NASA/TM-2001-210868

Fracture Behavior of a Stitched Warp-Knit Carbon Fabric Composite

Clarence C. Poe, Jr., and James R. Reeder
Langley Research Center, Hampton, Virginia

F. G. Yuan
North Carolina State University, Raleigh, North Carolina

National Aeronautics and
Space Administration

Langley Research Center
Hampton, Virginia 23681-2199

May 2001

ACKNOWLEDGMENTS

The authors would like to acknowledge the following people at NASA Langley Research Center for their assistance:

- Gary S. Johnson, Richard L. Chattin, Kenneth A. Deyerle, and James F. Linder of the Fabrication Division for manufacturing the stitched warp-knit composite panels.
- Benson H. Dexter of the Materials and Structures Competency for advice and assistance in manufacturing the stitched warp-knit composite panels.
- Lewis Simons of the Fabrication Division for making the notches.
- Diane C. Griffin and Richard S. Young of the Materials and Structures Competency for conducting the tests.

Available from:

NASA Center for AeroSpace Information (CASI)
7121 Standard Drive
Hanover, MD 21076-1320
(301) 621-0390

National Technical Information Service (NTIS)
5285 Port Royal Road
Springfield, VA 22161-2171
(703) 605-6000

TABLE OF CONTENTS

LIST OF FIGURES

LIST OF TABLES

ABSTRACT

Tests were conducted on several types of fracture specimens made from a carbon/epoxy composite. The composite material was stitched prior to introducing epoxy resin. Boeing used this material to develop a composite wing box for a transport aircraft in the NASA Advanced Composites Transport Program. The specimens included compact, extended compact, and center notched tension specimens. The specimens were cut from panels with three orientations in order to explore the effects of anisotropy. The panels were made with various thicknesses to represent a wing skin from tip to root. All fractures were not self-similar depending on specimen type and orientation. Unnotched tension specimens were also tested to measure elastic constants and strengths. The normal and shear strains were calculated on fracture planes using a series representation of strain fields for plane anisotropic crack problems. The fracture parameters were determined using a finite element method. Characteristic distances for critical tension and shear strains were calculated for each specimen and a failure criterion based on the interaction of tension and shear strains was proposed.

INTRODUCTION

Tests were conducted on a carbon/epoxy composite material to measure fracture properties that could be used in developing allowables to design for damage tolerance criteria. Unnotched tension specimens were also tested to measure elastic constants and strengths. ASTM standards were used. The carbon/epoxy composite material was made from a three dimensional preform using a resin film infusing process in an autoclave. The preform, which contained IM7 yarns in the spanwise (longitudinal) direction and AS4 yarns in the chordwise (transverse) and bias (±45°) directions, was stitched prior to introducing epoxy resin. Boeing used this material to develop a composite wing box for a transport aircraft in the NASA Advanced Composites Transport Program [1].

The crack-tip strain fields for planar anisotropic crack problems can be determined using a series expansion. Fracture parameters (stress intensity factor and T-stress) were determined using a J-integral method with finite element results [2]. The series expansion of the strain field contains a singular term which dominates the magnitude of the strains near the crack tip. The next largest term represents a uniform stress or strain field and is sometimes called the T-stress. This term was shown to govern the stability of the crack path in isotropic materials [3]. When the crack path is perturbed, the crack will naturally return to its original path only for a negative value of T-stress.

Panels were made with various numbers of fabric layers to represent the variation in thickness from tip to root. Fracture specimens of various configurations and loading directions were cut from the panels and tested to determine the influence of T-stress and anisotropy on fracture properties. The three specimen configurations were the center notch tension (CNT), the extended compact tension (ECT), and the compact tension (CT) specimen. For isotropic solids, the T-stress varies from negative to positive for these specimen configurations [4]. The specimens were cut with three orientations in order to apply the loads in the longitudinal, bias, and transverse directions. For longitudinal and transverse loading, the specimens are specially orthotropic. However for bias loading, the specimens are anisotropic, and shear and extension deformations are coupled.

For the elastic case, stresses and strains are infinite at the crack tip due to the singular terms. Thus, the distance from the crack tip to the point where the stress or strain reaches a critical value is often used as a fracture parameter. For a given critical value of stress or strain, fracture toughness is approximately proportional to the square root of this characteristic distance. With some specimen types and material orientations, the fracture path was not in the same direction as the original crack. In these cases when the crack growth was not self similar, both normal and shear strains are present along the fracture path. Thus, characteristic distances for critical values of shear and tension strains were calculated for these fracture paths, and an interaction equation was determined.

SYMBOLS

a	crack length for ECT and CT specimens measured from load line
a'	crack length for ECT specimens measured from specimen edge
$2a$	crack length for CNT specimens
B	biaxiality ratio, $T_s(\pi a)^{1/2}/K_I$
COD	crack opening displacement
d_o	characteristic distance
$g_{n\alpha}$	coefficient
E	Young's modulus
G	shear modulus
K	stress intensity factor
L	specimen length
n	index
$O(r^{1/2})$	terms of radius (r) higher than 1/2
P	applied load
r	radius from the crack tip
$\mathbf{S}$	compliance matrix
t	thickness normalized by fiber mass fraction of 66%
t'	measured thickness
$\mathbf{T}$	transformation matrix
T_s	T-stress
W	overall width of CNT specimen and width of ECT and CT specimens measured from load line
W'	overall width of ECT specimen
x_1, x_2	Cartesian coordinates where x_1 coincides with crack
x_1', x_2'	Cartesian coordinates where x_1' coincides with fracture path
$\bar{x}_1, \bar{x}_2$	Cartesian coordinates where $\bar{x}_1$ coincides with 0° fibers
δ_n	exponent
ε	engineering strain components
ς_α	functional
θ_{fiber}	inclination of 0° fiber from the cut direction
θ_{frac}	inclination of fracture path from the cut direction
λ	+1 for positive fracture strain and –1 for a negative fracture strain (see Eq. 6)
μ_α	roots of characteristic equation
ν	Poisson's ratio
σ	stress components

Subscripts:

frac	fracture path
1, 2	matrix component in Cartesian coordinate system oriented with the crack tip
max	pertaining to the max load

r, θ matrix component in polar coordinates system oriented with the direction of damage growth
u critical value
Q pertaining to 5% offset load
I mode I fracture
II mode II fracture

Abbreviations:
COD crack opening displacement
COV coefficient of variation
CNT center notch tension
CT compact tension
ECT extended compact tension
SIF stress intensity factor

EXPERIMENTS

Materials and Specimens

Preforms were made by stacking layers of a 50-inch-wide carbon warp-knit fabric to obtain various desired thicknesses. A three-dimensional preform was then made by stitching through the layers using a modified lock stitch. The yarns in the fabric were oriented in the 0°, ±45°, and 90° directions, resulting in what is commonly known as a fiber dominated composite. (The warp direction of the fabric was designated the 0° direction.) The orientation and areal weight of each ply of the fabric are given in Table 1. The areal weight of the fabric is equal to the fiber areal weight of 9 plies of 0.0324 lb/ft^2 (158 gm/m^2) prepreg tape. Also, composites made by stacking layers of this fabric are equivalent to balanced and symmetric laminates made from prepreg tape. The 0° yarns were 12K IM7 carbon, the ±45° yarns were 3K AS4 carbon, and the 90° yarns were 6K AS4 carbon. The 3K, 6K, and 12K designate the number in thousands of carbon fibers in a yarn. Both the warp and bias direction plies contribute approximately 44% of the yarns by weight while the remaining 12% were in the weft direction. The specified tolerance on areal weight per ply was ±3%.

Table 1. Warp knit fabric constituents.

Ply number	Yarn material	Yarn orien-tation	Areal weight, lb/ft^2 (gm/m^2)
1	3K-AS4	+45	0.0320 (156)
2	3K-AS4	-45	0.0320 (156)
3	12K-IM7	0	0.0643 (314)
4	6K-AS4	90	0.0350 (171)
5	12K-IM7	0	0.0643 (314)
6	3K-AS4	-45	0.0320 (156)
7	3K-AS4	+45	0.0320 (156)
		Total	0.2916 (1423)

Stitching was done with a numerically controlled single-needle stitching machine using Kevlar-29 thread and a modified lock stitch. The denier of the needle and bobbin threads were 1600 and 400, respectively. The rows of stitches

were made in the 0° direction 0.2 inches apart with 8 stitches per inch, resulting in 40 stitches per square inch. This pattern was determined by experiments to be optimum for maximum post-impact compression strength with minimum manufacturing costs [5].

Design studies for a 155 passenger commercial transport airplane indicated that the thickness of the tension wing skin would vary from 2 to 8 stacks of warp-knit fabric from wing tip to wing root. Thus, 11 flat panels 44 by 35 inches in length and width, and 2, 4, 6, and 8 stacks in thickness were made using 3501-6 epoxy resin. The resin was introduced in an autoclave using a resin-film infusion process where precast tiles of resin were placed between the lower caul plate and the preform. The resin tiles were sized with 2% excess resin which would flow through small holes uniformly distributed in the upper caul plate. All of the panels were made from the same batch of fabric and resin. Fiber mass and volume fractions were determined by acid digestion on 4 coupons taken from each panel. ASTM test method D3171 [6] was used. The average and coefficient of variation of the fiber mass fraction measurements were 66% and 2.7%, respectively. Detailed results are reported in the Appendix as Table A–1

Unnotched tension specimens to be loaded in the 0°-yarn (longitudinal) direction were cut from each panel. From most of the panels, specimens to be loaded in the 90° yarn (transverse) direction were also cut. At least one transverse specimen was taken from a panel of each thickness. The specimen configurations, which were 1.00-inches wide by 10.0-inches long, satisfy ASTM standard D3039/D3039M [7].

Three types of fracture specimens were cut from the composite panels—center notch tension (CNT), extended compact tension (ECT), and compact tension (CT) specimens. The specimens were cut from the panels with orientations parallel (longitudinal) and perpendicular (transverse) to the 0°-yarn direction. In addition, some CT specimens were cut on the bias of 45° and -45°. If the CT specimens cut on 45° and -45° biases are viewed from opposite sides, they are identical regarding laminate properties and loading direction so the results from these specimens are presented together as if they were all +45° specimen. They do differ slightly in that the ±45 plies within the laminate are reversed along with the stitch and bobbin thread sides of the laminate. Table 2 records the specimen sizes, thicknesses, range of cut lengths, and loading directions. Scaled sketches of the test specimens are given in Figure 1 while detailed dimensioned drawings are included in Appendix B. The configurations of the CT and ECT specimens were those prescribed in ASTM E399-90 [8] and E1922-97 [9], respectively.

The cuts were made using an ultrasonic machine with silicon carbide slurry. The blade of the tool was made from shim stock with a thickness that resulted in cuts with widths of approximately 0.020 inches. Thus, the aspect ratio of the cuts is small enough to be mathematically equivalent to cracks for analysis purposes.

Procedure

All specimens were tested in closed-loop, servo-hydraulic testing machines. The fracture specimens were tested in 100-kip capacity machines, and the unnotched

Table 2. List of fracture tests performed.

Specimen type	Width, W, inches	Length, L, inches	Thickness, inches	Cut length, a, inches	Loading direction
CNT	9.50	19.0	0.11, 0.33	3.33–4.75	Longitudinal
CNT	12.00	24.0	0.11, 0.33	4.85–5.67	Transverse
ECT	5.6	28.0	0.11, 0.22, 0.33, 0.44	2.10–2.80	Longitudinal
ECT	5.6	28.0	0.11, 0.22, 0.33, 0.44	2.10–2.80	Transverse
CT	5.6	6.7	0.11, 0.22, 0.33, 0.44	2.10–2.80	Longitudinal
CT	9.6	11.5	0.11, 0.22, 0.33, 0.44	2.10–2.80	Longitudinal
CT	5.6	6.7	0.11, 0.22, 0.33, 0.44	2.10–2.80	Transverse
CT	9.6	11.5	0.11, 0.22, 0.33, 0.44	2.10–2.80	Transverse
CT	5.6	6.7	0.22, 0.44	2.10–2.80	45° bias
CT	5.6	6.7	0.22, 0.44	2.10–2.80	-45° bias

tension specimens were tested in a 50-kip capacity machine. The testing machines were operated in stroke control, and the stroke rate was 0.050 inches per minute. A clip gage was used to measure crack opening displacement (COD). (See Appendix B for placement of gages.) The COD measurements were used to determine the applied load associated with a 5% increase in compliance. Load, stroke, date, and time were recorded on a digital data acquisition system. Strain for unnotched tension specimens and COD for fracture specimens were also recorded.

Radiographs were made of several failed specimens to reveal damage. The specimens were radiated with an industrial X-ray unit. The images were recorded on a self-developing film. A radiation-opaque dye penetrant was applied prior to radiation exposure. The penetrant was a liquid mixture of zinc iodide and a surfactant to facilitate penetration.

Unnotched tension specimens

The unnotched tension specimens were tested using hydraulically actuated wedge grips. Two inches of each specimen end were clamped by the grips. Instead of bonding loading tabs to specimens, plastic shims were placed between the serrated faces of the grips and the specimen. Carborundum coated screen, which is normally used for an abrasive, was placed between the plastic shims and the specimen to increase the coefficient of friction. The large failing loads for the 8-stack longitudinal specimens were the upper limit for this gripping method. The large hydraulic pressure necessary to prevent slip was about equal to that necessary to crush the composite.

Strain gages were bonded on the center of each face of the specimens. In some cases, a single gage was bonded on each face, and in other cases, a 0/90 rosette was bonded on each face. The modulus in the loading direction was determined according to ASTM standard D 3039/D 3039M [7], and Poisson's ratio was determined similarly from the 0/90 rosette data.

CNT specimens

The CNT specimens were loaded through friction grips similar to the unnotched tension specimens. However, 1-inch-diameter bolts were used to provide the normal force rather than hydraulically actuated wedges. The holes for the bolts are shown in Figure 1A and 1B. Transferring the load between the grips and the specimen through friction precludes stress concentrations in the specimen around the bolt holes. Also, clearance was sufficient between the bolts and edges of the holes in the specimen to preclude significant bearing forces.

To prevent Euler buckling in the compression regions above and below the cut, the specimens were sandwiched between aluminum guide plates. The plates were lined with 1/16-inch-thick Teflon sheet to minimize friction. A diamond shaped opening in the guide plates allowed access for a clip gage to be mounted over the cut along the centerline of the specimen. The clip gage measured the COD and had a gage length of approximately 0.5 inches. The gage was held in place by aluminum blocks that were bonded to the faces of a specimen using a room temperature epoxy. This method was believed suitable for obtaining the 5% offset load. Drawings of the test specimens, guide plates, test assembly and clip gage mounting are included in Appendix B.

ECT and CT specimens

The procedure for the CT specimens was patterned after ASTM E 399-90 [8], and the procedure for the ECT specimens is prescribed in ASTM E 1922-97 [9]. To prevent twisting and Euler buckling in regions with compression stresses, the specimens were sandwiched between aluminum guide plates. The plates were lined with 1/16-inch-thick Teflon sheet to minimize friction. Each ECT and CT specimen was loaded using a clevis and pin arrangement that prevent bending in either direction. A clip gage was mounted over the cut to measure COD. The clip gage was clipped to aluminum blocks bonded to the edge of the specimen. The clip gage assembly was similar to that used for the CNT specimens. Detail drawings of all test specimens, guide plates, and assembly drawings are documented in Appendix B.

ANALYSIS

Crack-tip Strain Field

Consider the coordinate systems in Figure 2. Three Cartesian coordinate systems with origins at the crack tip are shown. The primary coordinate system is defined with x_1 in crack direction or, in this application, the cut. The second coordinate system is defined with x_1' in the direction of the fracture path and finally the 0° fiber

direction of the material, $\bar{x}_1$, defines the third coordinate system. The angles θ_{fiber} and θ_{frac} define the orientations of the 0° fiber and the fracture direction, respectively, relative to the crack coordinate system.

For monoclinic materials with plane symmetry, Yuan has shown that the stress fields for a cracked body can be written as follows [2]:

$$\sigma_{11} = \sum_{n=1}(\delta_n+1)r^{\delta_n}\,\mathrm{Re}\left\{\frac{1}{\mu_1-\mu_2}\left[g_{n1}\left(\mu_2^2\varsigma_2^{\delta_n}-\mu_1^2\varsigma_1^{\delta_n}\right)+g_{n2}\mu_1\mu_2\left(\mu_2\varsigma_2^{\delta_n}-\mu_1\varsigma_1^{\delta_n}\right)\right]\right\}$$

$$\sigma_{22} = \sum_{n=1}(\delta_n+1)r^{\delta_n}\,\mathrm{Re}\left\{\frac{1}{\mu_1-\mu_2}\left[g_{n1}\left(\varsigma_2^{\delta_n}-\varsigma_1^{\delta_n}\right)+g_{n2}\left(\mu_1\varsigma_2^{\delta_n}-\mu_2\varsigma_1^{\delta_n}\right)\right]\right\} \qquad (1)$$

$$\sigma_{12} = \sum_{n=1}(\delta_n+1)r^{\delta_n}\,\mathrm{Re}\left\{\frac{1}{\mu_1-\mu_2}\left[g_{n1}\left(\mu_1\varsigma_1^{\delta_n}-\mu_2\varsigma_2^{\delta_n}\right)+g_{n2}\mu_1\mu_2\left(\varsigma_1^{\delta_n}-\varsigma_2^{\delta_n}\right)\right]\right\}$$

where $g_{n\alpha}$ are the unknown constants which are functions of loading and geometry. The $g_{n\alpha}$ terms are real for n = 1,3,5,... and imaginary for n = 2,4,6,... .

$$\delta_n = (n-2)/2$$

$$\varsigma_\alpha = \cos\theta + \mu_\alpha \sin\theta$$

μ_α are roots of the characteristic equation

$$S_{11}\mu^4 - 2S_{16}\mu^3 + (2S_{12}+S_{66})\mu^2 - 2S_{26}\mu + S_{22} = 0$$

and the S terms are from the compliance matrix such that

$$\varepsilon = \begin{bmatrix}\varepsilon_{11}\\ \varepsilon_{22}\\ \varepsilon_{12}\end{bmatrix} = \begin{bmatrix}S_{11} & S_{12} & S_{16}\\ S_{12} & S_{22} & S_{26}\\ S_{16} & S_{26} & S_{66}\end{bmatrix}\begin{bmatrix}\sigma_{11}\\ \sigma_{22}\\ \sigma_{12}\end{bmatrix} = [S]\sigma \qquad (2)$$

The first two terms of the series expansion for stress and strain can also be written in term of the fracture parameters as shown in equation 3 and 4

$$\sigma = \begin{bmatrix}\sigma_{11}\\ \sigma_{22}\\ \sigma_{12}\end{bmatrix} = \frac{1}{\sqrt{2\pi r}}\left(K_I\begin{bmatrix}\sigma_{11}\\ \sigma_{22}\\ \sigma_{12}\end{bmatrix}_I + K_{II}\begin{bmatrix}\sigma_{11}\\ \sigma_{22}\\ \sigma_{12}\end{bmatrix}_{II}\right) + T_s\begin{bmatrix}1\\0\\0\end{bmatrix} + O\left(r^{1/2}\right) \qquad (3)$$

$$\varepsilon = \begin{bmatrix}\varepsilon_{11}\\ \varepsilon_{22}\\ \varepsilon_{12}\end{bmatrix} = \frac{1}{\sqrt{2\pi r}}\left(K_I\begin{bmatrix}\varepsilon_{11}\\ \varepsilon_{22}\\ \varepsilon_{12}\end{bmatrix}_{II} + K_{II}\begin{bmatrix}\varepsilon_{11}\\ \varepsilon_{22}\\ \varepsilon_{12}\end{bmatrix}_{II}\right) + T_s\begin{bmatrix}S_{11}\\ S_{12}\\ S_{16}\end{bmatrix} + O\left(r^{1/2}\right) \qquad (4)$$

where K_I and K_{II} are the mode I and mode II stress intensity factors (SIF), T_s is the T-stress, and $O(r^{1/2})$ represents higher order terms. Comparing equation 3 to equation 1, it can be shown that [2]

$$K_I = \sqrt{\frac{\pi}{2}}\, g_{12}, \quad K_{II} = \sqrt{\frac{\pi}{2}}\, g_{11}, \quad T_s = -i\left(g_{21}\,\mathrm{Im}(\mu_1+\mu_2) + g_{22}\,\mathrm{Im}(\mu_1\mu_2)\right)$$

$$\sigma_I = \begin{bmatrix}\sigma_{11}\\ \sigma_{22}\\ \sigma_{12}\end{bmatrix}_I = \mathrm{Re}\begin{bmatrix} \frac{\mu_1\mu_2}{\mu_1-\mu_2}\left(\frac{\mu_2}{\sqrt{\varsigma_2}} - \frac{\mu_1}{\sqrt{\varsigma_1}}\right) \\ \frac{1}{\mu_1-\mu_2}\left(\frac{\mu_1}{\sqrt{\varsigma_2}} - \frac{\mu_2}{\sqrt{\varsigma_1}}\right) \\ \frac{\mu_1\mu_2}{\mu_1-\mu_2}\left(\frac{1}{\sqrt{\varsigma_1}} - \frac{1}{\sqrt{\varsigma_2}}\right)\end{bmatrix}, \quad \sigma_{II} = \begin{bmatrix}\sigma_{11}\\ \sigma_{22}\\ \sigma_{12}\end{bmatrix}_{II} = \mathrm{Re}\begin{bmatrix} \frac{1}{\mu_1-\mu_2}\left(\frac{\mu_2^2}{\sqrt{\varsigma_2}} - \frac{\mu_1^2}{\sqrt{\varsigma_1}}\right) \\ \frac{1}{\mu_1-\mu_2}\left(\frac{1}{\sqrt{\varsigma_2}} - \frac{1}{\sqrt{\varsigma_1}}\right) \\ \frac{1}{\mu_1-\mu_2}\left(\frac{\mu_1}{\sqrt{\varsigma_1}} - \frac{\mu_2}{\sqrt{\varsigma_2}}\right)\end{bmatrix}$$

and ε_I and ε_{II} can be obtained from σ_I and σ_{II} and equation 2.

The equations 1 through 4 are written in the crack-tip coordinate system. The strains along the fracture plane can be written

$$(\varepsilon)_{frac} = \begin{bmatrix}\varepsilon_{rr}\\ \varepsilon_{\theta\theta}\\ \varepsilon_{r\theta}\end{bmatrix}_{frac} = [T]\begin{bmatrix}\varepsilon_{11}\\ \varepsilon_{22}\\ \varepsilon_{12}\end{bmatrix} = [T]\varepsilon \tag{5}$$

where

$$T = \begin{bmatrix} \cos^2\theta_{frac} & \sin^2\theta_{frac} & \sin\theta_{frac}\cos\theta_{frac} \\ \sin^2\theta_{frac} & \cos^2\theta_{frac} & -\sin\theta_{frac}\cos\theta_{frac} \\ -2\sin\theta_{frac}\cos\theta_{frac} & 2\sin\theta_{frac}\cos\theta_{frac} & \cos^2\theta_{frac} - \sin^2\theta_{frac}\end{bmatrix}$$

Substituting equation 4 into 5,

$$\varepsilon_{frac} = \frac{1}{\sqrt{2\pi r}}\left[K_I(\varepsilon_I)_{frac} + K_{II}(\varepsilon_{II})_{frac}\right] + T_s(\varepsilon_T)_{frac} + O\left(r^{1/2}\right) \tag{6}$$

where

$$(\varepsilon_I)_{frac} = [T]\varepsilon_I, \quad (\varepsilon_{II})_{frac} = [T]\varepsilon_{II}, \quad (\varepsilon_T)_{frac} = [T]\begin{bmatrix}S_{11}\\ S_{12}\\ S_{16}\end{bmatrix},$$

The values of the coefficients $(\varepsilon_I)_{frac}$, $(\varepsilon_{II})_{frac}$, and $(\varepsilon_T)_{frac}$ in equations 6 depend only upon θ_{frac} and the elastic constants. The coefficients for normal and shear strains ($\varepsilon_{\theta\theta}$ and $\varepsilon_{r\theta}$, respectively) were calculated for the three loading directions (longitudinal, transverse and bias) and were normalized by the S_{22} compliance. The shear strains were then plotted against θ_{frac} in Figure 3. The coefficients for radial strain (ε_{rr}) are not considered because they do not contribute to the surface tractions on the fracture surface defined by θ_{frac}. Isotropic results are shown in each figure for comparison. Plane stress is assumed for all calculations in this report. The subscripts in S_{22} indicate the 2 direction of crack tip coordinate system. Thus, S_{22} is different for the three loading directions. The values of the coefficients are either symmetric or asymmetric with respect to θ_{frac} except for the bias loading direction where the principal material

axis is not aligned with the crack, resulting in anisotropy. The coefficients for isotropy and anisotropy are significantly different. The mode I coefficient for the normal strain and the mode II coefficient for the shear strain are maximum at $\theta_{frac} = 0$, whereas the others coefficients for longitudinal and transverse loading are minimum at $\theta_{frac} = 0$, and those for bias loading are minimum near $\theta_{frac} = 0$. For the normal strain, the coefficients for K_{II} and T-stress (T_s) can be much greater than that for K_I. The T_s coefficients for the normal strains at $\theta_{frac} = \pm 90°$ and the shear strains at $\theta_{frac} = \pm 45°$ can also be very large.

Fracture Criteria

Failure is assumed to occur on the plane θ_{frac} when either the normal or shear strain on that plane reaches a critical value $(\varepsilon_u)_{frac}$ at a characteristic distance d_o. Substituting $\varepsilon_{frac} = (\varepsilon_u)_{frac}$ and $r = d_o$ into equation 6, neglecting terms of $O(r^{1/2})$, and solving for $\sqrt{2\pi d_o}$,

$$\left(\sqrt{2\pi d_o}\right)_{\theta\theta} \cong \frac{K_I\left(\varepsilon_{(\theta\theta)I}\right)_{frac} + K_{II}\left(\varepsilon_{(\theta\theta)II}\right)_{frac}}{\lambda_{\theta\theta}\left(\varepsilon_{(\theta\theta)u}\right)_{frac} - T_s\left(\varepsilon_{(\theta\theta)T}\right)_{frac}} \qquad \left(\sqrt{2\pi d_o}\right)_{r\theta} \cong \frac{K_I\left(\varepsilon_{(r\theta)I}\right)_{frac} + K_{II}\left(\varepsilon_{(r\theta)II}\right)_{frac}}{\lambda_{r\theta}\left(\varepsilon_{(r\theta)u}\right)_{frac} - T_s\left(\varepsilon_{(r\theta)T}\right)_{frac}} \quad (7)$$

The λ in equation 7 is ± 1 depending on the sign of equation 6. The fracture parameter $\sqrt{2\pi d_o}$ is used instead of the distance d_o to obtain a fracture parameter proportional to the strength for small values of T_s. The use of the critical distance d_o directly, would have resulted in a failure parameter proportional to strength squared (assuming small values of T_s).

The five fracture paths θ_{frac} that correspond to planes normal to the fiber directions are 0°, 45°, 90°, -45°, and -90°. (Values of $\theta_{frac} < -90°$ or $\theta_{frac} > 90°$ are not considered.) The critical fibers are those normal to these paths. The critical fiber types are given in Table 3 for each of these paths. The value of $(\varepsilon_{\theta\theta(u)})_{frac}$ used for fiber tension failure is 0.0148 for AS4 fibers and 0.0171 for IM7 fibers [10] and the value of $(\varepsilon_{r\theta(u)})_{frac}$ used for shear failure is 0.022. (The average value of shear failing strain for woven and braided textile composites in reference 10 is 0.0110; however, use of twice the average value gave more satisfactory results. This seemed justified, because the variation in shear strength was very large among specimens of a given type and even larger between tubular and flat specimen types.)

Table 3. Critical fiber for different failure directions.

Loading Direction	θ_{fiber}	θ_{frac} 0°	45°	-45°	90°	-90°
Longitudinal	90°	IM7	AS4	AS4	AS4	AS4
Transverse	0°	AS4	AS4	AS4	IM7	IM7
Bias	45°	AS4	AS4	IM7	AS4	AS4
	-45°		IM7	AS4		

Calculations of K_I, K_{II}, and T_s

Values of K_I, K_{II}, and T_s were calculated using the procedure described in reference 2 which uses finite element results and a J integral calculation. In Figure 4, K_I is normalized by the applied load and plotted against 2a/W for the CNT specimens and against a/W for the ECT and CT specimens. T_s is also plotted in Figure 4 as a function crack length but is normalized by K_I. K_{II} is zero except for the CT specimens with bias loading, and the ratio of K_{II}/K_I for this case is plotted against a/W in Figure 5. Third-degree polynomial equations were fit to the data and plotted in each figure. The curve-fit equations which are listed in Table 4 were used to determine the critical stress intensity factors and T_s for each fracture test conducted.

Values for isotropic properties are also plotted in Figure 4 to show the influence of anisotropy. The equations that were used to calculate the curves in Figure 4 for the isotropic case are as follows:

Table 4. Curve fit equations for various figures.

Fig.	Specimen	y	x	Curve	Equation	R
4	CNT	$K_I/S(\pi a)^{1/2}$	2a/W	Longitudinal	$y= 0.8020 +1.408x -2.961x^2 +3.273x^3$	
				Transverse	$y= 0.8020 +1.408x -2.961x^2 +3.273x^3$	
		$T_s(\pi a)^{1/2}/K_I$	2a/W	Longitudinal	$y= -0.6204 -0.1803x$	
				Transverse	$y= -1.382 -0.4161x$	
	ECT	$K_I tW^{1/2}/P$	a/W	Longitudinal	$y= 9.418 -38.04x +88.05x^2 -26.50x^3$	
				Transverse	$y= 9.418 -38.04x +88.05x^2 -26.50x^3$	
		$T_s(\pi a)^{1/2}/K_I$	a/W	Longitudinal	$y= 0.4539 -3.843x +9.889x^2 -7.143x^3$	
				Transverse	$y= 0.3700 -4079x +11.58x^2 -7.841x^3$	
	CT	$K_I tW^{1/2}/P$	a/W	Longitudinal	$y= 7.880 -15.38x +37.88x^2 +4.251x^3$	
				Transverse	$y= 7.688 -21.37x +46.69x^2 +4.608x^3$	
				Bias	$y= 8.012 -20.86x +45.96x^2 +4.292x^3$	
		$T_s(\pi a)^{1/2}/K_I$	a/W	Longitudinal	$y= 0.02464 +.3098x +5.798x^2 -7.813x^3$	
				Transverse	$y= -0.6524 +4.401x -3.946x^2 +0.4100x^3$	
				Bias	$y= -0.6627 +4.417x -5.639x^2 +1.746x^3$	
5	CT	K_{II}/K_I	a/W	Bias	$y= 0.03507 +0.5602x -1.333x^2 +1.0159x^3$	
10	All	Δ Slope	$(P_{max}-P_O)/P_O$	Longitudinal	$y= 8.496 +1.220x$	0.638
				Transverse	$y= 15.25 +0.2792x$	0.157
	CT			Bias	$y= 16.103 +0.07053x$	0.047
11	CNT	K_Q	t/a	Longitudinal	$y= 25.85 -59.94 \log(x)$	0.950
				Transverse	$y= 41.39 -2.090 \log(x)$	0.352
		T_{sQ}	t/a	Longitudinal	$y= -8.433 -15.44 \log(x)$	0.901
				Transverse	$y= -24.28 -2.759 \log(x)$	0.770
		K_Q	t/a	Longitudinal	$y= 83.45 -10.01 \log(x)$	0.174
				Transverse	$y= 32.70 -6.211 \log(x)$	0.552
		T_{sQ}	t/a	Longitudinal	$y= 0.9746 -2.317 \log(x)$	0.511
				Transverse	$y= 0.2574 -1.739 \log(x)$	0.500
	CT	K_Q	t/a	Longitudinal	$y= 73.40 -14.66 \log(x)$	0.636
				Transverse	$y= 32.91 -6.046 \log(x)$	0.500
				Bias	$y= 14.59 -36.24 \log(x)$	0.857
		T_{sQ}	t/a	Longitudinal	$y= 17.33 -0.1991 \log(x)$	0.028
				Transverse	$y= 6.798 +0.1817 \log(x)$	0.006
				Bias	$y= 2.151 -3.837 \log(x)$	0.860
12	CT	K_{IIQ}	t/a	Bias	$y= 1424 -4216 \log(x)$	0.863

CNT specimen (references 12 and 4, respectively)

$$\frac{K_I t W}{P\sqrt{\pi a}} = \sqrt{\sec(\pi a / W)} \tag{8}$$

$$\frac{T_s\sqrt{\pi a}}{K_I} = \left[1 + 0.085(2a/W)\right] \tag{9}$$

ECT specimen (reference 9)

$$y = -0.08834 - 0.05964(a/W) + 1.146(a/W)^2 - 0.4537(a/W)^3 \tag{10}$$

where the a' and W' are measured from the specimen edge rather than the load line and a'/W' = (4a/W + 1)/5. No results were available for T_s.

CT specimen (reference 8 and 4, respectively)

$$y = -0.2014 - 0.1252(a/W) + 2.523(a/W)^2 - 0.9640(a/W)^3 \tag{11}$$

$$\frac{T_s\sqrt{\pi a}}{K_I} = -0.4199 + 4.408(a/W) - 6.211(a/W)^2 + 2.870(a/W)^3 \tag{12}$$

The above polynomial equation was fit to the biaxiality ratios that were tabulated in reference 4. For bias loading, $K_{II} = 0$ for the isotropic case.

Anisotropy did not affect values of K_I for the CNT and ECT specimens, but did influence the CT specimen. The longitudinal loading values were about 13% greater than those for transverse loading for this case. The values for bias loading were in between and were in agreement with the isotropic case. The values of K_I for the CNT specimen were between 1% and 2% less than those for the isotropic case. This difference was probably caused by the finite length of the specimen and uniform displacement boundary condition.

The value of K_{II} in Figure 5 for the CT specimen with bias loading was about 11% of K_I. The ratio declined only very slightly with increasing a/W. For the isotropic case, K_{II} is of course zero.

Anisotropy did strongly affect the magnitude of T_s, but not the sign. The values of T_s were negative for the CNT specimen and positive for the ECT and CT specimens. The absolute magnitudes of T_s were greatest for the CNT specimen and smallest for the ECT specimen, and those for the CT specimen were in between.

TEST RESULTS

Unnotched Tension Tests

Failure load and strain were measured for each test specimen. Stress was calculated using the width and a thickness that was normalized to a uniform 66% fiber mass fraction which was the average mass fraction for all panels. (See Table A-1.) Slopes of the stress strain curves were determined using a linear regression analysis for strains between 0.001 and 0.003. Young's modulus was taken as the slope for the strain parallel to the loading direction, and Poisson's ratio was calculated as the ratio of the slopes for the strains perpendicular and parallel to the loading directions.

Average values of strength, failing strain, Young's modulus, and Poisson's ratio are summarized in

Table 5 for longitudinal and transverse loading. The values are averages for all thicknesses, and each is the average of more than 15 measurements. Coefficients of variation, which are shown in parentheses, are reasonably low. Strength and Young's modulus for longitudinal loading are more than two times those for transverse loading because of the larger areal weight of the longitudinal yarns.

Strength and Young's modulus are plotted against thickness in Figure 6 and Figure 7 for longitudinal and transverse loading, respectively. The strengths and moduli decline noticeably with increasing thickness for longitudinal loading but not for transverse loading. The strengths of specimens that failed very near or in the grips were not included in the averages nor plotted in Figure 6 and Figure 7. Thus, it seems unlikely that the larger pressures necessary for gripping the thicker specimens caused the decrease in strength. Also, increasing gripping pressure should not have caused Young's modulus to decrease. Even though the decline in strength and modulus with thickness is noticeable, the coefficient of variation is only 6.5% for strengths and 4.7% for modulus.

All calculations in this report were made using the laminate elastic constants shown in Table 6. Here the subscript 1 and 2 in this case denote the primary 0° and 90° fiber directions, respectively. The laminate constants were calculated using lamination theory and the AS4/3501-6 and IM7/3501-6 lamina properties shown. The lamina moduli in the fiber direction were adjusted so that the laminate E_{11} would match the experimental unnotched tension results available at that time. Since that time,

Table 5. Results from tension tests.

Loading direction	Strength, Ksi (COV)	Failing strain, (COV)	Young's modulus, Msi (COV)	Poisson's ratio (COV)
Longitudinal	130 (6.5%)	0.0117 (7.5%)	11.3 (4.7%)	0.377 (8.1%)
Transverse	45.4 (5.9%)	0.0112 (9.8%)	4.70 (4.9%)	0.169 (4.1%)

Table 6. Material property values used in analysis.

	Laminate	AS4/3501-6	IM7/3501-6
E_{11} (Msi)	11.8	18.0	22.0
E_{22} (Msi)	5.16	1.60	1.60
G_{12} (Msi)	2.48	0.80	0.80
ν_{12}	0.401	0.34	0.34
ν_{21}	0.176	0.025	0.025

additional unnotched tension data was added to the data base causing a slight discrepancy between the E_{11} and E_{22} values derived by experiments and lamination theory (less than 5% and 9%, respectively). This difference is not believed to be important in the context of this report.

Detailed test results and calculated failure parameters to be discussed in the next section are listed in the tables of Appendix A for each test specimen. The data is grouped by type and loading direction.

Fracture Tests

COD and P_Q

Graphs of crack opening displacement (COD) plotted against load are shown in Figure 8. Two graphs each are shown for the CNT, ECT, and CT specimens. The 5% offset line is shown in each figure. Values of P_{max} and P_Q, which are the maximum load and the load corresponding to a 5% offset, are shown as symbols. For a given specimen type, the top graph represents the smallest P_{max}/P_Q case while the bottom represents the largest P_{max}/P_Q case. Thus, the variety of measured COD behaviors is represented. In most cases, the increase in COD due to stable damage progression was large, but in some the increase was small (bottom CNT response). Also, the difference between P_{max} and P_Q was significant in most cases, but in some cases the first peak was the largest (top CT response). The magnitude of the COD and applied load were quite different in each case because of differences in specimen thickness and crack length. The specimen number associated with each response is noted on each graph so that the response can be related to the detailed experimental data provided in Appendix A.

The values of P_{max}/P_Q were arranged in ascending order and plotted in Figure 9. A different symbol was used for each specimen type and loading direction. The mean value of P_{max}/P_Q is 1.0947 and the values for the mean plus and minus one standard deviation are 1.1701 and 1.0192, respectively. For each specimen type and loading direction, the ratios varied widely. However there does seem to be some segregation in values with specimen type. The eight lowest values of P_{max}/P_Q were for CT specimens (five were unity) and, the largest four values were for ECT specimens. The average values of P_{max}/P_Q were similar for each loading direction. The mean values for

longitudinal, transverse and bias were, 1.114, 1.070, and 1.106, respectively. The standard deviations were also similar, 0.0896, 0.0567,and 0.0510, respectively.

The crack length is approximately proportional to the value of COD/P. Thus an increase in slope of the COD versus load curve is an indication of failure at the notch tip of fibers in the loading direction. Figure 10 shows the percent increase in slope (COD/P) that occurs between P_{max} and P_Q plotted against the corresponding percent increase in load. The percentage in each case is taken with respect to the value at P_Q. Different specimen types are indicated by different symbols and a linear regression line is shown for each loading direction. The strongest correlation is for longitudinal loading with nearly a one for one correlation. The correlation is small for transverse loading and is nearly zero for bias loading. Thus, the damage evolution that occurs between P_Q and P_{max} for longitudinal loading may be characteristically different from that for transverse and bias loading.

Effect of thickness on values of K_{IQ}, K_{IIQ}, and T_{sQ}

In order to determine the effect of thickness on the fracture results, values of K_{IQ} and T_{sQ} are plotted against the logarithm of the thickness ratio t/a in Figure 11 for CNT, ECT, and CT specimens. Values of K_{IIQ} were zero for all cases except for the CT specimen loaded in the bias direction. These values of K_{IIQ} are plotted in Figure 12 against the logarithm of thickness. The subscript Q indicates that values of P_Q were used to make the calculations. The range of thickness ratios is nearly an order of magnitude for longitudinal and transverse loading but only a factor of two for bias loading. Different loading directions are indicated by different symbols. For the CNT specimens with longitudinal loading, the values of K_{IQ} decrease 40% from the smallest to largest values of t/a, whereas those with transverse loading are mostly unchanged with increasing thickness. This response is somewhat similar to that observed for the unnotched tension specimen where the strength in the longitudinal direction decreased with thickness while the strength in the transverse direction remained unchanged (Figure 6 and Figure 7). Scatter for the longitudinally loaded ECT specimens was much greater than for the other tests configurations and loading directions. The regression line for K_{IQ} in this case decreased only 9% with increasing t/a which is less than the coefficient of variation (15.8%). For the CT specimens, the values of K_{IQ} decrease less than 14% with increasing t/a for longitudinal and transverse loading and 19% for bias loading. The decrease is more significant for bias loading case because the range of t/a values is much smaller. The variation of T_{sQ} in Figure 11 and K_{IIQ} in Figure 12 with thickness is similar to the variation in K_{IQ} because K_{IIQ} and T_{sQ} are approximately proportional to K_{IQ}. Note that in the CNT case the magnitude of T_{sQ} is decreasing similar to the variation in K_{IQ} noted earlier but the slope of the curve is positive because the T_{sQ} values for this case are negative. For the ECT specimen, the effect on T_{sQ} due to increased thickness seems intensified over the effect on K_{IQ} while for the CT specimen the effect on T_{sQ} seems diminished.

Fracture paths

Fracture paths were self-similar ($\theta_{frac} = 0°$) for all specimen types with transverse loading and for all CNT specimens with longitudinal loading. Radiographs showing self similar crack growth are presented as Figure 13 and Figure 14 for a failed CNT specimen loaded longitudinally and a failed CT specimen loaded transversely. For the CNT specimen, radiographs are shown for both notch tips. The wide white lines are the cuts, and the wide dark regions indicate damage along the fracture paths. The small white spots within the damage region of the CNT specimen are gaps in the material indicating that the specimen was nearly pulled apart. The small dark spots near the damaged regions are stitch locations. On the other hand, the failure path for all CT specimens with longitudinal loading was $\theta_{frac} = 90°$ and with bias ($\theta_{fiber} = 45°$) loading was $\theta_{frac} = 45°$ as shown in Figure 15 and Figure 16 respectively.

The fracture paths for the longitudinally loaded ECT specimens were complex and varied. The radiographs of three failed ECT specimens are shown in Figure 17-Figure 19. In Figure 17, the fracture path is $\theta_{frac} = -45°$. In Figure 18, the overall fracture path is $\theta_{frac} = 0°$ but the path meanders. In Figure 17 and Figure 18, the initial fracture path appears to be $\theta_{frac} = \pm 90°$ but changes to $\theta_{frac} = -45°$ and 0°, respectively.

In Figure 19, two fracture paths are revealed in the failed ECT specimen. The fracture path originating at the end of the cut is $\theta_{frac} = \pm 90°$. The fracture that initiates at the free edge opposite the cut and propagates toward the cut has the appearance of a shear-kink type compression failure caused by the large bending stress in the net section. Similar failures occurred in longitudinally loaded ECT specimens with thicknesses of 2 and 4 stacks (0.11 and 0.22 inches) but not in specimens with a thickness of 8 stacks (0.44 inches). Of the two specimens with a thickness of 6 stacks (0.33 inches), a compression-like failure occurred in one but not in the other. Thus, the propensity for the compression-like failures varies inversely with thickness. The order of occurrence of the failures that initiated at the end of the cut and at the free edge is not obvious from the COD versus load graph (Bottom ECT graph in Figure 8). However, since compression failures were never observed alone, they may have been the second to initiate.

Use of $\sqrt{2\pi d_o}$ as a failure parameter

Values of $\sqrt{2\pi d_o}$ were calculated using equation 7 for each observed fracture path and for both the normal tension strain, $\varepsilon_{\theta\theta}$, and the shear strain, $\varepsilon_{r\theta}$. The critical values of K_{IQ}, K_{IIQ}, and T_{sQ} in Table 6 were calculated for $t/a = 0.1$ using the regression curves in Figure 11 and Figure 12. The value $t/a = 0.1$ is approximately the smallest value of t/a common to the CNT, ECT, and CT specimens. The coefficients $(\varepsilon_{\theta\theta(I)})_{frac}$, $(\varepsilon_{\theta\theta(II)})_{frac}$, $(\varepsilon_{\theta\theta(T)})_{frac}$, $(\varepsilon_{r\theta(I)})_{frac}$, $(\varepsilon_{r\theta(II)})_{frac}$, and $(\varepsilon_{r\theta(T)})_{frac}$ were determined for each value of θ_{frac} using the curves in Figure 3. The critical distance parameter $\sqrt{2\pi d_o}$ is plotted against crack extension direction in Figure 20 for each test specimen type and for both tension and shear strains. Even though the results are for the discrete values

of θ_{frac} = 0°, 45°, 90°, -45°, and –90°, continuous curves are drawn through the values to assist in visualizing the results. The curves were drawn using a spline fit method. A larger critical distance parameter can be interpreted as larger strains driving growth in that direction. Detailed calculations dealing with failure of specimens normalized to a t/a ratio of 0.1 are listed in Appendix A.

For longitudinal loading, the curves for the critical distance due to normal strain are similar in shape with all having a maximum at θ_{frac} = 0°. However, there is some separation between the curves. The failures for the CNT specimens and for one of the ECT specimens were self-similar (θ_{frac} = 0°). The other ECT specimens failed along θ_{frac} = -45° and ±90°. The maximum values of $\sqrt{2\pi d_o}$ due to normal strain and longitudinal loading was about 7% higher for the CNT and ECT specimen which exhibited self similar crack growth than it was for the CT which did not fail in the θ_{frac} = 0° direction. Because failures of the ECT and CT specimens failed in directions other than θ_{frac} = 0° where the critical distance parameter is highest for the normal strain, shear must contribute to the fracture in these cases. The curves for $\sqrt{2\pi d_o}$ due to shear strain with longitudinal loading reach a maximum at θ_{frac} = ±90°. The minimum value of $\sqrt{2\pi d_o}$ for shear occurs at θ_{frac} = 0°.

All tests conducted in transverse loading direction failed in a self-similar manner. The $\sqrt{2\pi d_o}$ curves due to the normal strain for the three specimen types are virtually identical for transverse loading and similar in shape to that seen for longitudinal loading The maximum $\sqrt{2\pi d_o}$ values were on average about 12% higher for the transverse direction than they were for the longitudinal loading direction. The curves for shear strain due to transverse loading are also quite close for the ECT and CT specimens, but the CNT curve is about 15% higher than the other two. The critical distance due to shear in the fracture direction (θ_{frac} = 0°) is zero indicating that shear did not help drive the fracture process for these tests. The shape of the shear curves are quite different from those seen for longitudinal loading. The values of $\sqrt{2\pi d_o}$ for shear in the transverse direction is a maximum at θ_{frac} = ±45° but no failures were observed in that direction for transversely loaded specimen.

Only CT specimens were tested with bias loading. The $\sqrt{2\pi d_o}$ curve for normal and shear strain for this case is plotted on Figure 20. The curve due to normal strain is somewhat similar in shape to those for transverse and longitudinal loading but it is skewed toward positive values of θ_{frac}. The value of $\sqrt{2\pi d_o}$ due to normal strain at θ_{frac} = 0° and -45° are about equal but all specimens failed in the θ_{frac} = 45° direction where the $\sqrt{2\pi d_o}$ due to shear strain was larger. The shear curve for bias loading is asymmetric and has two maxima, one at θ_{frac} = -45° and one at θ_{frac} = 90°. The fact that failure occurred in a direction that was not a maximum for either normal or shear strain but where both were large is an indication that there is an interaction between these two crack driving forces.

To examine the influence of normal and shear strain on fracture path, the critical values of $\sqrt{2\pi d_o}$ for normal strain were plotted against the critical $\sqrt{2\pi d_o}$ values for shear in Figure 21. The values for each type of specimen are plotted separately. Critical values in all five fracture directions ($\theta_{frac} = 0°$, $\pm 45°$, and $\pm 90°$) and in each loading direction were plotted, but actual failures were observed only in the directions marked with an "X". Because of material symmetry in the longitudinal and transverse loading cases, the critical values in the $\theta_{frac} = \pm\theta$ directions are the same. For longitudinal and transverse loading, self-similar failures lie on the ordinate, and non-self-similar failures lie to the right of the ordinate. For bias loading, all failures lie to the right of the ordinate.

Two failure criteria are also plotted in Figure 21. These failure criteria were fit to all the critical points corresponding to observed failures (those marked with an "X") from all of the specimen types. The "maximum $\sqrt{2\pi d_o}$ cirterion" requires that neither the normal or shear value of $\sqrt{2\pi d_o}$ be greater than their respective critical value. This criterion therefore ignores any interaction between the normal and the shear. The average value of $\sqrt{2\pi d_o}$ for specimens that failed with an absence of shear (in a self-similar manner) was 0.361 $\sqrt{\text{in.}}$ with a coefficient of variation of only 7.3%. Thus, a maximum normal strain criterion represents self-similar failures accurately. On the other hand, for failures that were not self similar, the values of $\sqrt{2\pi d_o}$ range from approximately 0.03 to 0.28 $\sqrt{\text{in.}}$ for normal strain and from 0.20 to 0.54 $\sqrt{\text{in.}}$ for shear strain. Thus, failures that were not self-similar are not well represented by maximum strain criteria, indicating a significant interaction between shear and tension.

The "polynomial criterion" was generated by fitting a second order polynomial through all the data marked with an "X" in Figure 21. Although the values of $\sqrt{2\pi d_o}$ were accurately represented for observed critical fracture paths, the criterion could not be used to accurately predict the fracture paths because the curve also fell though points representing failure directions that were not observed in testing. For example the polynomial criterion indicates that 0° and 45° fracture paths are equally likely for CNT specimens with transverse loading, but only 0° fracture paths were observed. Because the polynomial failure criterion does fall through all the observed critical values, it can be used to predict the strengths of the CNT, ECT, and CT specimens with longitudinal, transverse, and bias loading correctly. The strength of actual structures however might not be predicted accurately with this criterion because the fracture path could not be correctly predicted. The fracture path must be predicted correctly in order to determine the effect of structural elements on the ultimate strength of the structure and on the arrest and containment of the fracture.

The polynomial $\sqrt{2\pi d_o}$ criterion provides a failure criterion that is independent of loading direction which distinguishes it from a criterion based on K_{IQ} where the critical values change significantly with loading direction as seen in Table 7. The critical K_{IQ}

Table 7. Summary of fracture parameters for different specimen.

Specimen type	Loading	Fiber Direction θ_{fiber}	Observed Fracture Path θ_{frac}	$P = P_Q$ and $t/a = 0.1$			
				K_{IQ}, ksi $\sqrt{in.}$	K_{IIQ}, ksi $\sqrt{in.}$	T_{sQ}, ksi $\sqrt{in.}$	$\sqrt{2\pi d_o}$ for $\theta_{frac} = 0°$, $\sqrt{in.}$
CNT	Longitudinal	90°	0°	85.8	0	-23.87	0.329
ECT	Longitudinal	90°	0°,45°,90°	93.5	0	3.3	0.339
CNT	Transverse	0°	0°	41.4	0	-21.5	0.395
ECT	Transverse	0°	0°	38.9	0	2.0	0.372
CT	Transverse	0°	0°	39.0	0	6.78	0.369
						Average	0.361
						COV	7.3%
CT	Longitudinal	90°	90°	88.1	0	17.5	0.310
CT	Bias	45°,-45°	45°,-45°	50.8	5.6	5.988	0.340

values vary due to their dependence on modulus which varies with loading direction. Unlike K_{IQ}, the $\sqrt{2\pi d_o}$ parameter is also influenced by the T-stress.

Influence of T-stress

The T-factor is defined by $\left[\lambda_{ij} - T_s\left(\varepsilon_{ij(T)}\right)_{frac}/\left(\varepsilon_u\right)_{frac}\right]^{-1}$ and a separate T-factor can be calculated for each critical strain component (normal or shear). The sign of the T-factor indicates the sign of the critical strain but no negative (compression) values for normal strain were calculated for fracture paths observed in tests. The deviation of the T-factor from ± 1 indicates the relative magnitude of the T_s contribution to the failure strain calculated from equation 6. If |T-factor|>1, the T-stress augmented strains due to the stress intensity at the crack tip causing an early failure while if |T-factor|<1, the T-stress reduced these strains. Values of the T-factor for the fracture paths observed in the tests loaded in the longitudinal direction were ranked and plotted in Figure 22 for critical normal and shear strains. For critical tension, the values of T-factor range from 0.98 to 1.30, but the value of 1.30 is of no consequence because the resulting $\sqrt{2\pi d_o}$ is very small (The failure was dominated by shear instead of normal strain). Neglecting values that correspond to $\sqrt{2\pi d_o} < 0.1$, the values of T-factor, for normal strain, range only from 0.981 to 1.050. For critical shear, the values of T-factor range from 0.915 to 1.000. The range of the T-factor for observed fracture paths indicates that the T-stress influences values of $\sqrt{2\pi d_o}$ by less than 8% for either normal or shear strain.

Although the T-stress had less than a 8% effect on the magnitude of $\sqrt{2\pi d_o}$, the sense or sign of the T-stress has been shown to play an important role in influencing the stability of the fracture path. In reference 3, Cotterell determined the approximate isotropic stress field for a crack with a small kink at one end and showed that a negative T-stress would cause an extension of the kinked end to turn back toward the direction of

the main crack, resulting in overall self-similar crack extension. In the present investigation of orthotropic composites, the T-stress is only negative for the CNT specimens with both longitudinal and transverse loading, and indeed, the cracks did extend in a self-similar manner. (See Table 7.) The T-stress is positive for the longitudinal and bias loaded ECT and CT specimens, and cracks grew in a non-self similar manner. However, contrary to Cotterell's prediction, all transversely loaded ECT and CT specimens extended in a self-similar manner even though the T-stress was positive. Therefore, a negative T-stress was sufficient for self-similar crack extension but not necessary.

Comparisons to historical data.

An average value of $\sqrt{2\pi d_o} = 0.30\ \sqrt{in.}$ due to normal strain was reported by Poe[14] for CNT specimens of specially orthotropic composite materials with self-similar fracture paths. The shear component would be zero due to the self-similar fracture direction. The calculations by Poe were made using maximum loads and equation (6) with $\theta_{frac} = 0°$ but without the T-stress term. The median value of P_{max}/P_Q in Figure 9 is 1.095. Dividing $\sqrt{2\pi d_o} = 0.30$ by 1.095 gives $\sqrt{2\pi d_o} = 0.274\ \sqrt{in.}$, which is 24% less than the average value of 0.361 $\sqrt{in.}$ found in this study.

Harris and Morris[15] reported fracture test results for $[0/90]_{ns}$, $[0/\pm45/90]_{ns}$, and $[0/\pm45]_{ns}$ laminates of various thicknesses made from T300/5208 carbon/epoxy prepreg tape. CT and three-point-bend specimens (TPB) were used for the thicker laminates and CNT specimens for all thicknesses. Values of $\sqrt{2\pi d_o}$ were calculated using equation 7 and plotted against thickness in Figure 23. The calculations were made with the 5% offset load P_Q and $\theta_{frac} = 0°$, and the T-stress term was neglected. The elastic constants in reference 15 and a value of $(\varepsilon_{\theta\theta(u)})_{frac} = 0.010$ were used. The values of $\sqrt{2\pi d_o}$ for the $[0/90]_{ns}$ and $[0/\pm45/90]_{ns}$ laminates decrease with increasing thickness. They appear to have reached a minimum at t/a = 0.7. However, the values for the $[0/\pm45]_{ns}$ laminates increase with increasing thickness. For the $[0/90]_{ns}$ and $[0/\pm45/90]_{ns}$ laminates, the values of $\sqrt{2\pi d_o}$ for the various specimen types are in good agreement. For the $[0/\pm45]_{ns}$ laminates, on the other hand, the values for the TPB and CT specimens are significantly less than those for CNT specimens. All failures were self-similar except those for the $[0/\pm45]_{ns}$ CT specimens that were $\theta_{frac} = 45°$.

The values of $\sqrt{2\pi d_o}$ for the $[0/90]_{ns}$ laminates with t/a = 0.1 are in good agreement with the average value of 0.368 $\sqrt{in.}$ for the stitched warp-knit composites with self-similar failures found in this study. Those for the $[0/\pm45/90]_{ns}$ laminates are about 25% smaller, and those for $[0/\pm45]_{ns}$ are about 45% smaller.

CONCLUDING REMARKS

Tests were conducted on center notched tension (CNT), extended compact tension (ECT), and compact tension (CT) specimens made from a carbon/epoxy composite. The composite material, which was made from a stitched warp-knit fabric, contained 44% 0° yarns, 44% ±45° yarns, and 12% 90° yarns. The modulus in the longitudinal direction was twice that in the transverse direction. In order to determine the influence of anisotropy, specimens were cut with three orientations from panels – longitudinal, transverse, and on a 45° bias. The specimens loaded longitudinally and transversely were specially orthotropic, but the specimens loaded on the bias were anisotropic. Crack opening displacements (COD) were measured and loads P_Q corresponding to a 5% offset in the COD versus load curves were determined. The mean ratio of the maximum load P_{max} to P_Q was 1.09. The standard deviation was 0.07.

The panels were made with thicknesses ranging from 0.22 to 0.88 inches to represent a wing skin from tip to root. Values of fracture toughness were calculated for the offset loads P_Q. For CNT specimens with longitudinal loading, the mean value of fracture toughness for 0.33-inch-thick specimens was 40% less than the mean value for 0.11-inch-thick specimens. However, with transverse loading, the mean values were essentially equal. The difference was 19% or less for the other specimen types and loading directions.

Failures were self-similar for all specimens with transverse loading and for all CNT specimens with longitudinal loading. Except for one ECT specimen, failures were not self-similar for ECT and CT specimens with longitudinal loading nor for the CT specimens with bias loading. The ECT specimens with longitudinal loading were the only type to fail along more than one path. The thinner ECT specimens also failed in compression on the edge opposite the cut due to large bending stresses. The failure appeared to a shear-kinking type material failure. The compression failures never occurred alone.

The normal and shear strains were calculated on fracture planes using a series representation of strain fields for plane anisotropic crack problems developed by Yuan. The singular terms and the uniform stress term (T-stress) were included. For specimens with self-similar failures, shear strains were zero along the fracture paths. But for specimens with failures that were not self-similar, large shear strains were calculated along the fracture paths. Characteristic distances for tension and shear strains were calculated for each specimen. For specimens with self-similar failures, the values of the characteristic distance were reasonably constant and were in agreement with other values in the literature for carbon/epoxy composites. When failures were not self-similar, the values of characteristic distance for critical tension strain were smaller. A polynomial failure criterion was applied to the characteristic distances for critical tension and shear strains. The predictions of strength using this criterion were reasonably accurate, but the predictions of fracture paths were not accurate. A stability analysis for a kinked crack may be required to predict fracture paths.

REFERENCES

1. Kropp, Y.: Development of a Stitched /RFI Composite Transport Wing. Mechanics of Textile Composites Conference (Hampton, VA, Dec. 6-8, 1994). NASA CP-3311, Part 2, 1995, pp. 457-479.
2. Yuan, F. G.: Determination of Stress Coefficient Terms in Cracked Solids for Monoclinic Materials with Plane Symmetry at $x_3 = 0$. NASA CR-1998-208729, October 1998.
3. Cotterell, B.: Notes on the Paths and Stability of Cracks. International Journal of Fracture Mechanics, Vol. 2, 1966, pp. 526-533.
4. Levers, P. S. and Radon, J. C.: Inherent Stress Biaxiality in Various Fracture Specimen Geometries. International Journal of Fracture, Vol. 19, 1982, pp. 311-325.
5. Henrichs, Steve C.; Kropp, Yury; and Jegley, D.: Analysis and Testing of Stitched/RFI Subcomponents. in Sixth NASA/DOD Advanced Composites Technology Conference, Vol. 1, Part 1, NASA CP 3326, Aug. 1995, pp. 209-231.
6. ASTM: Standard Test Method for Fiber Content of Resin-Matrix Composites by Matrix Digestion. Annual Book of Standards, Vol. 15.03, D3171-99, 1999, pp. 110-112.
7. ASTM: Standard Test Method for Tensile Properties of Polymer Matrix Composite Materials, Annual Book of Standards, Vol. 15.03, D3039-95a,1999, pp 99-109.
8. ASTM: Standard Test Method for Plane-Strain Fracture Toughness of Metallic Materials. Annual Book of Standards, Vol. 03.01, E399-90, 1998, pp. 413-443.
9. ASTM: Standard Test Method for Translaminar Fracture Toughness of Laminated Polymer Matrix Composite Materials. Annual Book of Standards, Vol. 03.01, E1922-97, 1997, pp. 1085-1089
10. Minguet, Pierre J.; Fedro, Mark J.; and Gunther, Christian K.: Test Methods for Textile Composites. NASA CR-4609, July 1994.
11. Poe, Jr., C. C. and Sova, J. A.: Fracture Toughness of Boron/Aluminum Laminates with Various Proportions of 0° and ±45° Plies. NASA TP 1707, Nov. 1980.
12. Poe, Jr., C. C.; Harris, Charles E.; Coats, Timothy W.; and Walker, T. H.: Tension Strength with Discrete Source Damage. Fifth NASA/DoD Advanced Composites Technology Conference, Vol. I, Part 1, NASA CP-3294, pp. 369-437.
13. Yang, S.; and F.G. Yuan, "Kinked Crack in Anisotropic Bodies" in Int. J. of Solids and Structures, Vol. 37, No. 45, November 2000, pp. 6635-6682
14. Poe, C. C., Jr.: A Unifying Strain Criterion for Fracture of Fibrous Composite Laminates. Eng. Fract. Mech., Vol. 17, No. 2, 1983, pp. 153-171.
15. Harris, C. E.; and Morris, D. H.: Fracture Behavior of Thick, Laminated Graphite/Epoxy Composites. NASA CR-3784, 1984.
16. Poe, Jr. C. C., "Residual Strength of Composite Aircraft Structures with Damage," ASM Handbook, Vol. 19, Fatigue and Fracture, 1996, pp. 920-935.

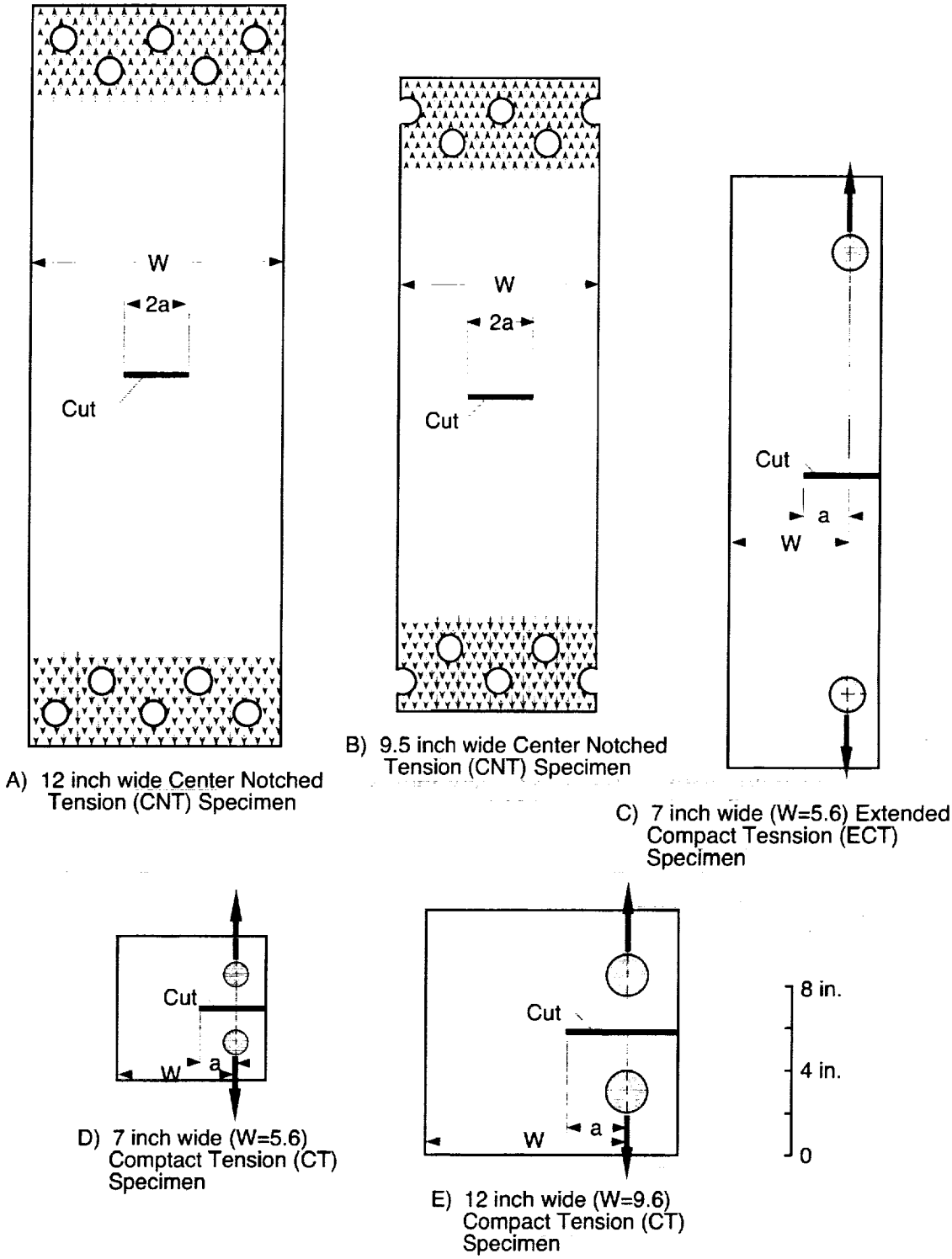

Figure 1. Fracture test specimen types.

Specimen	θ_{fiber}
Longitudinal	90°
Transverse	0°
Bias	45° or -45°(135°)

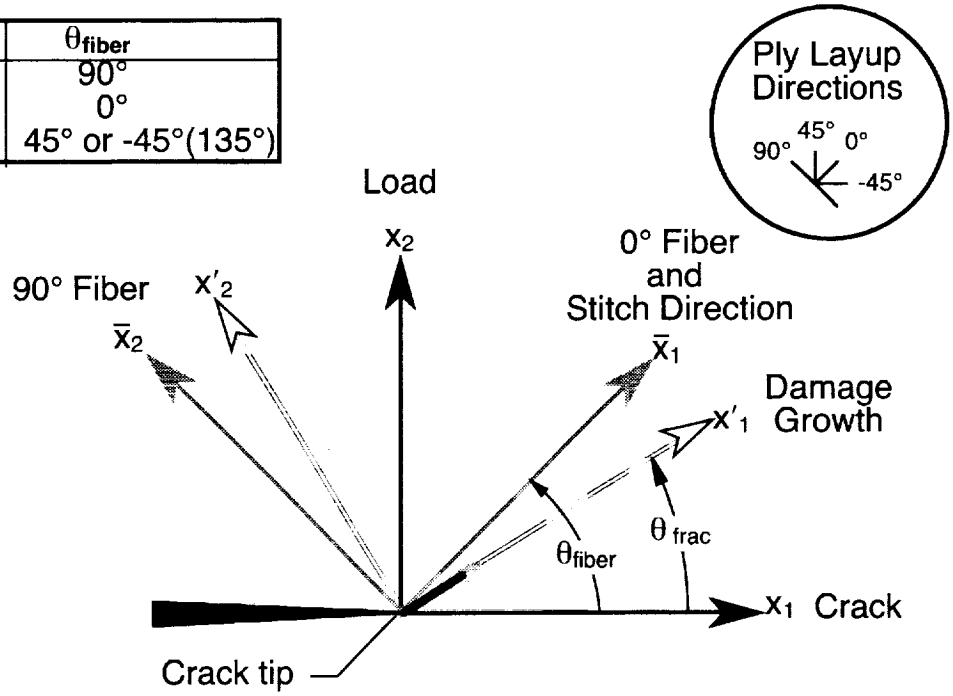

Figure 2. Sketch of crack tip coordinate systems.

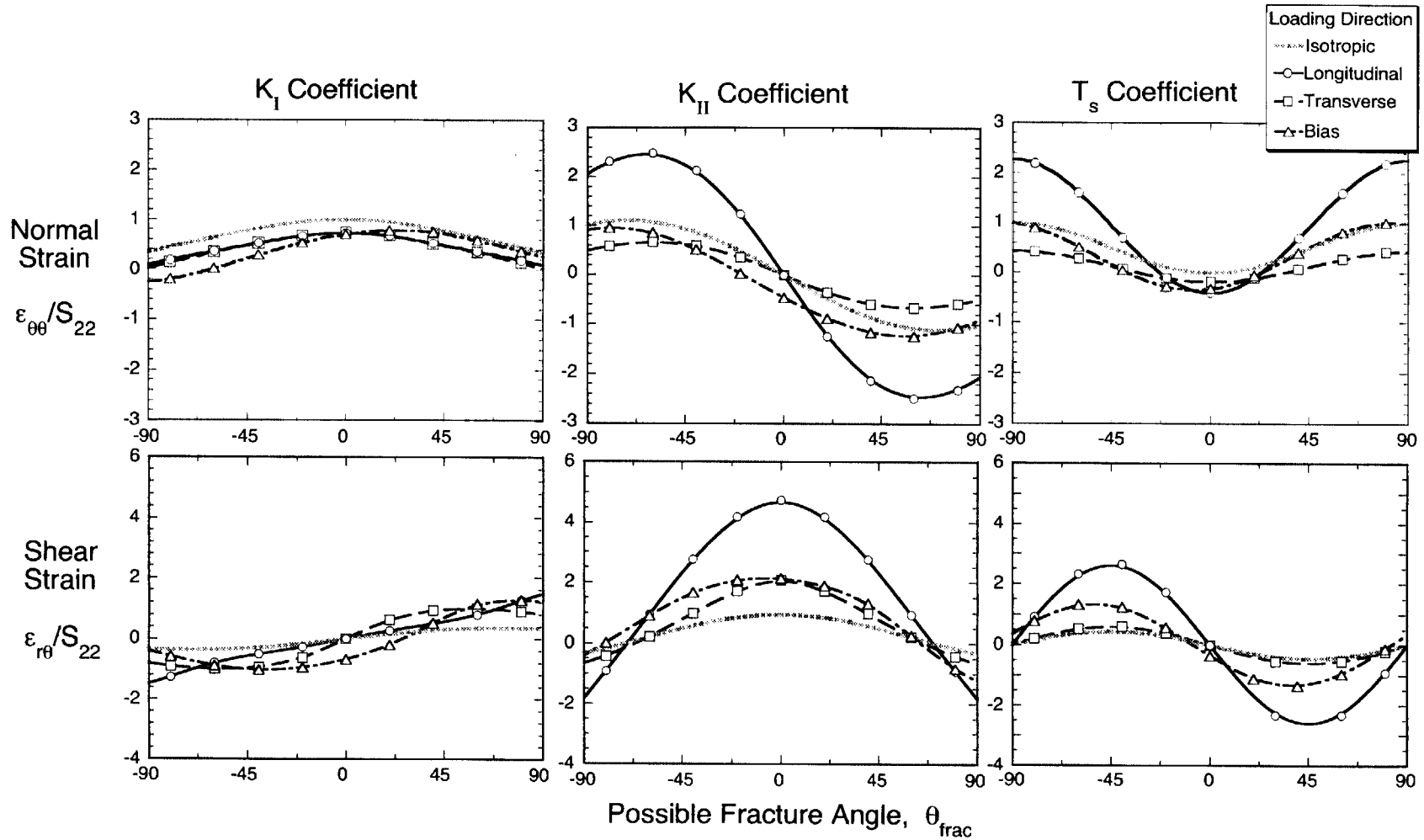

Figure 3. Normalized components of transverse and shear strain broken out by loading mode as a function of angle at which the crack might extend.

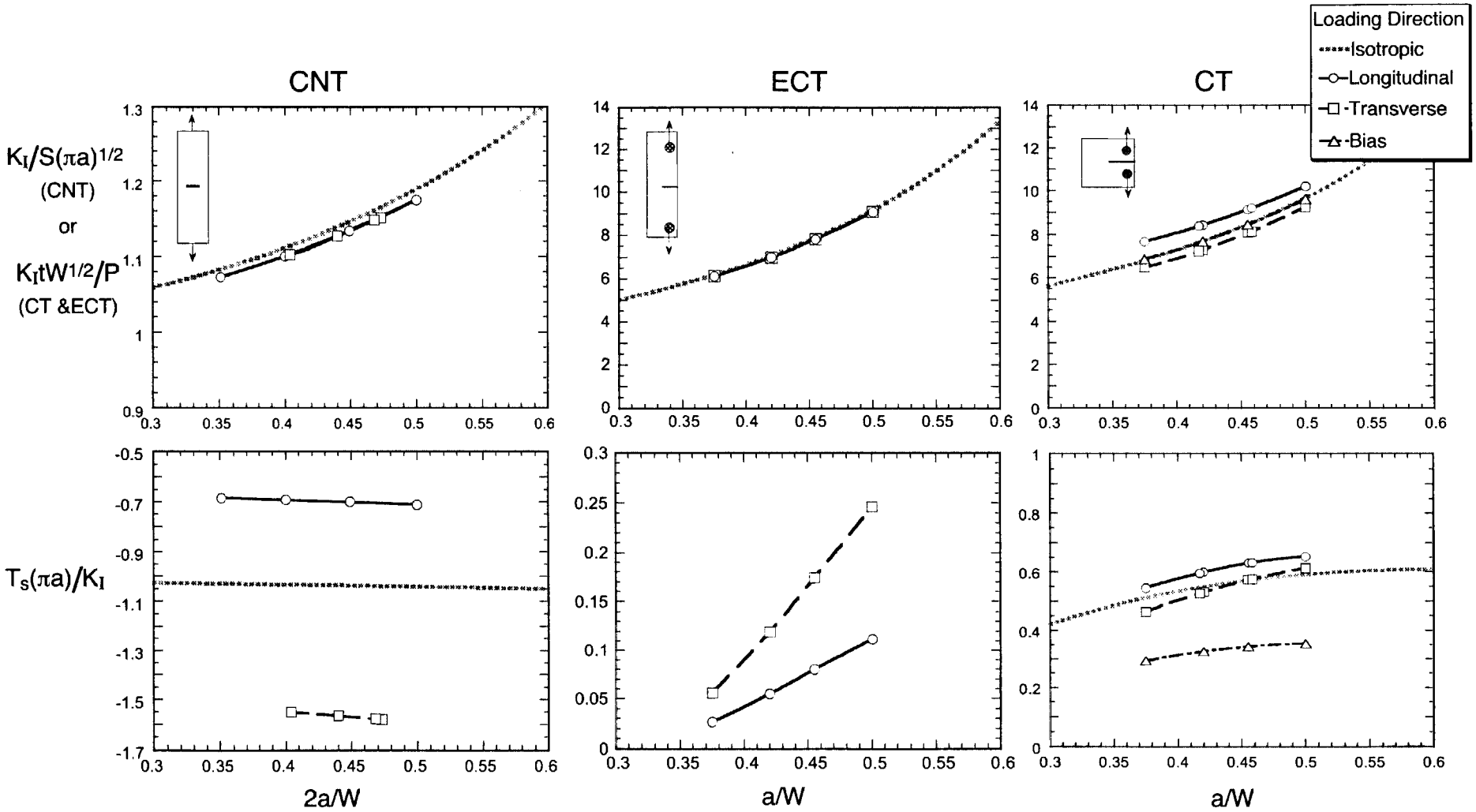

Figure 4. Normalized K_I and T_s as a function of crack length for each test specimen type and material direction.

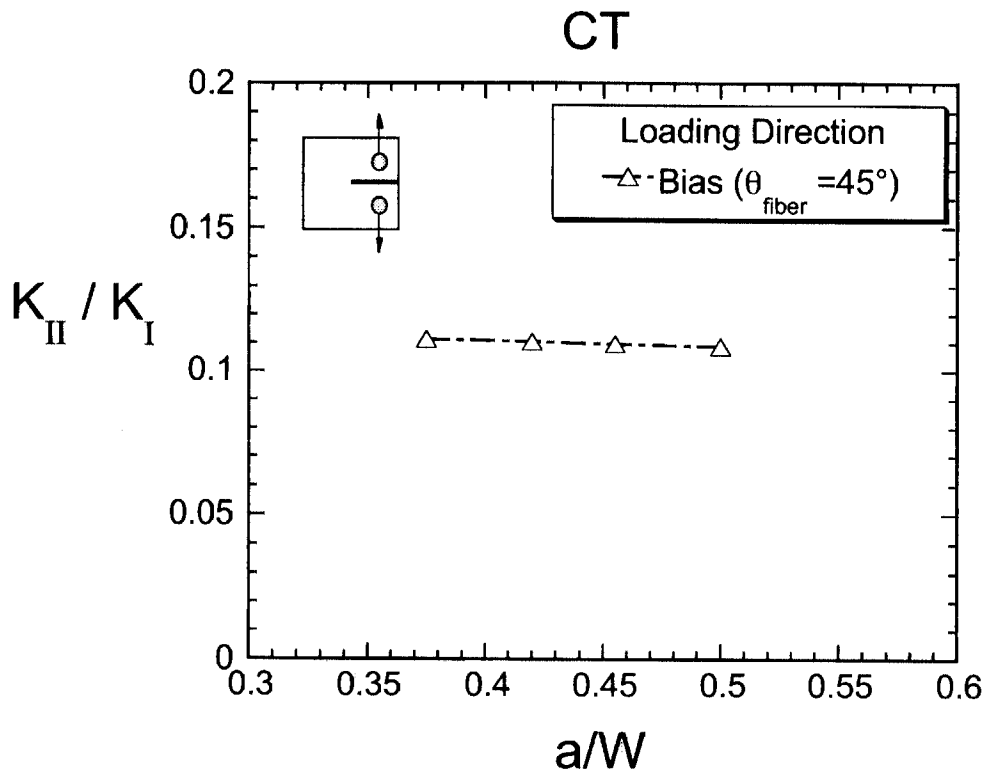

Figure 5. Plot of K_{II}/K_I versus a/W for CT specimens with bias loading.

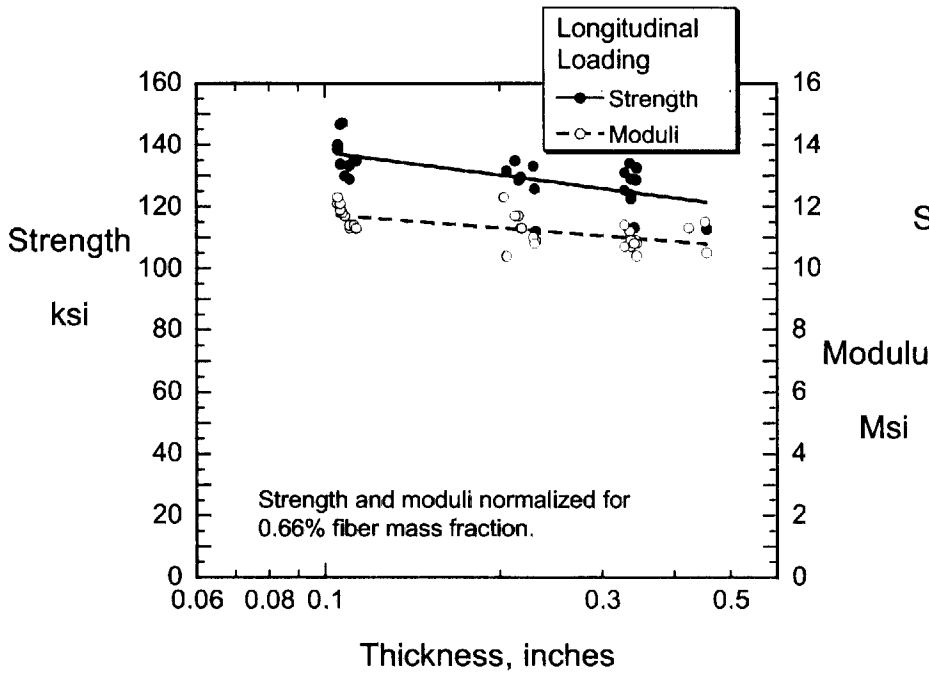

Figure 6. Plot of unnotched tension strengths and moduli versus thickness for longitudinal loading.

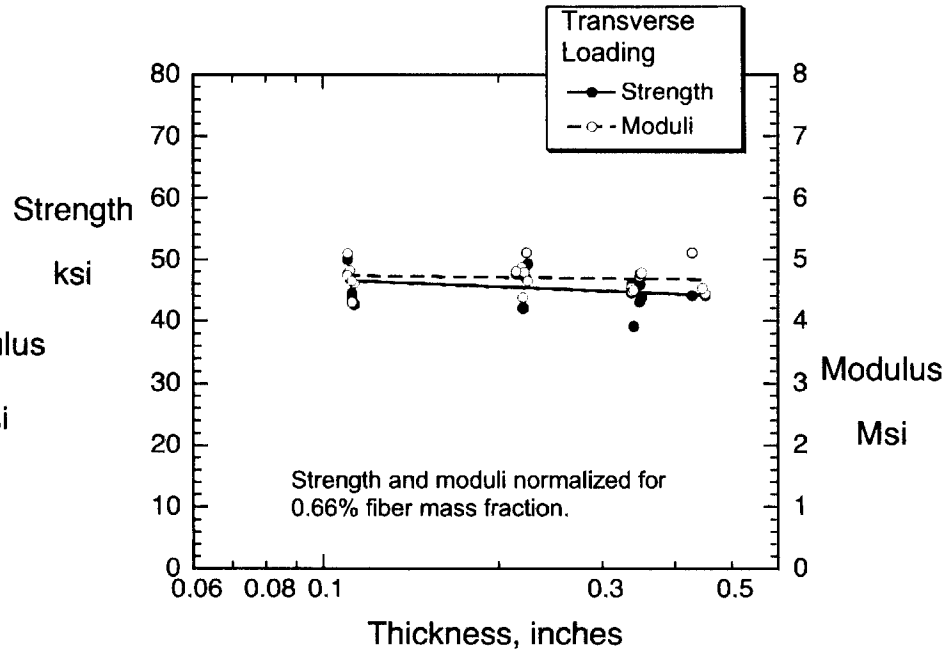

Figure 7. Plot of unnotched tension strengths and moduli versus thickness for transverse loading.

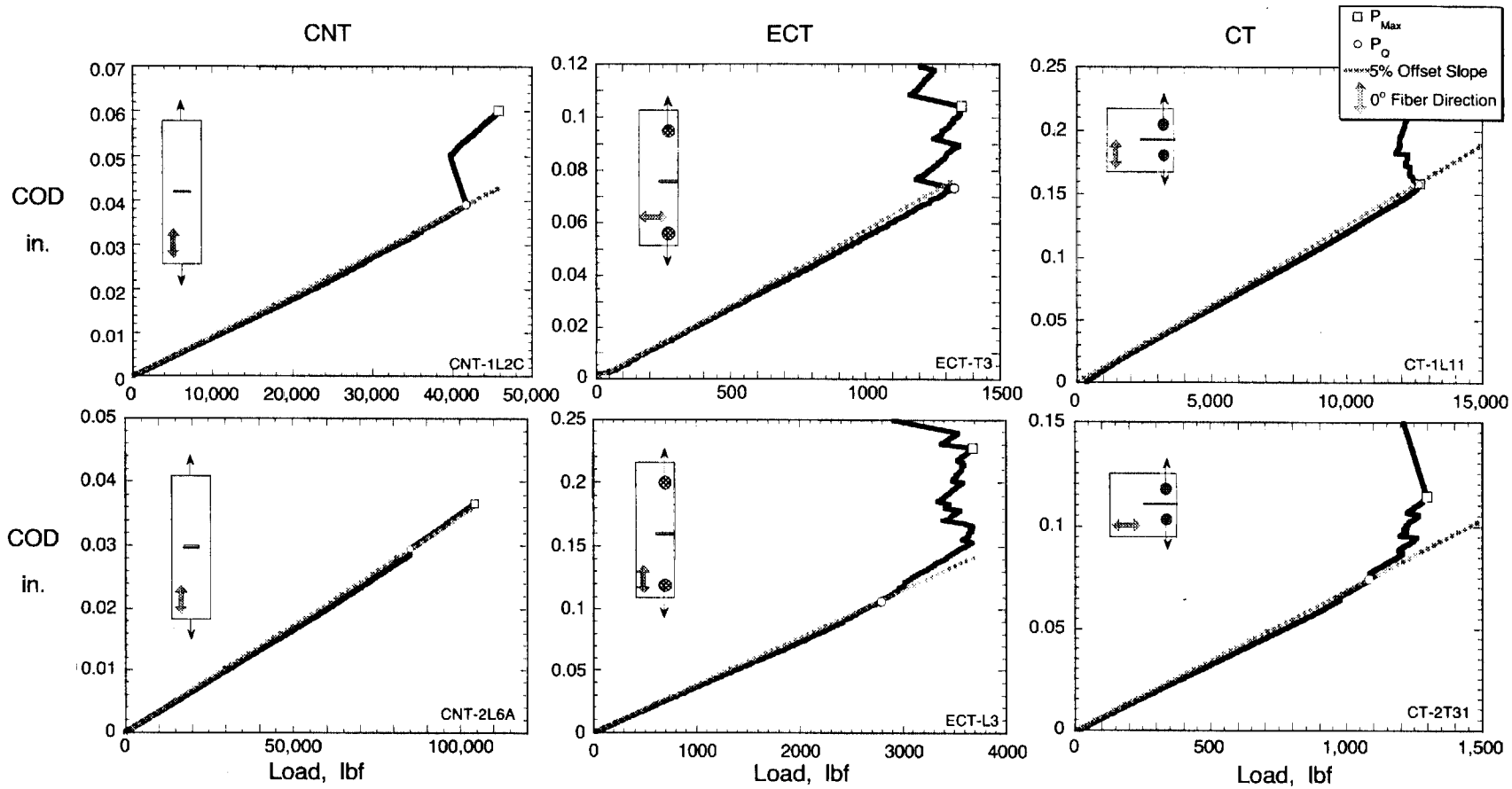

Figure 8. Crack opening displacement versus load for different specimen types.
(Top: Smallest P_{max}/P_Q,. Bottom: Largest P_{max}/P_Q)

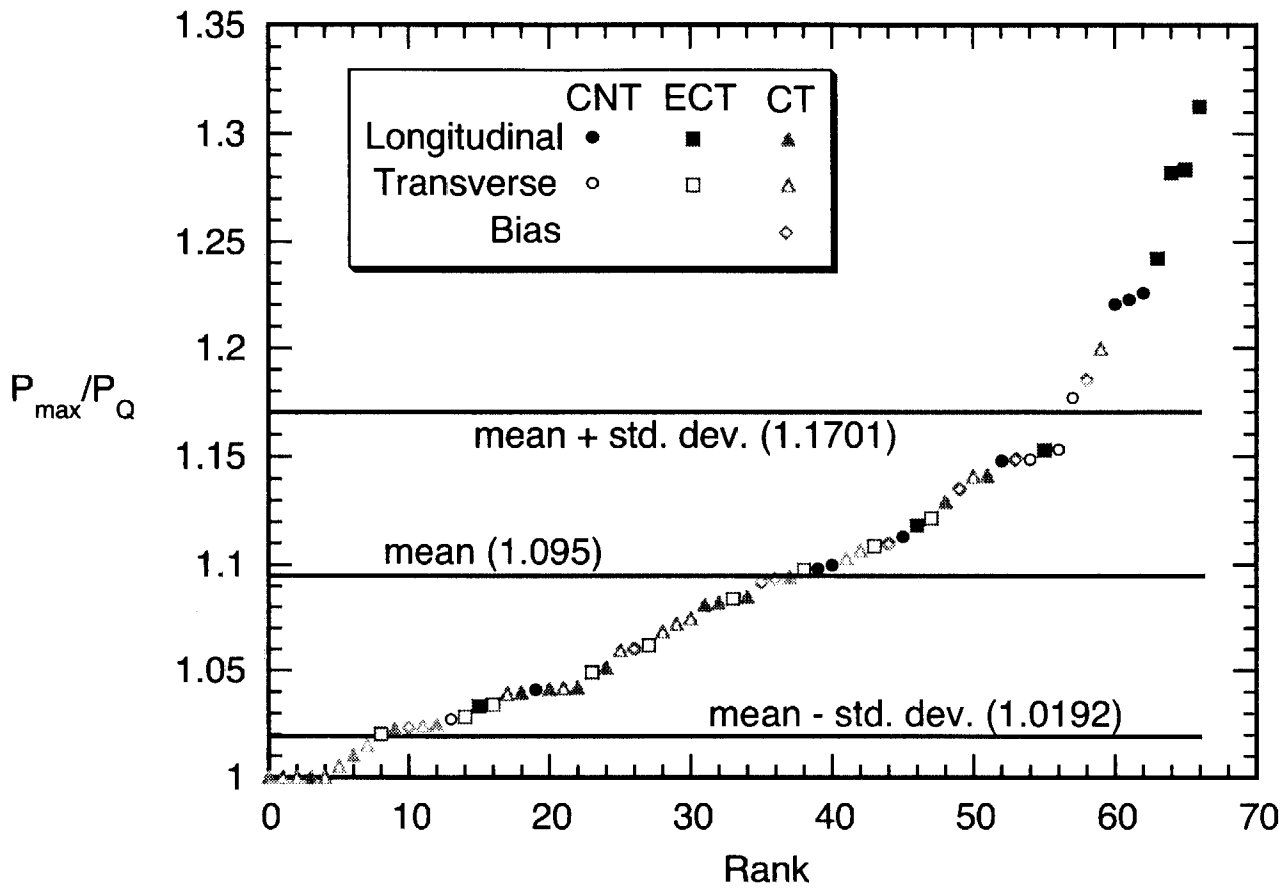

Figure 9. Ranking of values of P_{max}/P_Q.

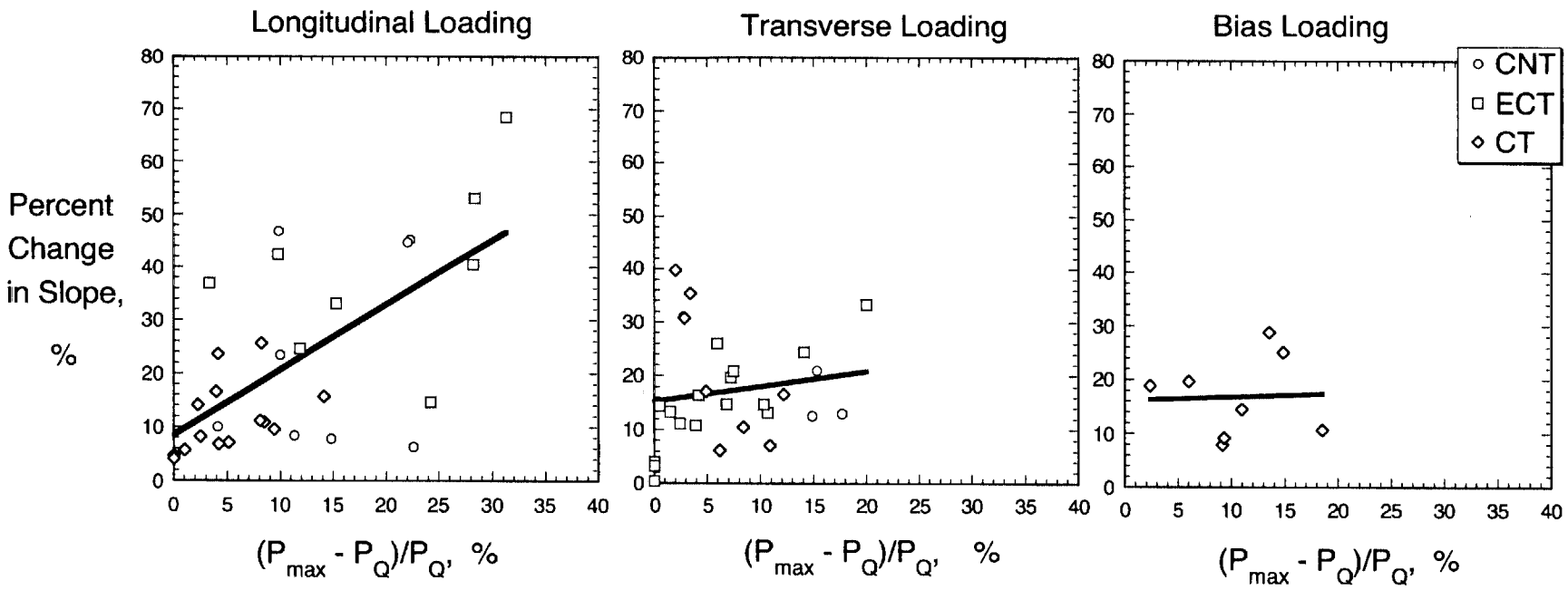

Figure 10. Change in slope of crack opening displacement curve versus % difference between P_{max} and P_Q.

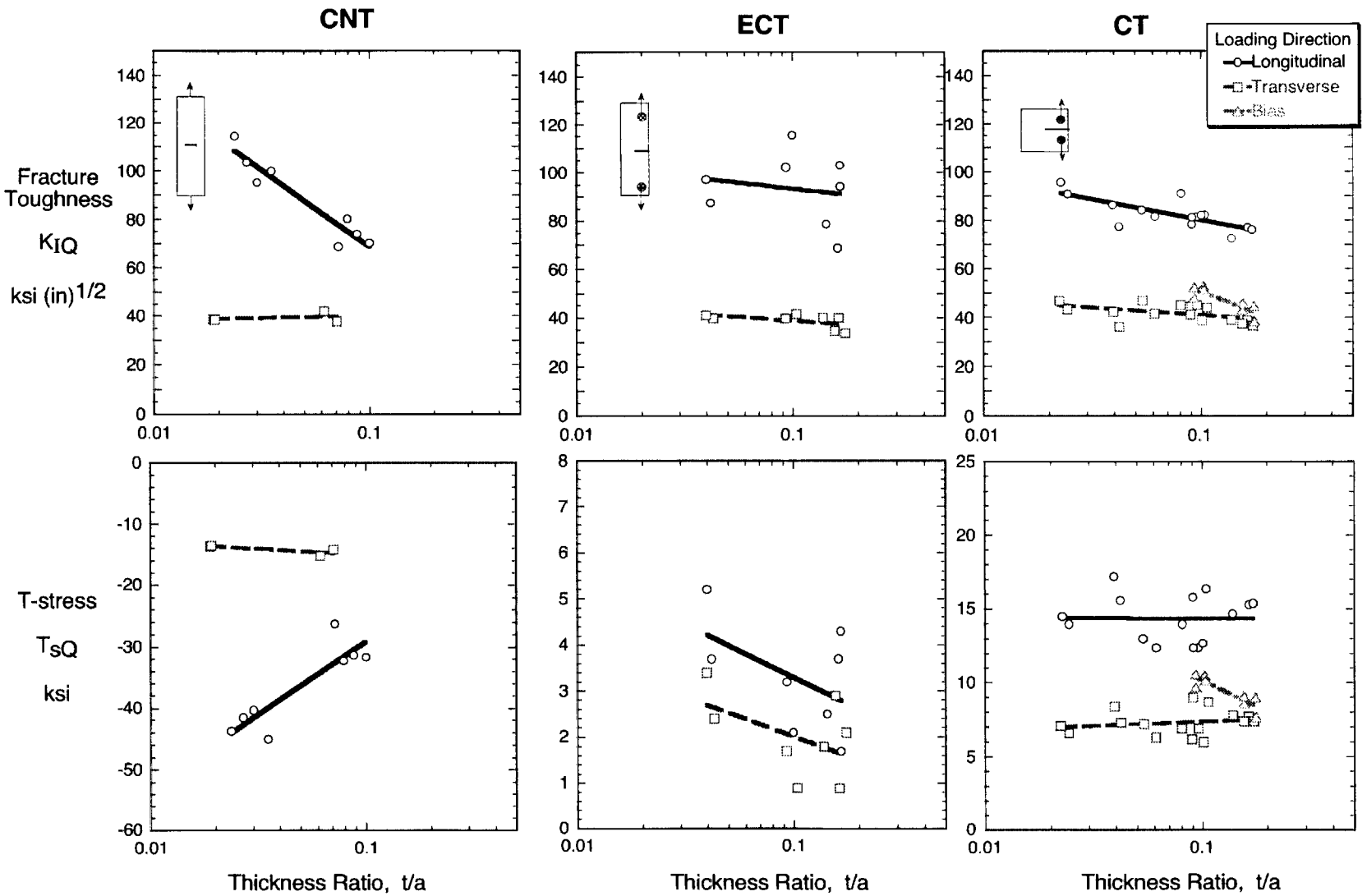

Figure 11. Critical values of K_{IQ} and T_{sQ} from various test specimen types.

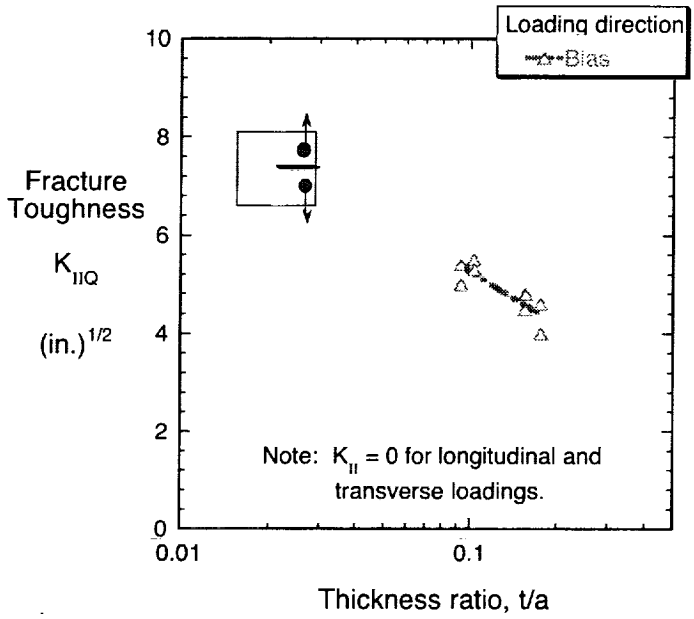

Figure 12. Critical values of K_{II} from bias direction CT tests.

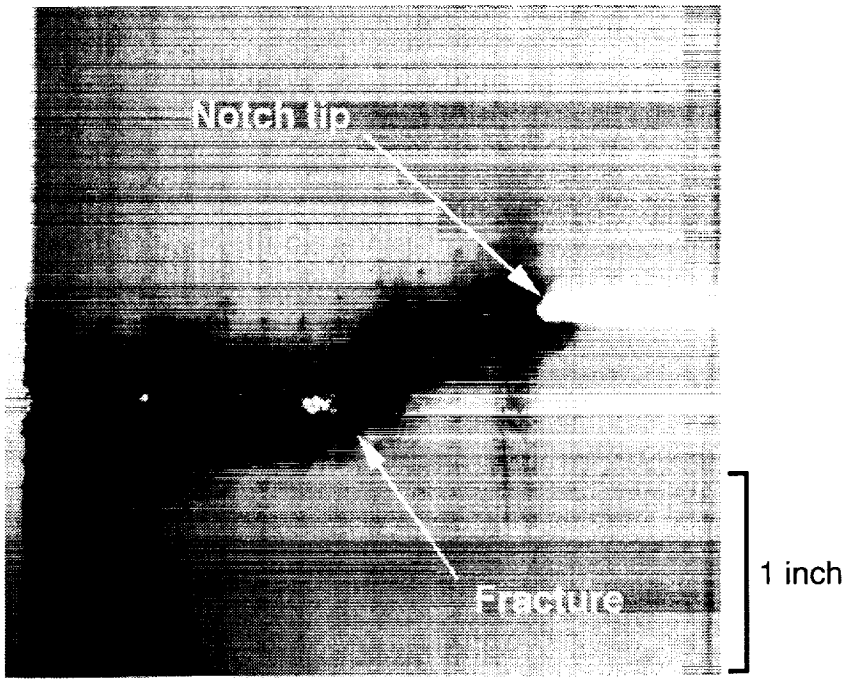

Left notch tip

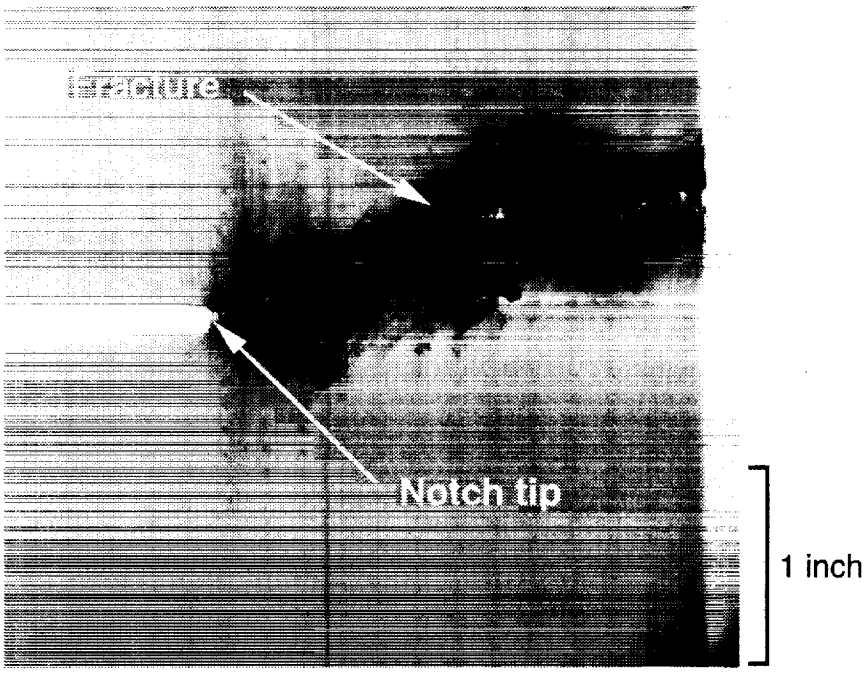

Right notch tip

Figure 13. Radiograph of longitudinally loaded CNT specimen (CNT-3L2C) .

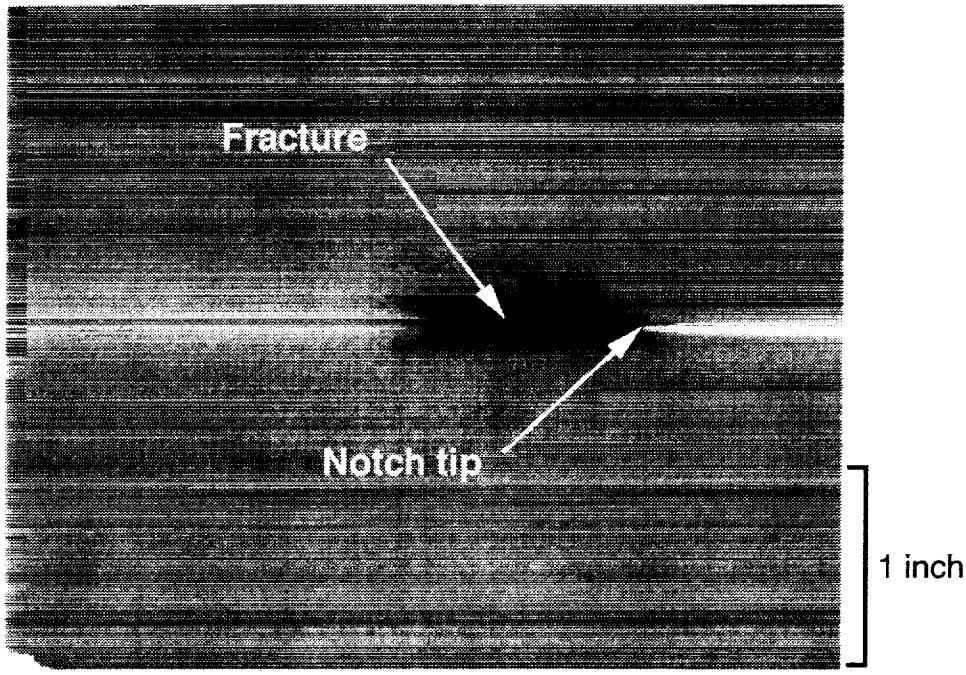

Figure 14. Radiograph of transversely loaded CTspecimen (CT-2T6).

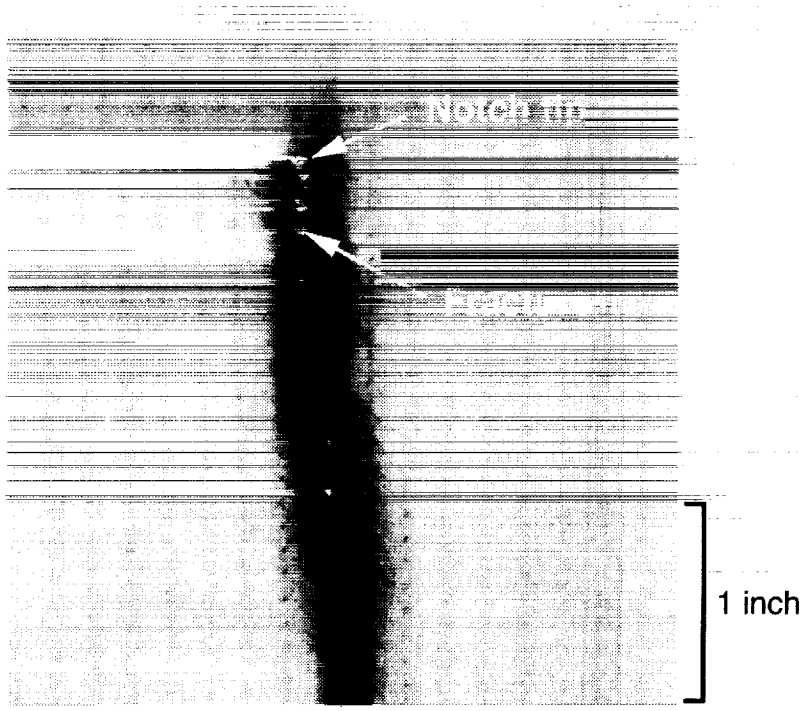

Figure 15. Radiograph of longitudinally loaded CT specimen (CT-2L6).

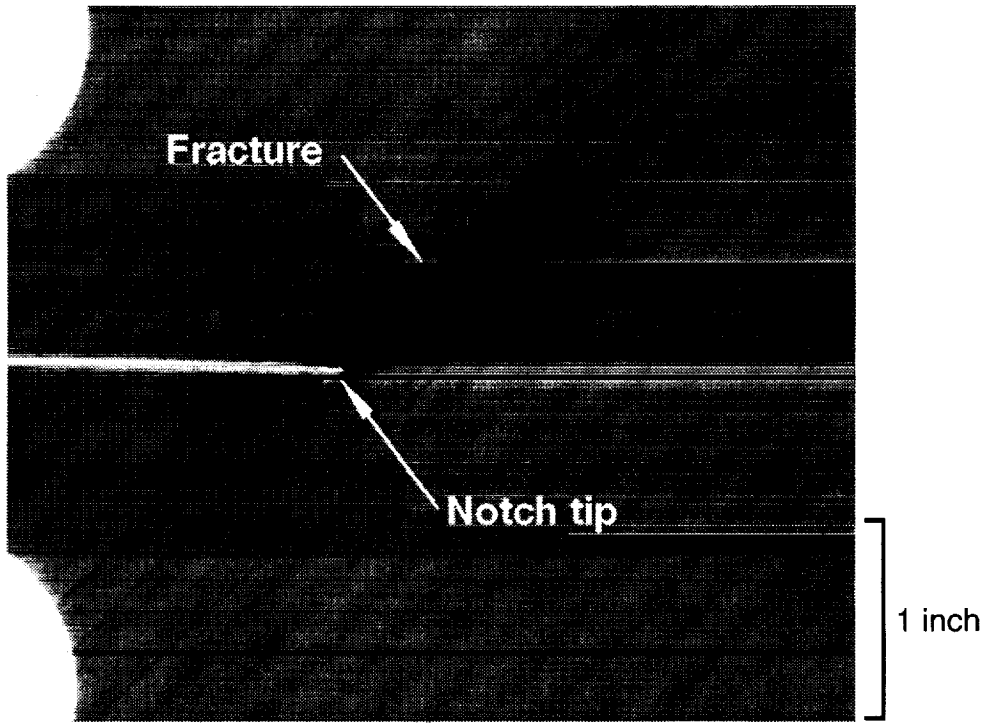

Figure 16. Radiograph of bias loaded (θ_{fiber}=45°) CT specimen (CT-2LT, ($\theta_{fracture}$=45°)).

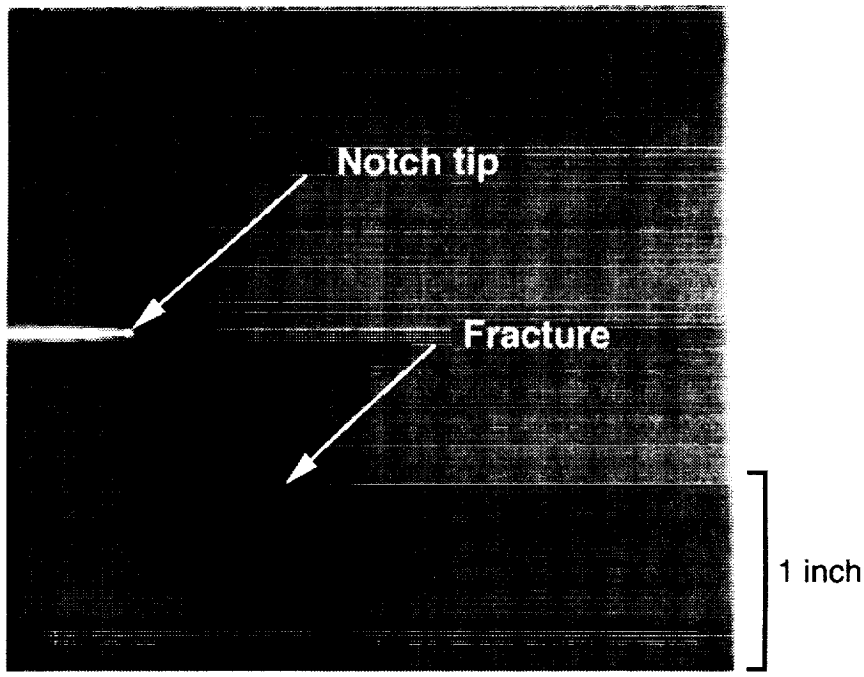

Figure 17. Radiograph of longitudinally loaded ECT specimen (ECT-L7).

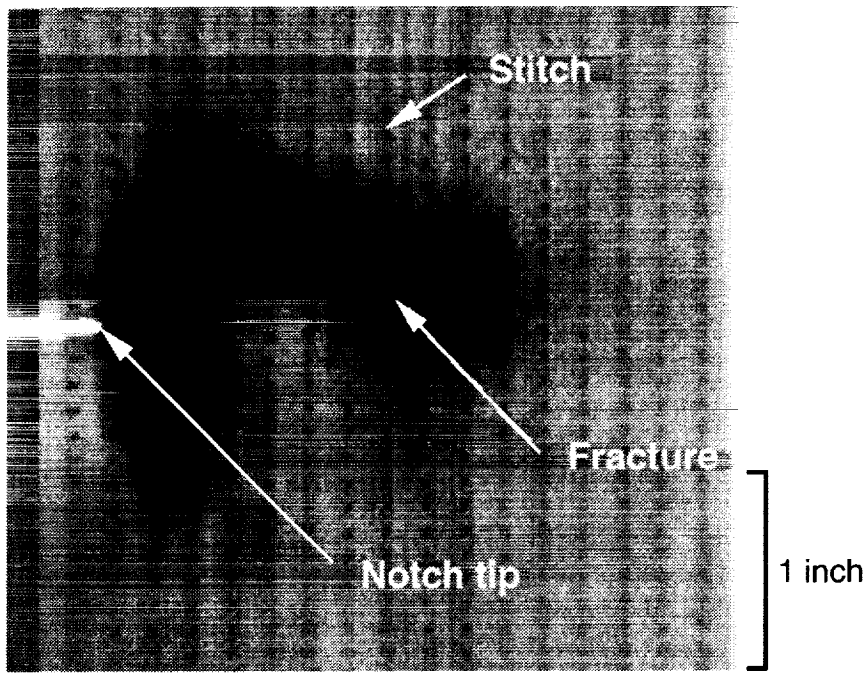

Figure 18. Radiograph of longitudinally loaded ECT specimen (ECT-L2).

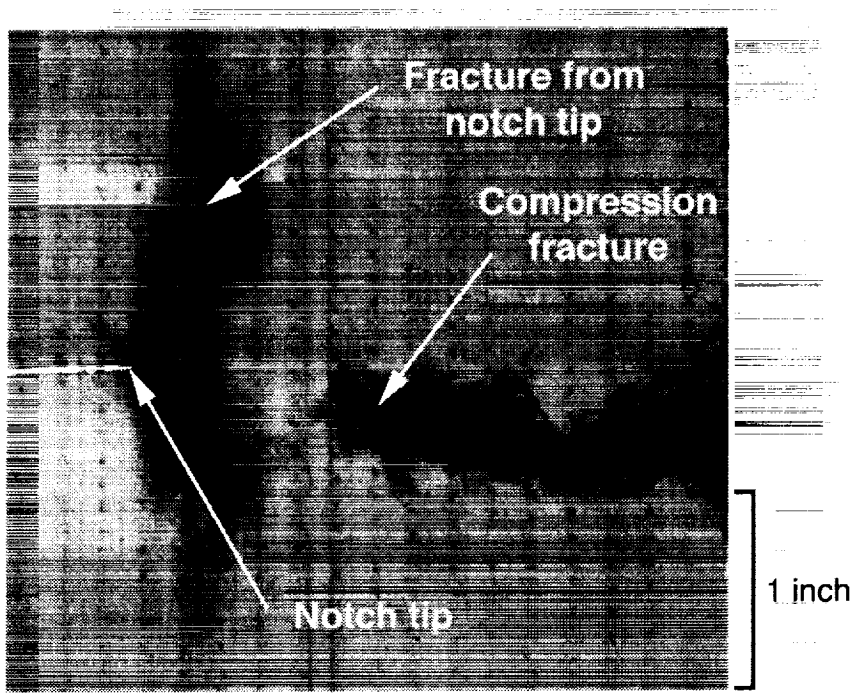

Figure 19. Radiograph of longitudinally loaded ECT specimen (ECT-L3).

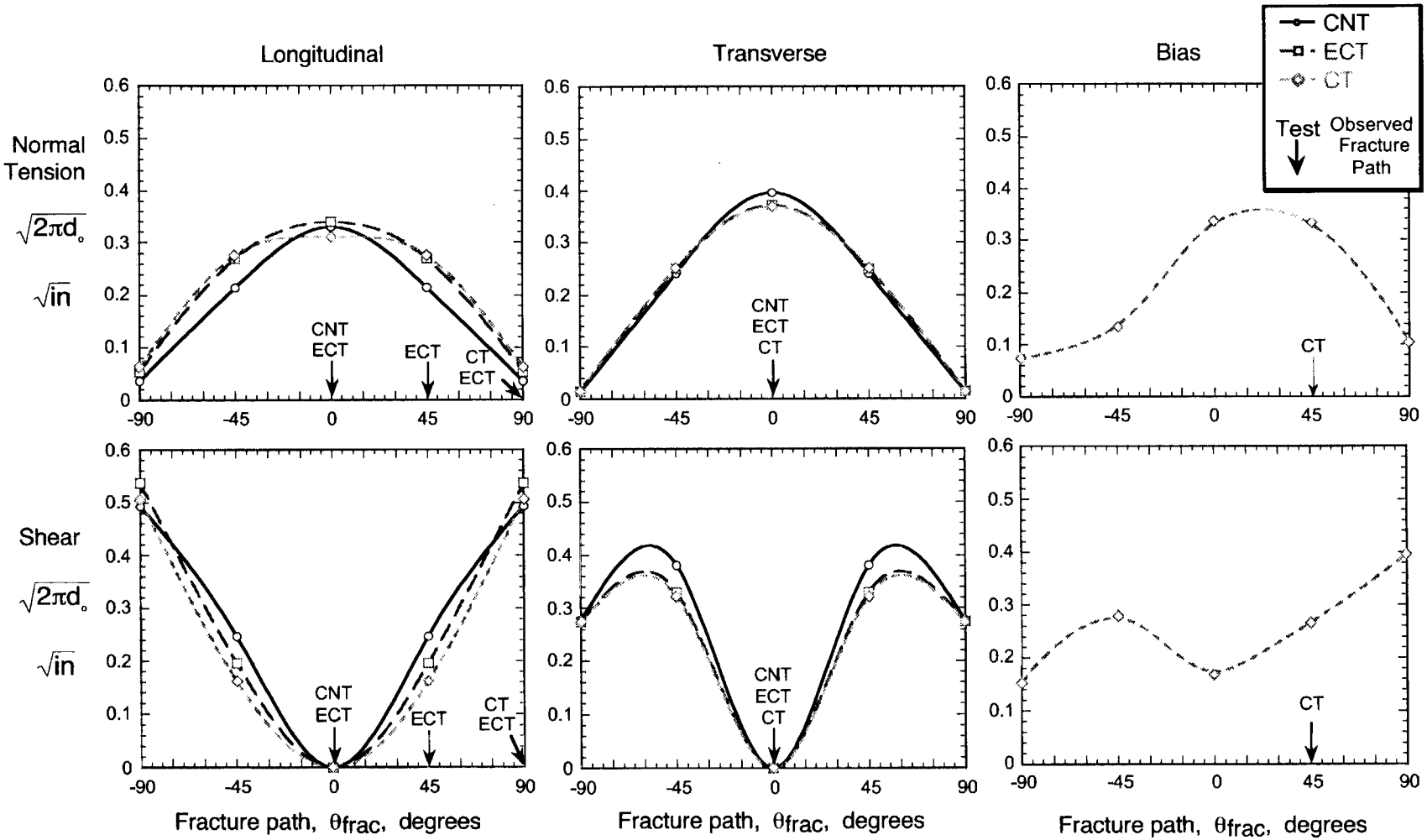

Figure 20. Critical distance parameter, $\sqrt{2\pi d_o}$ due to either normal tension or shear strains, versus angle of fracture path for diffferent loading directions (t/a = 0.1).

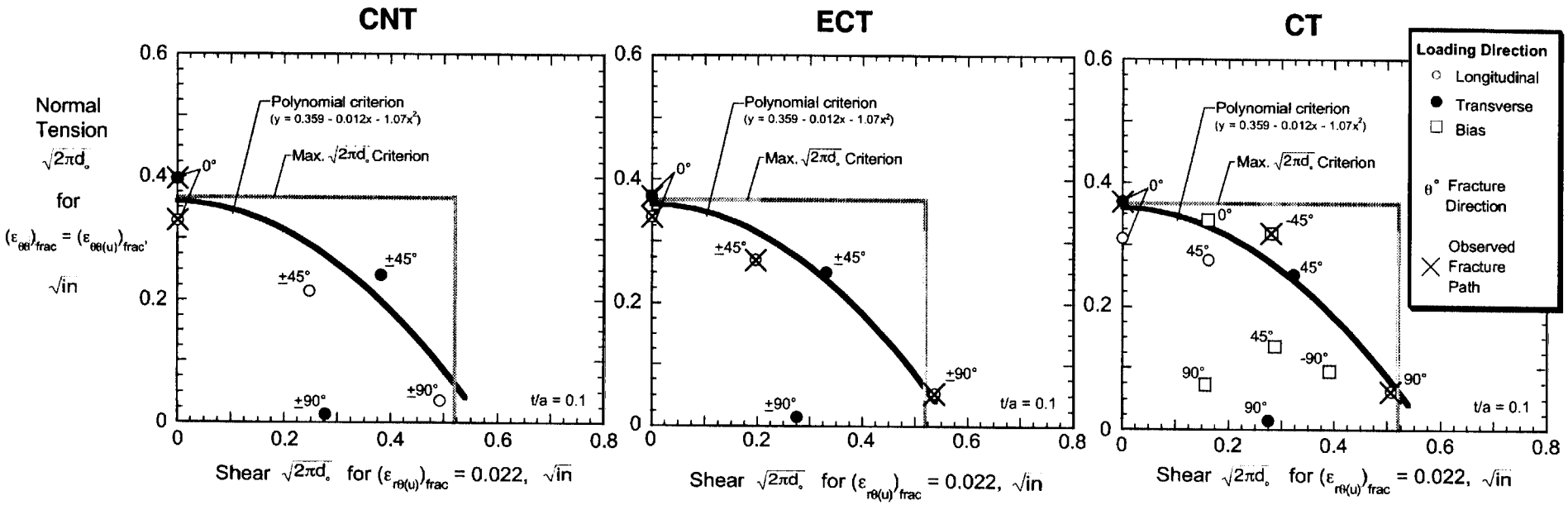

Figure 21. Interaction of $\sqrt{2\pi d_o}$ values for critcal normal tension and shear strains for different specimen types.

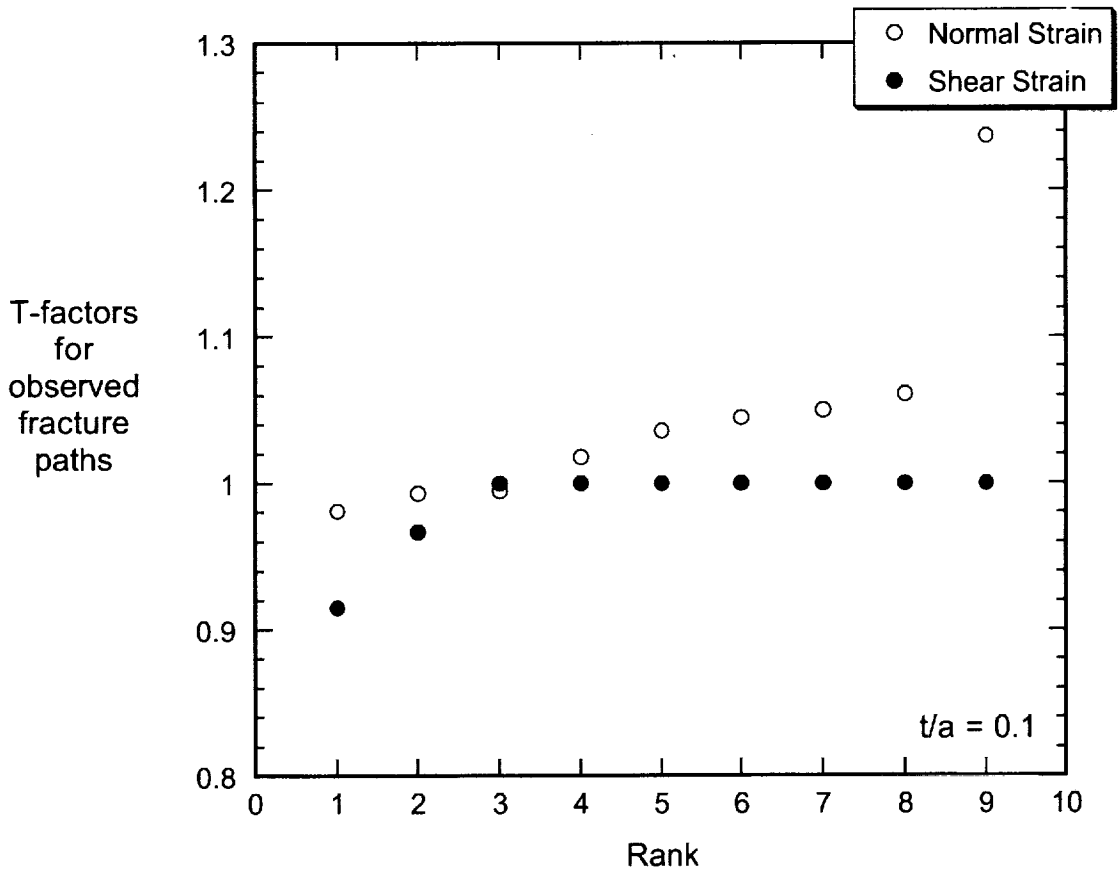

Figure 22. Ranking of T-factors for fracture paths observed in test specimens loaded in the longitudinal direction.

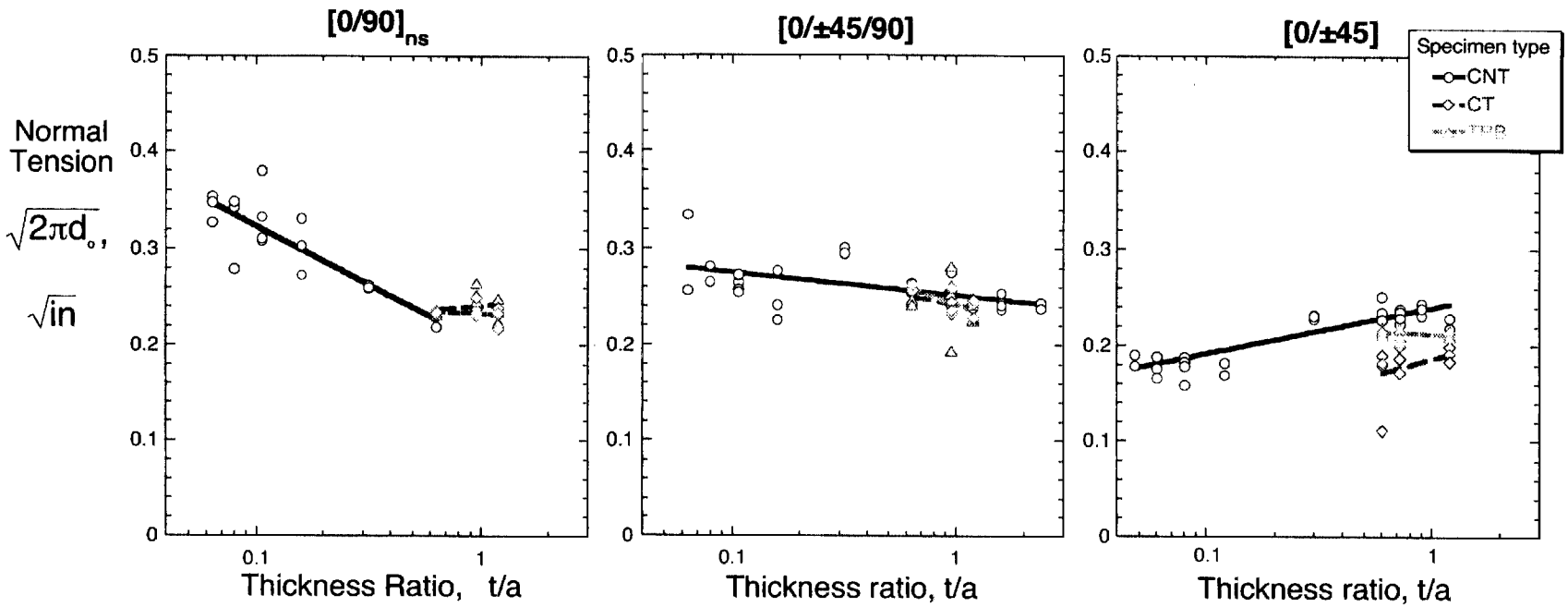

Figure 23. Critical distance parameter versus thickness ratio for T300/5208 laminates from reference 15.

APPENDICES

Appendix A. Tables of Raw Data

Appendix B. Detail Drawings of Tests specimen and apparatus

Table A–1. Fiber volume and mass fractions.

Sample number	Sheet number	Thickness, stacks	Thickness		Density, lb/ft^3	Fiber mass fraction	Fiber volume fraction
			inches	per stack, inches			
2C-1	2C	2	-	-	96.1	0.644	0.560
2C-2	2C	2	-	-	96.1	0.604	0.525
2C-3	2C	2	-	-	95.5	0.583	0.504
2C-4	2C	2	-	-	97.4	0.624	0.550
Average			0.1140	0.0570	96.3	0.614	0.535
Deviation					0.5	0.020	0.020
COV					0.6%	3.3%	3.8%
3-1	3	2	-	-	98.0	0.696	0.618
3-4	3	2	-	-	98.6	0.649	0.579
3-7	3	2	-	-	98.0	0.664	0.589
Average			0.1074	0.05370	98.2	0.670	0.595
Deviation					0.3	0.018	0.015
COV					0.3%	2.6%	2.5%
4-1	4	2	-	-	98.6	0.679	0.606
4-4	4	2	-	-	98.6	0.683	0.609
4-7	4	2	-	-	98.0	0.654	0.580
Average			0.1108	0.05540	98.4	0.672	0.598
Deviation					0.3	0.012	0.012
COV					0%	1.8%	2.0%
5-1	5	4	-	-	98.6	0.663	0.592
5-2	5	4	-	-	98.6	0.663	0.591
5-3	5	4	-	-	97.4	0.634	0.559
5-4	5	4	-	-	98.0	0.646	0.573
Average			0.2184	0.05460	98.2	0.652	0.579
Deviation					0.5	0.012	0.013
COV					0.5%	1.8%	2.2%
6-1	6	4	-	-	98.6	0.681	0.608
6-2	6	4	-	-	97.4	0.669	0.590
6-3	6	4	-	-	99.3	0.683	0.613
6-4	6	4	-	-	98.6	0.680	0.607
Average			0.2136	0.0534	98.5	0.678	0.605
Deviation					0.5	0.005	0.007
COV					0.6%	0.7%	1.2%
F44-1	F44	4	-	-	98.0	0.654	0.580
F44-2	F44	4	-	-	97.4	0.660	0.581
F44-3	F44	4	-	-	97.4	0.634	0.559
F44-4	F44	4	-	-	98.0	0.651	0.578
Average			0.2250	0.0563	97.7	0.650	0.575
Deviation					0.3	0.008	0.008
COV					0.3%	1.2%	1.3%

Table 1. Concluded.

Sample number	Sheet number	Thickness, stacks	Thickness		Density, g/cc	Fiber mass fraction	Fiber volume fraction
			inches	per stack, inches			
6A-1	6A	6	-	-	1.57	0.659	0.585
6A-2	6A	6	-	-	1.57	0.649	0.576
6A-3	6A	6	-	-	1.57	0.652	0.579
6A-4	6A	6	-	-	1.57	0.654	0.581
Average			0.3380	0.0563	1.57	0.654	0.580
Deviation					0.00	0.003	0.003
COV					0.0%	0.5%	0.5%
1 - 1	1	6	-	-	1.51	0.657	0.560
1 - 4	1	6	-	-	1.50	0.651	0.552
1 - 7	1	6	-	-	1.51	0.659	0.562
Average			0.3468	0.0578	1.51	0.656	0.558
Deviation					0.00	0.003	0.004
COV					0.3%	0.5%	0.7%
2 - 1	2	6	-	-	1.58	0.672	0.600
2 - 4	2	6	-	-	1.58	0.666	0.594
2 - 7	2	6	-	-	1.6	0.694	0.627
Average			0.3273	0.05455	1.59	0.677	0.607
Deviation					0.01	0.011	0.013
COV					0.6%	1.6%	2.2%
7 - 1	7	8	-	-	1.57	0.635	0.563
7 - 2	7	8	-	-	1.56	0.631	0.556
7 - 3	7	8	-	-	1.56	0.630	0.555
7 - 4	7	8	-	-	1.56	0.631	0.556
Average			0.4443	0.0555	1.57	0.632	0.558
Deviation					0.00	0.002	0.003
COV					0.2%	0.3%	0.5%
8 - 1	8	8	-	-	1.59	0.687	0.617
8 - 2	8	8	-	-	1.58	0.667	0.595
8 - 3	8	8	-	-	1.58	0.676	0.603
8 - 4	8	8	-	-	1.59	0.681	0.612
Average			0.4313	0.0539	1.59	0.678	0.607
Deviation					0.01	0.006	0.008
COV					0.3%	0.9%	1.3%
All Sheets							
Average				0.0557	1.57	0.656	0.581
Deviation				0.0016	0.02	0.018	0.020
COV				2.9%	1.0%	2.7%	3.5%

Table A–2. Unnotched tension test results for longitudinal loading.

Specimen no.	Thickness, inches		Width, inches	Failing load, lbf	[a]Strength, psi	Failing strain	[ab]Young's modulus, Msi	Poisson's ratio
	Actual	[a]Normal-ized						
Sheet 3								
TEN-1L3	0.106	0.108	0.995	13,951	129,924	0.0110	11.7	
TEN-2L3	0.108	0.110	1.013	14,314	128,875	0.0114	11.3	
TEN-3L3	0.108	0.110	1.013	14,819	133,360	0.0117	11.4	
Average	0.107	0.109	1.007	14,361	130,719	0.0114	11.5	
Deviation	0.001	0.001	0.010	436	2,346	0.0003	0.2	
COV	1.0%	1.0%	1.0%	3.0%	1.8%	2.9%	1.8%	
Sheet 4								
TEN-1L4	0.111	0.113	1.008	15,452	135,062	0.0125	11.3	
TEN-2L4	0.110	0.112	1.006	15,240	134,833	0.0119	11.4	
TEN-3L4	0.111	0.113	1.013	15,387	134,839	0.0122	11.3	
Average	0.111	0.113	1.009	15,360	134,911	0.0122	11.3	
Deviation	0.001	0.001	0.004	109	130	0.0003	0.1	
COV	0.5%	0.5%	0.4%	0.7%	0.1%	2.7%	0.7%	
Sheet 2C								
TEN-1L2C	0.115	0.107	0.998	15,747	147,301	0.0129	11.8	0.359
TEN-3L2C	0.114	0.106	0.999	14,129	133,787	0.0119	11.9	0.356
TEN-4L2C	0.112	0.105	1.003	14,694	140,034	0.0115	12.1	0.423
TEN-5L2C	0.114	0.106	1.006	15,671	146,737	0.0119	12.1	0.409
TEN-6L2C	0.113	0.105	1.008	14,694	138,553	0.0113	12.3	0.416
Average	0.114	0.106	1.003	14,987	141,282	0.0119	12.0	0.392
Deviation	0.001	0.001	0.004	699	5,726	0.0006	0.2	0.032
COV	0.9%	0.9%	0.4%	4.7%	4.1%	5.2%	1.6%	8.3%
Sheets 3, 4, and 2C								
Average	0.111	0.109	1.006	14,918	136,664	0.0119	11.7	0.392
Deviation	0.003	0.003	0.006	676	6,034	0.0006	0.4	0.032
COV	2.6%	2.9%	0.6%	4.5%	4.4%	4.6%	3.2%	8.3%
Sheet 5								
TEN-1L5	0.218	0.215	1.004	27,676	128,481	0.0111	11.7	0.384
TEN-2L5[e]	0.215	0.212	1.007	28,795	134,861	0.0117	11.7	0.370
TEN-3L5[f]	0.206	0.203	1.003	19,180	94,091	0.0078	12.3	0.370
Average	0.213	0.210	1.005	28,236	131,671	0.0114	11.9	0.375
Deviation	0.006	0.006	0.002	791	4,511	0.0004	0.4	0.010
COV	2.8%	2.8%	0.2%	2.8%	3.4%	3.4%	3.1%	2.8%
Sheet 6								
TEN-1L6	0.211	0.217	1.010	28,390	129,450	0.0124	11.3	0.372
TEN-2L6[ef]	0.213	0.218	1.005	26,090	118,811	0.0107	11.3	0.413
TEN-3L6	0.200	0.205	1.005	27,140	131,475	0.0107	10.4	0.324
Average	0.208	0.214	1.006	27,765	130,463	0.0116	11.0	0.348
Deviation	0.007	0.007	0.003	884	1,432	0.0012	0.6	0.034
COV	3.3%	3.3%	0.3%	3.2%	1.1%	10.2%	5.1%	9.6%

Table A-2. Continued.

Specimen no.	Thickness, inches		Width, inches	Failing load, lbf	[a]Strength, psi	Failing strain	[ab]Young's modulus, Msi	Poisson's ratio
	Actual	[a]Normal-ized						
Sheet F44								
TEN-1LF44	0.233	0.230	1.007	25,894	112,009	0.0103	10.9	0.369
TEN-2LF44	0.232	0.228	1.009	30,666	133,097	0.0118	11.0	0.393
TEN-3LF44	0.233	0.229	1.012	29,138	125,755	0.0115	10.8	0.337
Average	0.232	0.229	1.009	28,566	123,620	0.0112	10.9	0.366
Deviation	0.001	0.001	0.002	2,437	10,705	0.0008	0.1	0.028
COV	0.3%	0.3%	0.2%	8.5%	8.7%	6.8%	0.8%	7.6%
Sheets 5, 6, and F44								
Average	0.218	0.218	1.007	28,243	127,875	0.0114	11.3	0.370
Deviation	0.012	0.010	0.003	1,530	7,617	0.0007	0.6	0.025
COV	5.6%	4.5%	0.3%	5.4%	6.0%	6.1%	5.2%	6.7%
Sheet 1								
TEN-1L1[c]	0.347	0.344	1.001	44,315	128,586	0.0130	10.9	
TEN-2L1[g]	0.347	0.345	1.006	43,424	125,254	0.0114	10.8	
TEN-3L1	0.347	0.345	0.995	45,487	132,518	0.0144	10.4	
Average	0.347	0.345	1.000	44,901	130,552	0.0137	10.7	
Deviation	0.000	0.000	0.005	829	2,780	0.0010	0.2	
COV	0.1%	0.1%	0.5%	1.8%	2.1%	7.2%	2.3%	
Sheet 2								
TEN-1L2	0.328	0.337	1.003	43,567	129,027	0.0119	10.9	
TEN-2L2[g]	0.327	0.336	1.004	42,896	127,162	0.0115	11.0	
TEN-3L2[d]	0.326	0.335	1.004	45,078	134,106	0.0118	11.2	
Average	0.328	0.336	1.004	44,323	131,567	0.0119	11.0	
Deviation	0.000	0.000	0.001	1,068	3,592	0.0001	0.2	
COV	0.1%	0.1%	0.1%	2.4%	2.7%	0.5%	1.6%	
Sheet 6A								
TEN-1L6A	0.341	0.337	1.003	41,942	123,866	0.0113	10.7	0.356
TEN-2L6A	0.340	0.337	1.012	41,815	122,461	0.0112	10.9	0.362
TEN-3L6A	0.344	0.341	1.007	38,821	113,197	0.0105	10.8	0.376
TEN-4L6A	0.331	0.328	1.006	43,186	130,925	0.0127	10.7	0.391
TEN-5L6A	0.331	0.328	1.008	41,376	125,275	0.0107	11.4	0.449
Average	0.337	0.334	1.007	41,428	123,145	0.0113	10.9	0.387
Deviation	0.006	0.006	0.003	1,605	6,423	0.0009	0.3	0.037
COV	1.8%	1.8%	0.3%	3.9%	5.2%	7.6%	2.6%	9.6%
Sheets 1, 2, and 6A								
Average	0.337	0.337	1.005	42,843	126,662	0.0119	10.9	0.387
Deviation	0.008	0.006	0.004	2,091	6,382	0.0011	0.3	0.037
COV	2.5%	1.8%	0.4%	4.9%	5.0%	9.5%	2.4%	9.6%

Table A-2. Concluded.

Specimen no.	Thickness, inches		Width, inches	Failing load, lbf	[a]Strength, psi	Failing strain	[ab]Young's modulus, Msi	Poisson's ratio
	Actual	[a]Normal-ized						
Sheet 7								
TEN-1L7[f]	0.443	0.424	1.004	47,700	112,044	0.0103	11.3	0.334
Sheet 8								
TEN-1L8[f]	0.440	0.452	1.008	40,272	88,457	0.0076	11.5	0.371
TEN-2L8	0.443	0.455	1.010	51,700	112,624	0.0107	10.5	0.368
Average	0.441	0.453	1.009	51,700	112,624	0.0107	10.8	0.368
Deviation	0.002	0.002	0.001				0.7	0.002
COV	0.5%	0.5%	0.1%				6.5%	0.6%
Sheets 7 and 8								
Average	0.442	0.443	1.007	51,700	112,624	0.0107	11.1	0.358
Deviation	0.002	0.017	0.003				0.5	0.020
COV	0.4%	3.8%	0.3%				4.8%	5.7%
All sheets								
Average			1.006		130,393	0.0117	11.3	0.377
Deviation			0.005		8,511	0.0009	0.5	0.030
COV			0.5%		6.5%	7.5%	4.7%	8.1%

[a]Normalized to 66% fiber mass fraction.

[b]Modulus was calculated between 1000 and 3000 μstrain.

[c]Strain at 118.26 ksi; gages failed subsequently. Not included in average and deviation.

[d]Specimen slipped in the grips the first three times it was loaded.

[e]Transverse strain measured on only one side.

[f]Failed in grip.

[g]Specimen failed at or very near a grip.

Table A–3. Unnotched tension test results for transverse loading.

Specimen no.	Thickness, inches		Width, inches	Failing load, lbf	[a]Strength, psi	Failing strain	[ab]Young's modulus, Msi	Poisson's ratio
	Actual	[a]Normal-ized						
Sheet 3								
TEN-1T3	0.109	0.111	1.010	5,236	46,858	0.0115	4.82	
TEN-2T3	0.109	0.110	1.006	5,537	49,949	0.0111	5.10	
TEN-3T3	0.108	0.110	1.006	5,274	47,602	0.0115	4.74	
Average	0.109	0.110	1.007	5,349	48,136	0.0114	4.89	
Deviation	0.000	0.000	0.002	164	1613	0.0002	0.19	
COV	0.3%	0.3%	0.2%	3.1%	3.4%	2.1%	3.9%	
Sheet 4								
TEN-1T4	0.110	0.112	1.019	5,051	44,438	0.0117	4.30	
TEN-2T4	0.111	0.113	1.014	4,894	42,694	0.0106	4.61	
TEN-3T4	0.110	0.112	1.006	4,919	43,654	0.0110	4.65	
Average	0.110	0.112	1.013	4,955	43,596	0.0111	4.52	
Deviation	0.001	0.001	0.007	85	873	0.0006	0.19	
COV	0.7%	0.7%	0.6%	1.7%	2.0%	5.0%	4.2%	
Sheet 3 & 4								
Average	0.109	0.111	1.010	5,152	45,866	0.0112	4.70	
Deviation	0.001	0.001	0.005	245	2744	0.0004	0.26	
COV	0.9%	1.0%	0.5%	4.8%	6.0%	3.6%	5.6%	
Sheet 5								
TEN-1T5	0.222	0.219	1.006	10,456	47,496	0.0106	4.87	0.168
TEN-2T5	0.224	0.221	1.005	10,702	48,135	0.0123	4.79	0.165
TEN-3T5	0.216	0.214	1.008	10,278	47,716	0.0110	4.80	0.175
Average	0.221	0.218	1.006	10,479	47,783	0.0113	4.82	0.170
Deviation	0.004	0.004	0.001	213	325	0.0009	0.04	0.005
COV	1.7%	1.7%	0.1%	2.0%	0.7%	7.9%	0.9%	3.0%
Sheet 6								
TEN-1T6[c]	0.217	0.223	1.005	10,505	46,900	0.0101	5.11	0.171
TEN-2T6	0.218	0.224	1.006	11,094	49,223	0.0130	4.65	0.169
TEN-3T6	0.214	0.220	1.005	9,291	42,086	0.0106	4.38	0.168
Average	0.216	0.222	1.005	10,297	46,070	0.0112	4.72	0.169
Deviation	0.002	0.002	0.000	920	3640	0.0015	0.37	0.002
COV	1.0%	1.0%	0.0%	8.9%	7.9%	13.7%	7.8%	0.9%
Sheets 5 and 6								
Average	0.218	0.220	1.006	10,388	46,926	0.0113	4.70	0.169
Deviation	0.004	0.004	0	605	2495	0.0011	0.24	0.003
COV	1.7%	1.7%	0.1%	5.8%	5.3%	10.0%	5.1%	2.0%

Table A-3. Concluded.

Specimen no.	Thickness, inches		Width, inches	Failing load, lbf	[a]Strength, psi	Failing strain	[ab]Young's modulus, Msi	Poisson's ratio
	Actual	[a]Normal-ized						
Sheet 1								
TEN-1T1	0.339	0.337	1.004	15,068	44,519	0.0108	4.54	
TEN-2T1	0.340	0.338	1.005	15,585	45,906	0.0129	4.48	
TEN-3T1	0.343	0.340	1.002	13,356	39,169	0.0093	4.50	
Average	0.341	0.338	1.003	14,670	43,198	0.0110	4.51	
Deviation	0.002	0.002	0.002	1,167	3,558	0.0018	0.03	
COV	0.5%	0.5%	0.2%	8.0%	8.2%	16.4%	0.6%	
Sheet 2								
TEN-1T2	0.318	0.348	1.001	14,990	43,046	0.0121	4.73	
TEN-2T2	0.325	0.349	1.004	16,086	45,942	0.0114	4.77	
TEN-3T2	0.325	0.351	0.990	15,246	43,839	0.0113	4.78	
Average	0.323	0.349	0.998	15,441	44,276	0.0116	4.76	
Deviation	0.004	0.002	0.008	573	1497	0.000	0.02	
COV	1.2%	0.5%	0.8%	3.7%	3.4%	4.1%	0.5%	
Sheet 1 & 2								
Average	0.332	0.344	1.001	15,055	43,737	0.0113	4.63	
Deviation	0.010	0.006	0.006	924	2511	0.0012	0.14	
COV	3.1%	1.8%	0.6%	6.1%	5.7%	10.8%	3.1%	
Sheet 7								
TEN-1T7	0.447	0.428	1.004	18,947	44,114	0.0087	5.11	0.1812
Sheet 8								
TEN-1T8	0.439	0.451	1.004	19,997	44,136	0.0127	4.44	0.164
TEN-2T8[d]	0.434	0.446	1.005	17,204	38,367	0.0092	4.53	0.156
Average	0.437	0.449	1.005	19,997	44,364	0.0127	4.48	0.164
Deviation	0.004	0.004	0.001				0.06	
COV	0.8%	0.8%	0.1%				1.4%	
Sheets 7 and 8								
Average	0.440	0.442	1.005	19,472	44,125	0.0107	4.69	0.167
Deviation	0.006	0.012	0.001	742	15	0.0028	0.37	0.013
COV	1.4%	2.8%	0.1%	3.8%	0.0%	26.1%	7.8%	7.6%
All Sheets								
Average			1.005		45,371	0.0112	4.70	0.1687
Deviation			0.005		2,670	0.0011	0.23	0.0070
COV			0.5%		5.9%	9.8%	4.9%	4.1%

[a]Normalized to 66% fiber mass fraction.

[b]Modulus was calculated between 1000 and 3000 μstrain.

[c]Transverse strain measured on only one side.

[d]Specimen failed at or very near a grip.

Table A–4. CNT test results for longitudinal loading.

Specimen no.	Width, W, inches	Crack length, 2a, inches	Thick-ness, t', inches	Fiber mass fraction	[a]Adjusted thick-ness, t, inches	Thick-ness ratio, t/a	2a/W	P_Q, kips	P_{max}, kips	Fracture path θ_f, degrees	COD_Q, inches	COD_{max}, inches	Slope, COD t/P, psi-1		
													Initial	Final	Change
CNT-1L2C	9.50	3.33	0.117	0.614	0.109	0.0351	0.351	41.8	45.9	0	0.0392	0.0601	9.71E-08	1.43E-07	46.8%
CNT-2L2C	9.50	3.80	0.114	0.614	0.106	0.0301	0.400	35.5	43.4	0	0.0361	0.0624	1.05E-07	1.53E-07	45.2%
CNT-3L2C	9.50	4.27	0.115	0.614	0.107	0.0269	0.449	35.4	39.4	0	0.0438	0.0501	1.25E-07	1.36E-07	8.4%
CNT-4L2C	9.50	4.75	0.113	0.614	0.105	0.0237	0.500	35.1	38.6	0	0.0496	0.0641	1.41E-07	1.74E-07	23.4%
Average			0.114	0.614	0.106										
Std. dev.			0.002	0.000	0.001										
COV			1.4%	0.0%	1.4%										
CNT-1L6A	9.50	3.33	0.332	0.654	0.328	0.0995	0.351	88.5	108.0	0	0.0265	0.0456	9.58E-08	1.39E-07	44.7%
CNT-2L6A	9.50	3.80	0.332	0.654	0.329	0.0873	0.400	85.1	104.3	0	0.0296	0.0367	1.09E-07	1.16E-07	6.3%
CNT-3L6A	9.50	4.27	0.336	0.654	0.332	0.0786	0.449	85.5	89.0	0	0.0360	0.0408	1.39E-07	1.52E-07	10.0%
CNT-4L6A	9.50	4.75	0.340	0.654	0.337	0.0716	0.500	67.6	77.6	0	0.0319	0.0379	1.53E-07	1.65E-07	7.8%
Average			0.338	0.654	0.335										
Std. dev.			0.003	0.000	0.003										
COV			0.9%	0.0%	0.9%										
Average				0.634											
Std. dev.				0.021											
COV				3.4%											

[a]Values of thickness normalized to 66% fiber mass fraction

Table A-4. Continued.

$K_I t W / (\pi a)^{1/2}$	K_{II} / K_I	$T (\pi a)^{1/2} / K_I$	For P_Q			For P_{max}		
			K_I, ksi(in.)$^{1/2}$	K_{II}, ksi(in.)$^{1/2}$	T, ksi	K_I, ksi(in.)$^{1/2}$	K_{II}, ksi(in.)$^{1/2}$	T, ksi
1.07	0	-0.68	99.0	0	-29.6	108.8	0	-32.5
1.10	0	-0.69	94.4	0	-26.8	115.5	0	-32.7
1.13	0	-0.70	102.4	0	-27.7	113.9	0	-30.9
1.17	0	-0.71	113.2	0	-29.5	124.3	0	-32.3
			107.8	0	-28.6	119.1	0	-31.6
			8.0		1.4	6.4		0.9
			7.4%		-4.8%	5.4%		-2.7%
1.07	0	-0.68	69.6	0	-20.8	84.9	0	-25.4
1.10	0	-0.69	73.3	0	-20.8	89.8	0	-25.5
1.13	0	-0.70	79.5	0	-21.5	82.8	0	-22.4
1.17	0	-0.71	67.8	0	-17.6	77.8	0	-20.2
			73.7	0	-19.6	80.3	0	-21.3
			5.2		1.7	5.0		2.5
			7.0%		-8.8%	6.2%		-11.9%
			90.7	0	-24.1	99.7	0	-26.5
			17.1		4.6	17.8		5.0
			18.8%		-19.2%	17.9%		-18.8%

Table A-4. Continued.

For θ_{frac} = 0°												
$(\varepsilon_{\theta\theta(I)})_{frac.}$, Msi^{-1}	$(\varepsilon_{\theta\theta(II)})_{frac.}$, Msi^{-1}	$(\varepsilon_{r\theta(I)})_{frac.}$, Msi^{-1}	$(\varepsilon_{r\theta(II)})_{frac.}$, Msi^{-1}	$(\varepsilon_{\theta\theta(T)})_{frac.}$, Msi^{-1}	$(\varepsilon_{r\theta(T)})_{frac.}$, Msi^{-1}	For P_Q				For P_{max}			
						For $\varepsilon_{\theta\theta}$ = 0.0171		For $\varepsilon_{r\theta}$ = 0.0220		For $\varepsilon_{\theta\theta}$ = 0.0171		For $\varepsilon_{r\theta}$ = 0.0220	
						T factor	$(2\pi d_o)^{1/2}$, $(in.)^{1/2}$	T factor	$(2\pi d_o)^{1/2}$, $(in.)^{1/2}$	T factor	$(2\pi d_o)^{1/2}$, $(in.)^{1/2}$	T factor	$(2\pi d_o)^{1/2}$, $(in.)^{1/2}$
0.0624	0	0	0.403	-0.0341	0	1.063	0.384	1	0	1.069	0.424	1	0
0.0624	0	0	0.403	-0.0341	0	1.056	0.364	1	0	1.070	0.451	1	0
0.0624	0	0	0.403	-0.0341	0	1.058	0.395	1	0	1.065	0.443	1	0
0.0624	0	0	0.403	-0.0341	0	1.062	0.439	1	0	1.069	0.485	1	0
						1.060	0.395	1	0	1.068	0.451	1	0
						0.003	0.032			0.002	0.025	1	0
						0.3%	8.0%			0.2%	5.6%	1	0
0.0624	0	0	0.403	-0.0341	0	1.050	0.267	1	0	1.053	0.326	1	0
0.0624	0	0	0.403	-0.0341	0	1.050	0.281	1	0	1.053	0.345	1	0
0.0624	0	0	0.403	-0.0341	0	1.052	0.305	1	0	1.047	0.316	1	0
0.0624	0	0	0.403	-0.0341	0	1.042	0.258	1	0	1.042	0.296	1	0
						1.049	0.278	1	0	1.049	0.321	1	0
						0.004	0.021			0.006	0.021		
						0.4%	7.4%			0.5%	6.5%		
						1.054	0.337	1	0	1.059	0.386	1	0
						0.007	0.068			0.011	0.073		
						0.7%	20.1%			1.0%	18.8%		

Table A-4. Continued.

For θ_{frac} = 45°												
$(\varepsilon_{\theta\theta(I)})_{frac}$, Msi^{-1}	$(\varepsilon_{\theta\theta(II)})_{frac}$, Msi^{-1}	$(\varepsilon_{r\theta(I)})_{frac}$, Msi^{-1}	$(\varepsilon_{r\theta(II)})_{frac}$, Msi^{-1}	$(\varepsilon_{\theta\theta(T)})_{frac}$, Msi^{-1}	$(\varepsilon_{r\theta(T)})_{frac}$, Msi^{-1}	For P_Q				For P_{max}			
						For $\varepsilon_{\theta\theta}$ = 0.0148		For $\varepsilon_{r\theta}$ = 0.0220		For $\varepsilon_{\theta\theta}$ = 0.0148		For $\varepsilon_{r\theta}$ = 0.0220	
						T factor	$(2\pi d_o)^{1/2}$, $(in.)^{1/2}$	T factor	$(2\pi d_o)^{1/2}$, $(in.)^{1/2}$	T factor	$(2\pi d_o)^{1/2}$, $(in.)^{1/2}$	T factor	$(2\pi d_o)^{1/2}$, $(in.)^{1/2}$
0.0419	-0.193	0.0478	0.197	0.0798	-0.228	0.862	0.242	1.442	0.310	0.851	0.262	1.508	0.356
0.0419	-0.193	0.0478	0.197	0.0798	-0.228	0.874	0.234	1.383	0.283	0.850	0.278	1.513	0.379
0.0419	-0.193	0.0478	0.197	0.0798	-0.228	0.862	0.242	1.403	0.312	0.857	0.277	1.470	0.364
0.0419	-0.193	0.0478	0.197	0.0798	-0.228	0.874	0.234	1.439	0.354	0.852	0.300	1.503	0.406
						0.868	0.238	1.417	0.315	0.852	0.279	1.498	0.376
						0.007	0.005	0.029	0.029	0.003	0.015	0.020	0.022
						0.8%	2.0%	2.0%	9.2%	0.4%	5.5%	1.3%	5.8%
0.0419	-0.193	0.0478	0.197	0.0798	-0.228	0.899	0.177	1.275	0.193	0.880	0.212	1.357	0.250
0.0419	-0.193	0.0478	0.197	0.0798	-0.228	0.899	0.187	1.274	0.203	0.879	0.224	1.358	0.265
0.0419	-0.193	0.0478	0.197	0.0798	-0.228	0.896	0.202	1.287	0.222	0.892	0.209	1.302	0.234
0.0419	-0.193	0.0478	0.197	0.0798	-0.228	0.913	0.176	1.224	0.180	0.902	0.199	1.265	0.214
						0.902	0.185	1.265	0.199	0.888	0.211	1.320	0.241
						0.008	0.012	0.028	0.018	0.011	0.010	0.045	0.022
						0.8%	6.5%	2.2%	8.9%	1.2%	4.9%	3.4%	9.2%
						0.885	0.212	1.341	0.257	0.870	0.245	1.409	0.308
						0.019	0.029	0.085	0.066	0.020	0.039	0.100	0.075
						2.2%	13.9%	6.4%	25.5%	2.4%	15.7%	7.1%	24.4%

Table A-4. Concluded.

For θ_{frac} = 90°													
$(\varepsilon_{\theta\theta(I)})_{frac.}$, Msi^{-1}	$(\varepsilon_{\theta\theta(II)})_{frac.}$, Msi^{-1}	$(\varepsilon_{r\theta(I)})_{frac.}$, Msi^{-1}	$(\varepsilon_{r\theta(II)})_{frac.}$, Msi^{-1}	$(\varepsilon_{\theta\theta(T)})_{frac.}$, Msi^{-1}	$(\varepsilon_{r\theta(T)})_{frac.}$, Msi^{-1}	For P_Q				For P_{max}			
						For $\varepsilon_{\theta\theta}$ = 0.0148		For $\varepsilon_{r\theta}$ = 0.0220		For $\varepsilon_{\theta\theta}$ = 0.0148		For $\varepsilon_{r\theta}$ = 0.0220	
						T factor	$(2\pi d_o)^{1/2}$, $(in.)^{1/2}$	T factor	$(2\pi d_o)^{1/2}$, $(in.)^{1/2}$	T factor	$(2\pi d_o)^{1/2}$, $(in.)^{1/2}$	T factor	$(2\pi d_o)^{1/2}$, $(in.)^{1/2}$
0.0081	-0.175	0.126	-0.155	0.194	0	0.721	0.0391	1	0.569	0.701	0.0418	1	0.625
0.0081	-0.175	0.126	-0.155	0.194	0	0.741	0.0383	1	0.542	0.700	0.0443	1	0.663
0.0081	-0.175	0.126	-0.155	0.194	0	0.734	0.0411	1	0.588	0.712	0.0444	1	0.654
0.0081	-0.175	0.126	-0.155	0.194	0	0.722	0.0447	1	0.650	0.703	0.0478	1	0.714
						0.729	0.0408	1	0.587	0.704	0.0446	1	0.664
						0.010	0.0029		0.046	0.006	0.0025		0.037
						1.3%	7.1%		7.8%	0.8%	5.6%		5.6%
0.0081	-0.175	0.126	-0.155	0.194	0	0.786	0.0300	1	0.400	0.751	0.0349	1	0.488
0.0081	-0.175	0.126	-0.155	0.194	0	0.786	0.0315	1	0.421	0.750	0.0369	1	0.516
0.0081	-0.175	0.126	-0.155	0.194	0	0.780	0.0340	1	0.457	0.773	0.0350	1	0.475
0.0081	-0.175	0.126	-0.155	0.194	0	0.812	0.0302	1	0.390	0.791	0.0337	1	0.447
						0.791	0.0314	1	0.417	0.766	0.0351	1	0.481
						0.014	0.0018		0.030	0.020	0.0013		0.029
						1.8%	5.9%		7.1%	2.6%	3.8%		6.0%
						0.760	0.0361	1	0.502	0.735	0.0399	1	0.573
						0.035	0.0055		0.098	0.036	0.0054		0.102
						4.6%	15.2%		19.5%	4.9%	13.5%		17.9%

Table A–5. CNT test results for transverse loading.

Specimen no.	Width, W, inches	Crack length, 2a, inches	Thick-ness, t', inches	Fiber mass fraction	[a]Adjusted thick-ness, t, inches	Thick-ness ratio, t/a	2a/W	P_Q, kips	P_{max}, kips	Fracture path, θ_f, degrees	COD_Q, inches	COD_{max}, inches	Slope, COD t/P, psi-1		
													Initial	Final	Change
CNT-T3	12.00	5.67	0.107	0.670	0.109	0.0189	0.473	14.7	17.3	0	0.0278	0.0355	1.98E-04	2.23E-04	13.0%
CNT-T4	12.00	5.61	0.108	0.672	0.110	0.0192	0.468	14.8	17.0	0	0.0285	0.0347	1.99E-04	2.24E-04	12.6%
Average			0.108	0.671	0.109										
Std. dev.			0.000	0.001	0.001										
COV			0.3%	0.2%	0.5%										
CNT-T1	12.00	4.85	0.342	0.656	0.340	0.0705	0.404	50.3	58.0	0	0.0267	0.0363	1.75E-04	2.12E-04	21.0%
CNT-T2	12.00	5.28	0.324	0.677	0.333	0.0615	0.440	51.3	52.7	0	0.0299	0.0382	1.84E-04	2.41E-04	31.0%
Average			0.333	0.667	0.336										
Std. dev.			0.012	0.015	0.005										
COV			3.7%	2.2%	1.5%										
Average				0.669											
Std. dev.				0.009											
COV				1.3%											

[a]Values of thickness normalized to 66% fiber mass fraction

Table A-5. Continued.

$K_I t W / (\pi a)^{1/2}$	K_{II}/K_I	$T(\pi a)^{1/2}/K_I$	For P_Q			For P_{max}		
			K_{IQ}, ksi(in.)$^{1/2}$	K_{IIQ}, ksi(in.)$^{1/2}$	T_Q, ksi	K_{Imax}, ksi(in.)$^{1/2}$	K_{IImax}, ksi(in.)$^{1/2}$	T_{max}, ksi
1.15	0	-1.58	38.5	0	-20.4	45.5	0	-24.1
1.15	0	-1.58	38.2	0	-20.3	44.0	0	-23.4
			38.4	0	-20.3	44.8	0	-23.7
			0.3		0.1	1.0		0.5
			0.7%		-0.4%	2.3%		-2.1%
1.10	0	-1.55	37.6	0	-21.1	43.4	0	-24.4
1.13	0	-1.56	41.7	0	-22.7	42.8	0	-23.3
			39.6	0	-21.9	43.1	0	-23.8
			2.9		1.1	0.4		0.8
			7.3%		-5.0%	0.9%		-3.2%
			39.0	0	-21.1	43.9	0	-23.8
			1.8		1.1	1.2		0.5
			4.7%		-5.2%	2.6%		-2.2%

Table A-5. Continued.

For θ_{frac} = 0°													
$(\varepsilon_{\theta\theta(I)})_{frac}$, Msi^{-1}	$(\varepsilon_{\theta\theta(II)})_{frac}$, Msi^{-1}	$(\varepsilon_{r\theta(I)})_{frac}$, Msi^{-1}	$(\varepsilon_{r\theta(II)})_{frac}$, Msi^{-1}	$(\varepsilon_{\theta\theta(T)})_{frac}$, Msi^{-1}	$(\varepsilon_{r\theta(T)})_{frac}$, Msi^{-1}	For P_Q				For P_{max}			
						For $\varepsilon_{\theta\theta}$ = 0.0148		For $\varepsilon_{r\theta}$ = 0.0220		For $\varepsilon_{\theta\theta}$ = 0.0148		For $\varepsilon_{r\theta}$ = 0.0220	
						T - factor	$(2\pi d_o)^{1/2}$, $(in.)^{1/2}$	T - factor	$(2\pi d_o)^{1/2}$, $(in.)^{1/2}$	T - factor	$(2\pi d_o)^{1/2}$, $(in.)^{1/2}$	T - factor	$(2\pi d_o)^{1/2}$, $(in.)^{1/2}$
0.142	0	0	0.403	-0.0341	0	1.049	0.389	1	0	1.059	0.463	1	0
0.142	0	0	0.403	-0.0341	0	1.049	0.385	1	0	1.057	0.447	1	0
						1.049	0.387	1	0	1.058	0.455	1	0
						0.000	0.003			0.001	0.011		
						0.0%	0.7%			0.1%	2.5%		
0.142	0	0	0.403	-0.0341	0	1.051	0.380	1	0	1.059	0.442	1	0
0.142	0	0	0.403	-0.0341	0	1.055	0.423	1	0	1.057	0.435	1	0
						1.053	0.401	1	0	1.058	0.438	1	0
						0.003	0.030			0.002	0.003		
						0.3%	7.6%			0.2%	0.7%		
						1.051	0.394	1	0	1.058	0.447	1	0
						0.003	0.019			0.001	0.008		
						0.3%	4.9%			0.1%	1.9%		

Table A-5. Continued.

For θ_{frac} = 45°													
$(\varepsilon_{\theta\theta(I)})_{frac}$, Msi^{-1}	$(\varepsilon_{\theta\theta(II)})_{frac}$, Msi^{-1}	$(\varepsilon_{r\theta(I)})_{frac}$, Msi^{-1}	$(\varepsilon_{r\theta(II)})_{frac}$, Msi^{-1}	$(\varepsilon_{\theta\theta(T)})_{frac}$, Msi^{-1}	$(\varepsilon_{r\theta(T)})_{frac}$, Msi^{-1}	For P_Q				For P_{max}			
						For $\varepsilon_{\theta\theta}$ = 0.0148		For $\varepsilon_{r\theta}$ = 0.0220		For $\varepsilon_{\theta\theta}$ = 0.0148		For $\varepsilon_{r\theta}$ = 0.0220	
						T - factor	$(2\pi d_o)^{1/2}$, $(in.)^{1/2}$	T - factor	$(2\pi d_o)^{1/2}$, $(in.)^{1/2}$	T - factor	$(2\pi d_o)^{1/2}$, $(in.)^{1/2}$	T - factor	$(2\pi d_o)^{1/2}$, $(in.)^{1/2}$
0.0947	-0.122	0.1883	0.153	0.0254	-0.119	0.966	0.238	1.124	0.371	0.960	0.280	1.150	0.448
0.0947	-0.122	0.1883	0.153	0.0254	-0.119	0.966	0.236	1.123	0.367	0.961	0.271	1.145	0.431
						0.966	0.237	1.124	0.369	0.961	0.275	1.147	0.440
						0.000	0.002	0.001	0.003	0.001	0.006	0.003	0.008
						0.0%	0.7%	0.0%	0.7%	0.1%	2.3%	0.3%	1.9%
0.0947	-0.122	0.1883	0.153	0.0254	-0.119	0.965	0.232	1.129	0.363	0.960	0.266	1.152	0.428
0.0947	-0.122	0.1883	0.153	0.0254	-0.119	0.963	0.257	1.140	0.407	0.962	0.264	1.144	0.420
						0.964	0.244	1.134	0.385	0.961	0.265	1.148	0.424
						0.002	0.017	0.008	0.031	0.001	0.002	0.005	0.006
						0.2%	7.1%	0.7%	8.0%	0.1%	0.7%	0.5%	1.3%
						0.965	0.241	1.129	0.377	0.961	0.270	1.148	0.432
						0.002	0.011	0.008	0.020	0.001	0.007	0.004	0.012
						0.2%	4.5%	0.7%	5.3%	0.1%	2.6%	0.3%	2.8%

Table A-5. Concluded.

For θ_{frac} = 90°													
$(\varepsilon_{\theta\theta(I)})_{frac.}$ Msi^{-1}	$(\varepsilon_{\theta\theta(II)})_{frac.}$ Msi^{-1}	$(\varepsilon_{r\theta(I)})_{frac.}$ Msi^{-1}	$(\varepsilon_{r\theta(II)})_{frac.}$ Msi^{-1}	$(\varepsilon_{\theta\theta(T)})_{frac.}$ Msi^{-1}	$(\varepsilon_{r\theta(T)})_{frac.}$ Msi^{-1}	For P_Q				For P_{max}			
						For $\varepsilon_{\theta\theta}$ = 0.0148		For $\varepsilon_{r\theta}$ = 0.0220		For $\varepsilon_{\theta\theta}$ = 0.0148		For $\varepsilon_{r\theta}$ = 0.0220	
						T - factor	$(2\pi d_o)^{1/2}$, $(in.)^{1/2}$	T - factor	$(2\pi d_o)^{1/2}$, $(in.)^{1/2}$	T - factor	$(2\pi d_o)^{1/2}$, $(in.)^{1/2}$	T - factor	$(2\pi d_o)^{1/2}$, $(in.)^{1/2}$
0.0066	-0.094	0.1553	-0.126	0.0849	0.000	0.895	0.015	1.000	0.272	0.879	0.018	1.000	0.321
0.0066	-0.094	0.1553	-0.126	0.0849	0.000	0.896	0.015	1.000	0.269	0.882	0.017	1.000	0.311
						0.896	0.015	1.000	0.271	0.880	0.018	1.000	0.316
						0.000	0.000	0.000	0.002	0.002	0.000	0.000	0.005
						0.0%	0.6%	0.0%	0.7%	0.2%	2.1%	0.0%	1.7%
0.0066	-0.094	0.1553	-0.126	0.0849	0.000	0.892	0.015	1.000	0.265	0.877	0.017	1.000	0.306
0.0066	-0.094	0.1553	-0.126	0.0849	0.000	0.885	0.016	1.000	0.294	0.882	0.017	1.000	0.302
						0.888	0.016	1.000	0.280	0.880	0.017	1.000	0.304
						0.005	0.001	0.000	0.020	0.003	0.000	0.000	0.003
						0.6%	6.7%	0.0%	7.3%	0.4%	0.5%	0.0%	0.9%
						0.892	0.015	1.000	0.275	0.880	0.017	1.000	0.310
						0.005	0.001	0.000	0.013	0.002	0.000	0.000	0.008
						0.6%	4.2%	0.0%	4.7%	0.3%	2.5%	0.0%	2.6%

Table A–6. ECT test results for longitudinal loading.

Specimen no.	Width, W, inches	Crack length, a, inches	Thick-ness, t', inches	Fiber mass fraction	[b]Adjusted thick-ness, t, inches	Thick-ness, ratio, t/a	a/W	P_Q, lbf	P_{max}, lbf	Fracture path, θ_{frac}, degrees	COD_Q, inches	COD_{max}, inches	Slope, COD t/P, psi-1		
													Initial	Final	Change
ECT-L3[a]	5.6	2.55	0.104	0.670	0.106	0.0416	0.455	2,802	3,678	90	0.108	0.228	3.89E-06	6.56E-06	68.5%
ECT-L4[a]	5.6	2.80	0.109	0.672	0.111	0.0397	0.500	2,814	3,495	90	0.137	0.189	5.24E-06	6.01E-06	14.7%
Average			0.107	0.671	0.109										
Std. dev.			0.003	0.001	0.004										
COV			3.2%	0.2%	3.4%										
ECT-L5[a]	5.6	2.10	0.211	0.652	0.208	0.0991	0.375	9,288	10,194	45	0.115	0.171	2.45E-06	3.48E-06	42.4%
ECT-L6[a]	5.6	2.35	0.213	0.678	0.218	0.0929	0.420	7,530	8,680	45,90	0.118	0.172	3.25E-06	4.32E-06	33.1%
Average			0.212	0.665	0.213										
Std. dev.			0.001	0.018	0.007										
COV			0.6%	2.8%	3.4%										
ECT-L1[a]	5.6	2.10	0.348	0.656	0.346	0.1649	0.375	12,611	14,103	45,90	0.105	0.140	2.77E-06	3.45E-06	24.6%
ECT-L2	5.6	2.35	0.325	0.677	0.334	0.1420	0.420	8,891	11,411	0,90	0.097	0.182	3.47E-06	5.31E-06	53.1%
Average			0.337	0.667	0.340										
Std. dev.			0.016	0.015	0.009										
COV			4.9%	2.2%	2.6%										
ECT-L7	5.6	2.55	0.438	0.632	0.419	0.1644	0.455	13,044	13,478	45,90	0.122	0.164	3.73E-06	5.11E-06	36.9%
ECT-L8	5.6	2.80	0.436	0.678	0.448	0.1599	0.500	8,018	10,279	45,90	0.096	0.169	5.22E-06	7.34E-06	40.5%
Average			0.437	0.655	0.434										
Std. dev.			0.001	0.033	0.020										
COV			0.3%	5.0%	4.6%										
Average				0.664											
Std. dev.				0.016											
COV				2.5%											

[a]Compression failure on edge opposite cut.

[b]Values of thickness normalized to 66% fiber mass fraction

Table A-6. Continued.

$K_I t(W')^{1/2}$ / P	K_{II}/K_I	$T(\pi a)^{1/2}$ / K_I	For P_Q			For P_{max}		
			K_I, ksi(in.)$^{1/2}$	K_{II}, ksi(in.)$^{1/2}$	T, ksi	K_I, ksi(in.)$^{1/2}$	K_{II}, ksi(in.)$^{1/2}$	T, ksi
7.85	0.000	0.080	87.7	0	3.7	116.9	0	4.9
9.10	0.000	0.112	97.3	0	5.2	123.0	0	6.6
			92.5	0	4.4	119.9	0	5.7
			6.8		1.1	4.3		1.2
			7.3%		23.8%	3.6%		20.1%
6.14	0.000	0.027	115.7	0	2.1	125.5	0	2.3
7.00	0.000	0.055	102.1	0	3.2	120.9	0	3.8
			108.9	0	2.7	123.2	0	3.0
			9.7		0.8	3.3		1.1
			8.9%		30.6%	2.7%		36.5%
6.14	0.000	0.027	94.4	0	1.7	105.0	0	1.9
7.00	0.000	0.055	78.8	0	2.5	103.8	0	3.3
			86.6	0	2.1	104.4	0	2.6
			11.0		0.6	0.8		1.0
			12.7%		26.9%	0.8%		38.2%
7.85	0.000	0.080	103.2	0	4.3	102.1	0	4.3
9.10	0.000	0.112	68.8	0	3.7	90.7	0	4.8
			86.0	0	4.0	96.4	0	4.6
			24.3		0.5	8.1		0.4
			28.2%		11.9%	8.4%		8.3%
			93.5	0	3.3	111.0	0	4.0
			14.8		1.2	12.3		1.5
			15.8%		35.5%	11.1%		38.1%

Table A-6. Continued.

For θ_{frac} = 0°													
$(\varepsilon_{\theta\theta(I)})_{frac.}$, Msi^{-1}	$(\varepsilon_{\theta\theta(II)})_{frac.}$, Msi^{-1}	$(\varepsilon_{r\theta(I)})_{frac.}$, Msi^{-1}	$(\varepsilon_{r\theta(II)})_{frac.}$, Msi^{-1}	$(\varepsilon_{\theta\theta(T)})_{frac.}$, Msi^{-1}	$(\varepsilon_{r\theta(T)})_{frac.}$, Msi^{-1}	For P_Q				For P_{max}			
						For $\varepsilon_{\theta\theta}$ = 0.0171		For $\varepsilon_{r\theta}$ = 0.0220		For $\varepsilon_{\theta\theta}$ = 0.0171		For $\varepsilon_{r\theta}$ = 0.0220	
						T - factor	$(2\pi d_o)^{1/2}$, $(in.)^{1/2}$	T - factor	$(2\pi d_o)^{1/2}$, $(in.)^{1/2}$	T - factor	$(2\pi d_o)^{1/2}$, $(in.)^{1/2}$	T - factor	$(2\pi d_o)^{1/2}$, $(in.)^{1/2}$
0.0624	0	0	0.403	-0.0341	0	0.993	0.318	1	0	0.990	0.422	1	0
0.0624	0	0	0.403	-0.0341	0	0.990	0.351	1	0	0.987	0.443	1	0
						0.991	0.334	1	0	0.989	0.433	1	0
						0.002	0.024			0.002	0.015		
						0.2%	7.1%			0.2%	3.4%		
0.0624	0	0	0.403	-0.0341	0	0.996	0.420	1	0	0.996	0.456	1	0
0.0624	0	0	0.403	-0.0341	0	0.994	0.370	1	0	0.992	0.438	1	0
						0.995	0.395	1	0	0.994	0.447	1	0
						0.002	0.036			0.002	0.013		
						0.2%	9.0%			0.2%	2.9%		
0.0624	0	0	0.403	-0.0341	0	0.997	0.343	1	0	0.996	0.381	1	0
0.0624	0	0	0.403	-0.0341	0	0.995	0.286	1	0	0.993	0.376	1	0
						0.996	0.315	1	0	0.995	0.379	1	0
						0.001	0.040			0.002	0.004		
						0.1%	12.8%			0.2%	1.0%		
0.0624	0	0	0.403	-0.0341	0	0.991	0.373	1	0	0.992	0.369	1	0
0.0624	0	0	0.403	-0.0341	0	0.993	0.249	1	0	0.990	0.328	1	0
						0.992	0.311	1	0	0.991	0.349	1	0
						0.001	0.088			0.001	0.030		
						0.1%	28.2%			0.1%	8.5%		
						0.993	0.339	1	0	0.992	0.402	1	0
						0.002	0.054			0.003	0.045		
						0.2%	15.9%			0.3%	11.1%		

Table A-6. Continued.

For θ_{frac} = 45°												
$(\varepsilon_{\theta\theta(I)})_{frac.}$ Msi^{-1}	$(\varepsilon_{\theta\theta(II)})_{frac.}$ Msi^{-1}	$(\varepsilon_{r\theta(I)})_{frac.}$ Msi^{-1}	$(\varepsilon_{r\theta(II)})_{frac.}$ Msi^{-1}	$(\varepsilon_{\theta\theta(T)})_{frac.}$ Msi^{-1}	$(\varepsilon_{r\theta(T)})_{frac.}$ Msi^{-1}	For P_Q				For P_{max}			
						For $\varepsilon_{\theta\theta}$ = 0.0148		For $\varepsilon_{r\theta}$ = 0.0220		For $\varepsilon_{\theta\theta}$ = 0.0148		For $\varepsilon_{r\theta}$ = 0.0220	
						T - factor	$(2\pi d_o)^{1/2}$, $(in.)^{1/2}$	T - factor	$(2\pi d_o)^{1/2}$, $(in.)^{1/2}$	T - factor	$(2\pi d_o)^{1/2}$, $(in.)^{1/2}$	T - factor	$(2\pi d_o)^{1/2}$, $(in.)^{1/2}$
0.0419	-0.193	0.0478	0.197	0.0798	-0.228	1.020	0.254	0.963	0.183	1.027	0.340	0.952	0.241
0.0419	-0.193	0.0478	0.197	0.0798	-0.228	1.029	0.284	0.949	0.200	1.037	0.361	0.936	0.250
						1.025	0.269	0.956	0.192	1.032	0.351	0.944	0.246
						0.006	0.021	0.010	0.012	0.007	0.015	0.011	0.006
						0.6%	7.9%	1.0%	6.3%	0.6%	4.2%	1.1%	2.5%
0.0419	-0.193	0.0478	0.197	0.0798	-0.228	1.011	0.332	0.979	0.246	1.012	0.360	0.977	0.266
0.0419	-0.193	0.0478	0.197	0.0798	-0.228	1.018	0.294	0.968	0.214	1.021	0.350	0.962	0.252
						1.015	0.313	0.973	0.230	1.017	0.355	0.969	0.259
						0.005	0.026	0.008	0.022	0.006	0.007	0.011	0.010
						0.4%	8.4%	0.8%	9.7%	0.6%	2.0%	1.1%	3.8%
0.0419	-0.193	0.0478	0.197	0.0798	-0.228	1.009	0.270	0.983	0.201	1.010	0.301	0.981	0.224
0.0419	-0.193	0.0478	0.197	0.0798	-0.228	1.014	0.226	0.975	0.167	1.018	0.299	0.967	0.218
						1.011	0.248	0.979	0.184	1.014	0.300	0.974	0.221
						0.003	0.031	0.006	0.024	0.005	0.001	0.010	0.004
						0.3%	12.4%	0.6%	13.3%	0.5%	0.2%	1.0%	1.8%
0.0419	-0.193	0.0478	0.197	0.0798	-0.228	1.024	0.300	0.957	0.214	1.024	0.296	0.957	0.212
0.0419	-0.193	0.0478	0.197	0.0798	-0.228	1.020	0.199	0.963	0.144	1.027	0.264	0.952	0.187
						1.022	0.249	0.960	0.179	1.025	0.280	0.955	0.200
						0.003	0.071	0.005	0.050	0.002	0.023	0.004	0.018
						0.3%	28.5%	0.5%	27.8%	0.2%	8.2%	0.4%	8.8%
						1.018	0.270	0.967	0.196	1.022	0.321	0.961	0.231
						0.007	0.043	0.011	0.031	0.009	0.036	0.014	0.026
						0.6%	15.8%	1.2%	16.0%	0.8%	11.2%	1.5%	11.1%

Table A-6. Concluded.

For θ_{frac} = 90°													
$(\varepsilon_{\theta\theta(I)})_{frac.}$ Msi^{-1}	$(\varepsilon_{\theta\theta(II)})_{frac.}$ Msi^{-1}	$(\varepsilon_{r\theta(I)})_{frac.}$ Msi^{-1}	$(\varepsilon_{r\theta(II)})_{frac.}$ Msi^{-1}	$(\varepsilon_{\theta\theta(T)})_{frac.}$ Msi^{-1}	$(\varepsilon_{r\theta(T)})_{frac.}$ Msi^{-1}	For P_Q				For P_{max}			
						For $\varepsilon_{\theta\theta}$ = 0.0148		For $\varepsilon_{r\theta}$ = 0.0220		For $\varepsilon_{\theta\theta}$ = 0.0148		For $\varepsilon_{r\theta}$ = 0.0220	
						T - factor	$(2\pi d_o)^{1/2}$, $(in.)^{1/2}$	T - factor	$(2\pi d_o)^{1/2}$, $(in.)^{1/2}$	T - factor	$(2\pi d_o)^{1/2}$, $(in.)^{1/2}$	T - factor	$(2\pi d_o)^{1/2}$, $(in.)^{1/2}$
0.0081	-0.175	0.126	-0.155	0.194	0	1.051	0.0505	1	0.504	1.069	0.0684	1	0.671
0.0081	-0.175	0.126	-0.155	0.194	0	1.073	0.0571	1	0.559	1.094	0.0737	1	0.706
						1.062	0.0538	1	0.531	1.081	0.0710	1	0.689
						0.0156	0.0047		0.0388	0.0177	0.0037		0.0248
						1.5%	8.8%		7.3%	1.6%	5.2%		3.6%
0.0081	-0.175	0.126	-0.155	0.194	0	1.028	0.0651	1	0.665	1.031	0.0708	1	0.721
0.0081	-0.175	0.126	-0.155	0.194	0	1.044	0.0584	1	0.586	1.053	0.0697	1	0.694
						1.036	0.0618	1	0.625	1.042	0.0702	1	0.707
						0.0114	0.0048		0.0555	0.0158	0.0008		0.0187
						1.1%	7.8%		8.9%	1.5%	1.1%		2.7%
0.0081	-0.175	0.126	-0.155	0.194	0	1.023	0.0529	1	0.542	1.025	0.0589	1	0.603
0.0081	-0.175	0.126	-0.155	0.194	0	1.034	0.0446	1	0.453	1.045	0.0594	1	0.596
						1.028	0.0488	1	0.498	1.035	0.0592	1	0.599
						0.0078	0.0058		0.0633	0.0139	0.0003		0.0047
						0.8%	12.0%		12.7%	1.3%	0.6%		0.8%
0.0081	-0.175	0.126	-0.155	0.194	0	1.060	0.0599	1	0.593	1.060	0.0592	1	0.586
0.0081	-0.175	0.126	-0.155	0.194	0	1.050	0.0396	1	0.395	1.068	0.0530	1	0.521
						1.055	0.0498	1	0.494	1.064	0.0561	1	0.554
						0.0070	0.0144		0.1395	0.0056	0.0044		0.0465
						0.7%	28.9%		28.2%	0.5%	7.9%		8.4%
						1.045	0.0535	1	0.537	1.055	0.0641	1	0.637
						0.0168	0.0084		0.0850	0.0222	0.0074		0.0709
						1.6%	15.7%		15.8%	2.1%	11.5%		11.1%

Table A–7. ECT results for transverse loading.

Specimen no.	Width, W, inches	Crack length, a, inches	Thick-ness, t', inches	Fiber mass fraction	[a]Adjusted thick-ness, t, inches	Thick-ness, ratio, t/a	a/W	P_Q, lbf	P_{max}, lbf	Fracture path, θ_{frac}, degrees	COD_Q, inches	COD_{max}, inches	Slope, COD t/P, psi-1		
													Initial	Final	Change
ECT-T3	5.6	2.55	0.109	0.670	0.110	0.0427	0.455	1,331	1,358	0	0.074	0.104	6.07E-06	8.49E-06	39.8%
ECT-T4	5.6	2.80	0.111	0.672	0.113	0.0395	0.500	1,206	1,337	0	0.090	0.102	8.02E-06	8.59E-06	7.1%
Average			0.110	0.671	0.112										
Std. dev.			0.001	0.001	0.002										
COV			0.8%	0.2%	1.4%										
ECT-T5	5.6	2.10	0.217	0.652	0.214	0.1034	0.375	3,446	3,544	0	0.066	0.085	3.94E-06	5.15E-06	30.8%
ECT-T6	5.6	2.35	0.217	0.678	0.223	0.0924	0.420	2,994	3,141	0	0.073	0.086	5.19E-06	6.07E-06	17.1%
Average			0.217	0.665	0.219										
Std. dev.			0.000	0.018	0.006										
COV			0.0%	2.8%	2.8%										
ECT-T1	5.6	2.10	0.341	0.656	0.339	0.1622	0.375	5,222	5,659	0	0.070	0.080	4.34E-06	4.80E-06	10.5%
ECT-T2	5.6	2.35	0.322	0.677	0.331	0.1372	0.420	4,487	5,033	0	0.074	0.092	5.21E-06	6.08E-06	16.6%
Average			0.332	0.667	0.335										
Std. dev.			0.009	0.015	0.006										
COV			2.7%	2.2%	1.7%										
ECT-T7	5.6	2.55	0.444	0.632	0.425	0.1743	0.455	4,355	4,624	0	0.064	0.070	6.10E-06	6.48E-06	6.2%
ECT-T8	5.6	2.80	0.433	0.678	0.445	0.1546	0.500	4,023	4,160	0	0.071	0.098	7.75E-06	1.05E-05	35.4%
Average			0.439	0.655	0.435										
Std. dev.			0.006	0.033	0.014										
COV			1.3%	5.0%	3.1%										
Average				0.664											
Std. dev.				0.016											
COV				2.5%											

[a]Values of thickness normalized to 66% fiber mass fraction

Table A-7. Continued.

$K_I t(W')^{1/2}$ / P	K_{II}/K_I	$T(\pi a)^{1/2}$ / K_I	For P_Q			For P_{max}		
			K_I, ksi(in.)$^{1/2}$	K_{II}, ksi(in.)$^{1/2}$	T, ksi	K_I, ksi(in.)$^{1/2}$	K_{II}, ksi(in.)$^{1/2}$	T, ksi
7.85	0	0.173	40.0	0	2.4	41.4	0	2.5
9.10	0	0.245	41.1	0	3.4	46.4	0	3.8
			40.5	0	2.9	43.9	0	3.2
			0.8		0.7	3.6		0.9
			2.1%		23.1%	8.1%		29.0%
6.14	0	0.055	41.7	0	0.9	42.3	0	0.9
7.00	0	0.118	39.7	0	1.7	42.8	0	1.9
			40.7	0	1.3	42.6	0	1.4
			1.4		0.6	0.3		0.7
			3.4%		44.7%	0.8%		48.4%
6.14	0	0.055	40.0	0	0.9	43.1	0	0.9
7.00	0	0.118	40.1	0	1.7	46.2	0	2.0
			40.1	0	1.3	44.6	0	1.5
			0.1		0.6	2.2		0.8
			0.2%		47.9%	4.9%		52.0%
7.85	0	0.173	34.0	0	2.1	34.5	0	2.1
9.10	0	0.245	34.8	0	2.9	37.0	0	3.1
			34.4	0	2.5	35.7	0	2.6
			0.6		0.6	1.7		0.7
			1.7%		22.8%	4.8%		25.8%
			38.9	0	2.0	41.7	0	2.2
			2.9		0.9	4.1		1.0
			7.4%		44.6%	9.9%		46.3%

Table A-7. Continued.

For $\theta_{frac} = 0°$												
$(\varepsilon_{\theta\theta(I)})_{frac.}$ Msi^{-1}	$(\varepsilon_{\theta\theta(II)})_{frac.}$ Msi^{-1}	$(\varepsilon_{r\theta(I)})_{frac.}$ Msi^{-1}	$(\varepsilon_{r\theta(II)})_{frac.}$ Msi^{-1}	$(\varepsilon_{\theta\theta(T)})_{frac.}$ Msi^{-1}	$(\varepsilon_{r\theta(T)})_{frac.}$ Msi^{-1}	For P_Q				For P_{max}			
						For $\varepsilon_{\theta\theta} = 0.0148$		For $\varepsilon_{r\theta} = 0.0220$		For $\varepsilon_{\theta\theta} = 0.0148$		For $\varepsilon_{r\theta} = 0.0220$	
						T - factor	$(2\pi d_o)^{1/2}$, $(in.)^{1/2}$	T - factor	$(2\pi d_o)^{1/2}$, $(in.)^{1/2}$	T - factor	$(2\pi d_o)^{1/2}$, $(in.)^{1/2}$	T - factor	$(2\pi d_o)^{1/2}$, $(in.)^{1/2}$
0.1423	0	0	0.403	-0.0341	0	0.994	0.382	1	0	0.994	0.396	1	0
0.1423	0	0	0.403	-0.0341	0	0.992	0.392	1	0	0.991	0.443	1	0
						0.993	0.387	1	0	0.993	0.419	1	0
						0.002	0.007			0.002	0.033		
						0.2%	1.9%			0.2%	7.9%		
0.1423	0	0	0.403	-0.0341	0	0.998	0.400	1	0	0.998	0.406	1	0
0.1423	0	0	0.403	-0.0341	0	0.996	0.380	1	0	0.996	0.410	1	0
						0.997	0.390	1	0	0.997	0.408	1	0
						0.001	0.014			0.002	0.003		
						0.1%	3.5%			0.2%	0.6%		
0.1423	0	0	0.403	-0.0341	0	0.998	0.384	1	0	0.998	0.413	1	0
0.1423	0	0	0.403	-0.0341	0	0.996	0.384	1	0	0.995	0.442	1	0
						0.997	0.384	1	0	0.997	0.428	1	0
						0.001	0.000			0.002	0.020		
						0.1%	0.1%			0.2%	4.7%		
0.1423	0	0	0.403	-0.0341	0	0.995	0.325	1	0	0.995	0.330	1	0
0.1423	0	0	0.403	-0.0341	0	0.993	0.332	1	0	0.993	0.353	1	0
						0.994	0.329	1	0	0.994	0.342	1	0
						0.001	0.005			0.002	0.016		
						0.1%	1.6%			0.2%	4.7%		
						0.995	0.372	1	0	0.995	0.399	1	0
						0.002	0.028			0.002	0.040		
						0.2%	7.5%			0.2%	9.9%		

Table A-7. Continued.

For θ_{frac} = 45°														
$(\varepsilon_{\theta\theta(I)})_{frac.}$ Msi^{-1}	$(\varepsilon_{\theta\theta(II)})_{frac.}$ Msi^{-1}	$(\varepsilon_{r\theta(I)})_{frac.}$ Msi^{-1}	$(\varepsilon_{r\theta(II)})_{frac.}$ Msi^{-1}	$(\varepsilon_{\theta\theta(T)})_{frac.}$ Msi^{-1}	$(\varepsilon_{r\theta(T)})_{frac.}$ Msi^{-1}	For P_Q				For P_{max}			
						For $\varepsilon_{\theta\theta}$ = 0.0148		For $\varepsilon_{r\theta}$ = 0.0220		For $\varepsilon_{\theta\theta}$ = 0.0148		For $\varepsilon_{r\theta}$ = 0.0220	
						T - factor	$(2\pi d_o)^{1/2}$, $(in.)^{1/2}$	T - factor	$(2\pi d_o)^{1/2}$, $(in.)^{1/2}$	T - factor	$(2\pi d_o)^{1/2}$, $(in.)^{1/2}$	T - factor	$(2\pi d_o)^{1/2}$, $(in.)^{1/2}$
0.0947	-0.122	0.1883	0.153	0.0254	-0.119	1.004	0.257	0.987	0.338	1.004	0.266	0.986	0.350
0.0947	-0.122	0.1883	0.153	0.0254	-0.119	1.006	0.265	0.982	0.346	1.007	0.299	0.980	0.389
						1.005	0.261	0.984	0.342	1.006	0.283	0.983	0.370
						0.001	0.006	0.004	0.006	0.002	0.023	0.005	0.028
						0.1%	2.2%	0.4%	1.7%	0.2%	8.3%	0.5%	7.6%
0.0947	-0.122	0.1883	0.153	0.0254	-0.119	1.002	0.267	0.995	0.355	1.002	0.271	0.995	0.361
0.0947	-0.122	0.1883	0.153	0.0254	-0.119	1.003	0.255	0.991	0.337	1.003	0.275	0.990	0.363
						1.002	0.261	0.993	0.346	1.002	0.273	0.993	0.362
						0.001	0.009	0.003	0.013	0.001	0.002	0.004	0.002
						0.1%	3.3%	0.3%	3.7%	0.1%	0.9%	0.4%	0.4%
0.0947	-0.122	0.1883	0.153	0.0254	-0.119	1.001	0.256	0.995	0.341	1.002	0.276	0.995	0.367
0.0947	-0.122	0.1883	0.153	0.0254	-0.119	1.003	0.258	0.991	0.340	1.003	0.296	0.989	0.391
						1.002	0.257	0.993	0.341	1.003	0.286	0.992	0.379
						0.001	0.001	0.003	0.000	0.001	0.014	0.004	0.017
						0.1%	0.4%	0.3%	0.1%	0.1%	5.0%	0.4%	4.5%
0.0947	-0.122	0.1883	0.153	0.0254	-0.119	1.004	0.218	0.989	0.287	1.004	0.222	0.989	0.292
0.0947	-0.122	0.1883	0.153	0.0254	-0.119	1.005	0.224	0.985	0.293	1.005	0.238	0.984	0.311
						1.004	0.221	0.987	0.290	1.004	0.230	0.986	0.302
						0.001	0.004	0.003	0.004	0.001	0.011	0.004	0.013
						0.1%	1.8%	0.3%	1.4%	0.1%	4.9%	0.4%	4.5%
						1.003	0.250	0.989	0.330	1.004	0.268	0.988	0.353
						0.002	0.018	0.005	0.025	0.002	0.027	0.005	0.035
						0.2%	7.4%	0.5%	7.6%	0.2%	9.9%	0.5%	9.9%

Table A-7. Concluded.

For θ_{frac} = 90°													
$(\varepsilon_{\theta\theta(I)})_{frac.}$ Msi^{-1}	$(\varepsilon_{\theta\theta(II)})_{frac.}$ Msi^{-1}	$(\varepsilon_{r\theta(I)})_{frac.}$ Msi^{-1}	$(\varepsilon_{r\theta(II)})_{frac.}$ Msi^{-1}	$(\varepsilon_{\theta\theta(T)})_{frac.}$ Msi^{-1}	$(\varepsilon_{r\theta(T)})_{frac.}$ Msi^{-1}	For P_Q				For P_{max}			
						For $\varepsilon_{\theta\theta}$ = 0.0171		For $\varepsilon_{r\theta}$ = 0.0220		For $\varepsilon_{\theta\theta}$ = 0.0171		For $\varepsilon_{r\theta}$ = 0.0220	
						T - factor	$(2\pi d_o)^{1/2}$, $(in.)^{1/2}$	T - factor	$(2\pi d_o)^{1/2}$, $(in.)^{1/2}$	T - factor	$(2\pi d_o)^{1/2}$, $(in.)^{1/2}$	T - factor	$(2\pi d_o)^{1/2}$, $(in.)^{1/2}$
0.0066	-0.094	0.155	-0.126	0.085	0	1.012	0.0156	1	0.282	1.013	0.0162	1	0.292
0.0066	-0.094	0.155	-0.126	0.085	0	1.017	0.0161	1	0.290	1.019	0.0183	1	0.328
						1.015	0.0159	1	0.286	1.016	0.0172	1	0.310
						0.003	0.0004		0.006	0.005	0.0015		0.025
						0.3%	2.4%		2.1%	0.5%	8.6%		8.1%
0.0066	-0.094	0.155	-0.126	0.085	0	1.004	0.0161	1	0.294	1.005	0.0164	1	0.299
0.0066	-0.094	0.155	-0.126	0.085	0	1.009	0.0155	1	0.280	1.009	0.0167	1	0.302
						1.007	0.0158	1	0.287	1.007	0.0165	1	0.300
						0.003	0.0005		0.010	0.003	0.0002		0.002
						0.3%	3.1%		3.4%	0.3%	1.1%		0.8%
0.0066	-0.094	0.155	-0.126	0.085	0	1.004	0.0155	1	0.282	1.005	0.0167	1	0.304
0.0066	-0.094	0.155	-0.126	0.085	0	1.009	0.0156	1	0.283	1.010	0.0180	1	0.326
						1.007	0.0156	1	0.283	1.007	0.0173	1	0.315
						0.003	0.0001		0.001	0.004	0.0009		0.015
						0.3%	0.6%		0.2%	0.4%	5.3%		4.9%
0.0066	-0.094	0.155	-0.126	0.085	0	1.010	0.0132	1	0.240	1.011	0.0135	1	0.244
0.0066	-0.094	0.155	-0.126	0.085	0	1.015	0.0136	1	0.245	1.015	0.0145	1	0.261
						1.012	0.0134	1	0.243	1.013	0.0140	1	0.252
						0.003	0.0003		0.004	0.003	0.0007		0.012
						0.3%	2.0%		1.7%	0.3%	5.1%		4.8%
						1.010	0.0152	1	0.275	1.011	0.0163	1	0.294
						0.005	0.001		0.020	0.005	0.002		0.029
						0.4%	7.3%		7.4%	0.5%	10.0%		9.9%

Table A–8. CT results for longitudinal loading.

Specimen no.	Width, W, inches	Crack length, a, inches	Thick-ness, t', inches	Fiber mass fraction	Adjusted thick-ness[a], t, inches	Thick-ness, ratio, t/a	a/W	P_Q, lbf	P_{max}, lbf	Crack path, θ_f, degrees	COD_Q, inches	COD_{max}, inches	Slope, COD t/P, psi-1		
													Initial	Final	Change
CT-2L31	5.6	2.55	0.107	0.670	0.109	0.0420	0.455	2,354	2,658	90	0.150		6.76E-06		
CT-2L41	5.6	2.80	0.110	0.672	0.112	0.0393	0.500	2,370	2,491	90	0.183	0.199	8.34E-06	8.94E-06	7.1%
CT-1L31	9.6	4.40	0.107	0.670	0.109	0.0243	0.458	3,585	3,674	90	0.171	0.186	5.08E-06	5.50E-06	8.2%
CT-1L41	9.6	4.80	0.108	0.672	0.110	0.0226	0.500	3,386	3,386	90	0.194	0.194	6.05E-06	6.34E-06	4.7%
Average			0.108	0.671	0.110										
Std. dev.			0.001	0.001	0.002										
COV			1.2%	0.2%	1.4%										
CT-2L5	5.6	2.10	0.218	0.652	0.216	0.1040	0.375	6,166	6,229	90	0.154	0.157	5.13E-06	5.43E-06	5.7%
CT-2L6	5.6	2.35	0.212	0.678	0.218	0.0903	0.420	5,275	5,771	90	0.162	0.185	6.36E-06	6.97E-06	9.6%
CT-1L5	9.6	3.60	0.220	0.652	0.218	0.0612	0.375	8,078	9,218	90	0.182	0.228	4.66E-06	5.39E-06	15.7%
CT-1L6	9.6	4.00	0.213	0.678	0.219	0.0533	0.417	7,515	8,151	90	0.207	0.237	5.73E-06	6.36E-06	10.9%
Average			0.216	0.665	0.218										
Std. dev.			0.004	0.015	0.000										
COV			1.9%	2.3%	0.1%										
CT-2L11	5.6	2.10	0.344	0.656	0.342	0.1640	0.375	9,156	9,518	90	0.156	0.182	5.62E-06	6.56E-06	16.6%
CT-2L21	5.6	2.35	0.325	0.677	0.333	0.1383	0.420	7,469	8,072	90	0.150	0.171	6.35E-06	7.06E-06	11.2%
CT-1L11	9.6	3.60	0.344	0.656	0.342	0.0955	0.375	12,660	12,660	90	0.159	0.159	4.12E-06	4.29E-06	4.1%
CT-1L21	9.6	4.00	0.323	0.677	0.332	0.0808	0.417	12,293	12,571	90	0.177	0.201	4.63E-06	5.29E-06	14.1%
Average			0.334	0.667	0.337										
Std. dev.			0.012	0.012	0.000										
COV			3.4%	1.8%	0.1%										
CT-2L7	5.6	2.55	0.438	0.632	0.420	0.1718	0.455	8,941	9,310	90	0.155	0.190	6.91E-06	8.54E-06	23.6%
CT-2L8[b]	5.6	2.80	0.437	0.678	0.449	0.1560	0.500		8,840	90					
CT-1L7	9.6	4.40	0.441	0.632	0.422	0.1003	0.458	12,603	13,131	90	0.210	0.222	6.68E-06	7.13E-06	6.8%
CT-1L8	9.6	4.80	0.435	0.678	0.447	0.0907	0.500	11,661	12,615	90	0.222	0.288	8.12E-06	1.02E-05	25.6%
Average			0.438	0.655	0.434										
Std. dev.			0.003	0.027	0.016										
COV			0.6%	4.1%	3.6%										
Average				0.664											
Std. dev.				0.016											
COV				2.4%											

[a]Values of thickness normalized to 66% fiber mass fraction

[b]Only maximum load was recorded.

Table A-8. Continued.

$K_I t(W)^{1/2}$ / P	K_{II}/K_I	$T(\pi a)^{1/2}$ / K_I	For P_Q			For P_{max}		
			K_I, ksi(in.)$^{1/2}$	K_{II}, ksi(in.)$^{1/2}$	T, ksi	K_I, ksi(in.)$^{1/2}$	K_{II}, ksi(in.)$^{1/2}$	T, ksi
9.140	0	0.630	83.5	0	18.6	94.3	0	21.0
10.199	0	0.652	91.3	0	20.1	95.9	0	21.1
9.206	0	0.632	98.0	0	16.7	100.4	0	17.1
10.199	0	0.652	101.0	0	17.0	101.0	0	17.0
			93.5	0	18.1	97.9	0	19.0
			7.8		1.6	3.3		2.3
			8.3%		8.7%	3.4%		12.2%
7.672	0	0.544	92.6	0	19.6	93.6	0	19.8
8.419	0	0.598	86.1	0	18.9	94.1	0	20.7
7.672	0	0.544	91.8	0	14.9	104.8	0	17.0
8.364	0	0.595	92.7	0	15.6	100.5	0	16.9
			90.8	0	17.2	98.3	0	18.6
			3.2		2.4	5.4		2.0
			3.5%		13.8%	5.5%		10.6%
7.672	0	0.544	86.7	0	18.4	90.2	0	19.1
8.419	0	0.598	79.7	0	17.5	86.1	0	19.0
7.672	0	0.544	91.7	0	14.8	91.7	0	14.8
8.364	0	0.595	100.1	0	16.8	102.4	0	17.2
			89.6	0	16.9	92.6	0	17.5
			8.6		1.5	6.9		2.0
			9.6%		8.9%	7.5%		11.3%
9.140	0	0.630	82.3	0	18.3	85.7	0	19.1
10.199	0	0.652				84.9	0	18.7
9.206	0	0.632	88.6	0	15.1	92.4	0	15.7
10.199	0	0.652	85.9	0	14.4	92.9	0	15.6
			85.6	0	15.9	89.0	0	17.3
			3.2		2.1	4.2	0	1.9
			3.7%		13.1%	4.8%		10.8%
			90.1	0	17.1	94.4	0	18.1
			6.3		1.9	6.1		2.0
			7.0%		10.8%	6.5%		10.9%

Table A-8. Continued.

For θ_{frac} = 0°													
$(\varepsilon_{\theta\theta(I)})_{frac.}$ Msi^{-1}	$(\varepsilon_{\theta\theta(II)})_{frac.}$ Msi^{-1}	$(\varepsilon_{r\theta(I)})_{frac.}$ Msi^{-1}	$(\varepsilon_{r\theta(II)})_{frac.}$ Msi^{-1}	$(\varepsilon_{\theta\theta(T)})_{frac.}$ Msi^{-1}	$(\varepsilon_{r\theta(T)})_{frac.}$ Msi^{-1}	For P_Q				For P_{max}			
						For $\varepsilon_{\theta\theta}$ = 0.0171		For $\varepsilon_{r\theta}$ = 0.0220		For $\varepsilon_{\theta\theta}$ = 0.0171		For $\varepsilon_{r\theta}$ = 0.0220	
						T factor	$(2\pi d_o)^{1/2}$, $(in.)^{1/2}$	T factor	$(2\pi d_o)^{1/2}$, $(in.)^{1/2}$	T factor	$(2\pi d_o)^{1/2}$, $(in.)^{1/2}$	T factor	$(2\pi d_o)^{1/2}$, $(in.)^{1/2}$
0.0624	0	0	0.403	-0.0341	0	0.964	0.294	1	0	0.960	0.330	1	0
0.0624	0	0	0.403	-0.0341	0	0.962	0.320	1	0	0.960	0.336	1	0
0.0624	0	0	0.403	-0.0341	0	0.968	0.346	1	0	0.967	0.354	1	0
0.0624	0	0	0.403	-0.0341	0	0.967	0.356	1	0	0.967	0.356	1	0
						0.965	0.329	1	0	0.963	0.344	1	0
						0.003	0.028			0.004	0.013		
						0.3%	8.5%			0.4%	3.8%		
0.0624	0	0	0.403	-0.0341	0	0.962	0.325	1	0	0.962	0.328	1	0
0.0624	0	0	0.403	-0.0341	0	0.964	0.303	1	0	0.960	0.330	1	0
0.0624	0	0	0.403	-0.0341	0	0.971	0.325	1	0	0.967	0.370	1	0
0.0624	0	0	0.403	-0.0341	0	0.970	0.328	1	0	0.967	0.355	1	0
						0.967	0.320	1	0	0.964	0.346	1	0
						0.004	0.012			0.004	0.020	1	0
						0.5%	3.7%			0.4%	5.8%	1	0
0.0624	0	0	0.403	-0.0341	0	0.965	0.305	1	0	0.963	0.317	1	0
0.0624	0	0	0.403	-0.0341	0	0.966	0.281	1	0	0.964	0.303	1	0
0.0624	0	0	0.403	-0.0341	0	0.971	0.325	1	0	0.971	0.325	1	0
0.0624	0	0	0.403	-0.0341	0	1.000	0.365	1	0	0.967	0.361	1	0
						0.975	0.319	1	0	0.966	0.326	1	0
						0.016	0.036			0.004	0.025	1	0
						1.7%	11.2%			0.4%	7.6%	1	0
0.0624	0	0	0.403	-0.0341	0	0.965	0.290	1	0	0.963	0.301	1	0
0.0624	0	0	0.403	-0.0341	0					0.964	0.299	1	0
0.0624	0	0	0.403	-0.0341	0	0.971	0.314	1	0	0.970	0.327	1	0
0.0624	0	0	0.403	-0.0341	0	0.972	0.305	1	0	0.970	0.329	1	0
						0.969	0.303	1	0	0.967	0.314	1	0
						0.004	0.012			0.003	0.016		
						0.4%	4.0%			0.4%	5.1%		
						0.969	0.319	1	0	0.965	0.333	1	0
						0.009	0.024			0.004	0.022		
						0.9%	7.5%			0.4%	6.6%		

Table A-8. Continued.

For θ_{frac} = 45°													
$(\varepsilon_{\theta\theta(I)})_{frac.}$ Msi^{-1}	$(\varepsilon_{\theta\theta(II)})_{frac.}$ Msi^{-1}	$(\varepsilon_{r\theta(I)})_{frac.}$ Msi^{-1}	$(\varepsilon_{r\theta(II)})_{frac.}$ Msi^{-1}	$(\varepsilon_{\theta\theta(T)})_{frac.}$ Msi^{-1}	$(\varepsilon_{r\theta(T)})_{frac.}$ Msi^{-1}	For P_Q				For P_{max}			
						For $\varepsilon_{\theta\theta}$ = 0.0148		For $\varepsilon_{r\theta}$ = 0.0220		For $\varepsilon_{\theta\theta}$ = 0.0148		For $\varepsilon_{r\theta}$ = 0.0220	
						T factor	$(2\pi d_o)^{1/2}$, $(in.)^{1/2}$	T factor	$(2\pi d_o)^{1/2}$, $(in.)^{1/2}$	T factor	$(2\pi d_o)^{1/2}$, $(in.)^{1/2}$	T factor	$(2\pi d_o)^{1/2}$, $(in.)^{1/2}$
0.0419	-0.193	0.0478	0.197	0.0798	-0.228	1.112	0.263	0.839	0.152	1.128	0.301	0.821	0.168
0.0419	-0.193	0.0478	0.197	0.0798	-0.228	1.121	0.290	0.828	0.164	1.128	0.307	0.821	0.171
0.0419	-0.193	0.0478	0.197	0.0798	-0.228	1.099	0.305	0.853	0.182	1.102	0.314	0.850	0.185
0.0419	-0.193	0.0478	0.197	0.0798	-0.228	1.101	0.315	0.851	0.187	1.101	0.315	0.851	0.187
						1.108	0.293	0.842	0.171	1.115	0.309	0.836	0.178
						0.010	0.023	0.012	0.016	0.016	0.006	0.017	0.010
						0.9%	7.7%	1.4%	9.3%	1.4%	2.0%	2.0%	5.4%
0.0419	-0.193	0.0478	0.197	0.0798	-0.228	1.118	0.294	0.831	0.167	1.120	0.297	0.830	0.169
0.0419	-0.193	0.0478	0.197	0.0798	-0.228	1.114	0.272	0.836	0.156	1.126	0.300	0.823	0.168
0.0419	-0.193	0.0478	0.197	0.0798	-0.228	1.087	0.283	0.867	0.173	1.101	0.327	0.851	0.194
0.0419	-0.193	0.0478	0.197	0.0798	-0.228	1.092	0.287	0.861	0.173	1.100	0.313	0.851	0.186
						1.103	0.284	0.849	0.167	1.112	0.309	0.839	0.179
						0.016	0.009	0.018	0.008	0.013	0.014	0.014	0.013
						1.4%	3.2%	2.1%	4.8%	1.2%	4.4%	1.7%	7.1%
0.0419	-0.193	0.0478	0.197	0.0798	-0.228	1.110	0.273	0.840	0.158	1.115	0.285	0.835	0.163
0.0419	-0.193	0.0478	0.197	0.0798	-0.228	1.105	0.249	0.846	0.146	1.114	0.272	0.836	0.156
0.0419	-0.193	0.0478	0.197	0.0798	-0.228	1.087	0.283	0.867	0.173	1.087	0.283	0.867	0.173
0.0419	-0.193	0.0478	0.197	0.0798	-0.228	1.100	0.312	0.852	0.185	1.102	0.320	0.849	0.189
						1.100	0.279	0.851	0.166	1.105	0.290	0.847	0.170
						0.010	0.026	0.011	0.017	0.013	0.021	0.015	0.014
						0.9%	9.3%	1.3%	10.2%	1.2%	7.2%	1.8%	8.2%
0.0419	-0.193	0.0478	0.197	0.0798	-0.228	1.110	0.259	0.841	0.150	1.115	0.271	0.835	0.155
0.0419	-0.193	0.0478	0.197	0.0798	-0.228					1.112	0.268	0.838	0.155
0.0419	-0.193	0.0478	0.197	0.0798	-0.228	1.089	0.273	0.865	0.166	1.093	0.286	0.860	0.172
0.0419	-0.193	0.0478	0.197	0.0798	-0.228	1.084	0.264	0.870	0.162	1.092	0.287	0.861	0.174
						1.094	0.265	0.859	0.160	1.103	0.278	0.848	0.164
						0.014	0.007	0.016	0.008	0.012	0.010	0.014	0.010
						1.2%	2.8%	1.8%	5.3%	1.1%	3.7%	1.6%	6.4%
						1.102	0.281	0.850	0.166	1.108	0.297	0.842	0.173
						0.012	0.019	0.014	0.012	0.013	0.019	0.015	0.012
						1.1%	6.9%	1.6%	7.5%	1.2%	6.2%	1.7%	7.1%

Table 8. Concluded.

For θ_{frac} = 90°													
$(\varepsilon_{\theta\theta(II)})_{frac.}$ Msi^{-1}	$(\varepsilon_{\theta\theta(II)})_{frac.}$ Msi^{-1}	$(\varepsilon_{r\theta(I)})_{frac.}$ Msi^{-1}	$(\varepsilon_{r\theta(II)})_{frac.}$ Msi^{-1}	$(\varepsilon_{\theta\theta(T)})_{frac.}$ Msi^{-1}	$(\varepsilon_{r\theta(T)})_{frac.}$ Msi^{-1}	For P_Q				For P_{max}			
						For $\varepsilon_{\theta\theta}$ = 0.0148		For $\gamma_{r\theta}$ = 0.0220		For $\varepsilon_{\theta\theta}$ = 0.0148		For $\gamma_{r\theta}$ = 0.0220	
						T factor	$(2\pi d_c)^{1/2}$, $(in.)^{1/2}$	T factor	$(2\pi d_c)^{1/2}$, $(in.)^{1/2}$	T factor	$(2\pi d_c)^{1/2}$, $(in.)^{1/2}$	T factor	$(2\pi d_c)^{1/2}$, $(in.)^{1/2}$
0.00810	-0.175	0.126	-0.155	0.194	0	1.322	0.060	1	0.480	1.379	0.071	1	0.542
0.00810	-0.175	0.126	-0.155	0.194	0	1.357	0.068	1	0.524	1.382	0.073	1	0.551
0.00810	-0.175	0.126	-0.155	0.194	0	1.279	0.069	1	0.563	1.288	0.071	1	0.577
0.00810	-0.175	0.126	-0.155	0.194	0	1.286	0.071	1	0.580	1.286	0.071	1	0.580
						1.311	0.067	1	0.537	1.334	0.071	1	0.562
						0.036	0.005		0.045	0.054	0.001		0.019
						2.7%	6.8%		8.3%	4.1%	1.1%		3.4%
0.00810	-0.175	0.126	-0.155	0.194	0	1.346	0.068	1	0.532	1.350	0.069	1	0.537
0.00810	-0.175	0.126	-0.155	0.194	0	1.330	0.063	1	0.494	1.372	0.071	1	0.541
0.00810	-0.175	0.126	-0.155	0.194	0	1.241	0.062	1	0.527	1.285	0.074	1	0.602
0.00810	-0.175	0.126	-0.155	0.194	0	1.256	0.064	1	0.532	1.284	0.071	1	0.577
						1.293	0.064	1	0.521	1.323	0.071	1	0.564
						0.052	0.003		0.018	0.045	0.002		0.031
						4.0%	4.2%		3.5%	3.4%	2.7%		5.5%
0.00810	-0.175	0.126	-0.155	0.194	0	1.317	0.063	1	0.498	1.333	0.066	1	0.518
0.00810	-0.175	0.126	-0.155	0.194	0	1.298	0.057	1	0.458	1.330	0.063	1	0.495
0.00810	-0.175	0.126	-0.155	0.194	0	1.241	0.062	1	0.527	1.241	0.062	1	0.527
0.00810	-0.175	0.126	-0.155	0.194	0	1.282	0.070	1	0.575	1.290	0.072	1	0.588
						1.284	0.063	1	0.514	1.299	0.066	1	0.532
						0.032	0.006		0.049	0.043	0.005		0.040
						2.5%	8.9%		9.6%	3.3%	7.0%		7.5%
0.00810	-0.175	0.126	-0.155	0.194	0	1.316	0.059	1	0.473	1.333	0.063	1	0.492
0.00810	-0.175	0.126	-0.155	0.194	0					1.324	0.062	1	0.488
0.00810	-0.175	0.126	-0.155	0.194	0	1.246	0.060	1	0.509	1.259	0.064	1	0.530
0.00810	-0.175	0.126	-0.155	0.194	0	1.233	0.058	1	0.493	1.257	6.4%	1	0.533
						1.265	0.059	1	0.492	1.293	0.063	1	0.511
						0.044	0.001		0.018	0.041	0.001		0.024
						3.5%	2.1%		3.7%	3.2%	1.7%		4.8%
						1.290	0.064	1	0.518	1.312	0.068	1	0.542
						0.040	0.005		0.036	0.045	0.004		0.035
						3.1%	7.1%		7.0%	3.4%	6.5%		6.5%

Table A–9. CT results for transverse loading.

Specimen no.	Width, W, inches	Crack length, a, inches	Thick-ness, t', inches	Fiber mass fraction	Adjusted thick-ness[a], t, inches	Thick-ness, ratio, t/a	a/W	P_Q, lbf	P_{max}, lbf	Crack path, θ_f, degrees	COD_Q, inches	COD_{max}, inches	Slope, COD t/P, psi-1		
													Initial	Final	Change
CT-2T31	5.6	2.55	0.107	0.670	0.109	0.0421	0.455	1,081	1,297	0	0.075	0.114	7.20E-06	9.60E-06	33.3%
CT-2T41	5.6	2.80	0.111	0.672	0.113	0.0395	0.500	1,144	1,212	0	0.071	0.090	6.66E-06	8.40E-06	26.0%
CT-1T31	9.6	4.40	0.106	0.670	0.108	0.0242	0.458	1,668	1,788	0	0.091	0.111	5.62E-06	6.73E-06	19.7%
CT-1T41	9.6	4.80	0.107	0.672	0.109	0.0222	0.500	1,600	1,624	0	0.106	0.118	6.96E-06	7.88E-06	13.3%
Average			0.108	0.671	0.110										
Std. dev.			0.002	0.001	0.002										
COV			1.9%	0.2%	2.0%										
CT-2T5	5.6	2.10	0.223	0.652	0.221	0.1064	0.375	3,401	3,401	0	0.081	0.081	5.23E-06	5.26E-06	0.4%
CT-2T6	5.6	2.35	0.212	0.678	0.218	0.0903	0.420	2,922	2,993	0	0.087	0.095	6.22E-06	6.91E-06	11.1%
CT-1T5	9.6	3.60	0.219	0.652	0.217	0.0610	0.375	4,138	4,721	0	0.095	0.132	4.87E-06	6.06E-06	24.4%
CT-1T6	9.6	4.00	0.215	0.678	0.221	0.0537	0.417	4,089	4,089	0	0.115	0.115	5.97E-06	6.21E-06	4.0%
Average			0.217	0.665	0.219										
Std. dev.			0.005	0.015	0.002										
COV			2.3%	2.3%	0.9%										
CT-2T11	5.6	2.10	0.343	0.656	0.341	0.1633	0.375	4,620	4,813	0	0.078	0.091	5.51E-06	6.41E-06	16.4%
CT-2T21	5.6	2.35	0.325	0.677	0.333	0.1381	0.420	3,893	4,159	0	0.082	0.095	6.64E-06	7.62E-06	14.7%
CT-1T11	9.6	3.60	0.344	0.656	0.342	0.0956	0.375	7,063	7,099	0	0.101	0.111	4.69E-06	5.36E-06	14.4%
CT-1T21	9.6	4.00	0.321	0.677	0.329	0.0803	0.417	5,877	6,107	0	0.094	0.104	5.05E-06	5.59E-06	10.8%
Average			0.333	0.667	0.336										
Std. dev.			0.010	0.012	0.006										
COV			3.1%	1.8%	1.8%										
CT-2T7	5.6	2.55	0.441	0.632	0.422	0.1729	0.455	4,503	4,983	0	0.079	0.095	7.09E-06	8.02E-06	13.2%
CT-2T8	5.6	2.80	0.434	0.678	0.446	0.1551	0.500	3,977	4,386	0	0.085	0.104	9.23E-06	1.06E-05	14.7%
CT-1T7	9.6	4.40	0.444	0.632	0.425	0.1010	0.458	6,245	6,245	0	0.104	0.104	6.85E-06	7.08E-06	3.3%
CT-1T8	9.6	4.80	0.428	0.678	0.440	0.0892	0.500	5,645	6,066	0	0.117	0.144	8.65E-06	1.05E-05	20.9%
Average			0.437	0.655	0.433										
Std. dev.			0.006	0.027	0.011										
COV			1.3%	4.1%	2.6%										
Average				0.664											
Std. dev.				0.162											
COV				24.4%											

[a]Values of thickness normalized to 66% fiber mass fraction

Table A-9. Continued.

$K_I t (W)^{1/2}$ / P	K_{II}/K_I	$T(\pi a)^{1/2}$ / K_I	For P_Q			For P_{max}		
			K_I, ksi(in.)$^{1/2}$	K_{II}, ksi(in.)$^{1/2}$	T, ksi	K_I, ksi(in.)$^{1/2}$	K_{II}, ksi(in.)$^{1/2}$	T, ksi
8.073	0	0.572	34.4	0	7.0	41.3	0	8.3
9.252	0	0.613	40.4	0	8.3	42.8	0	8.8
8.145	0	0.575	41.2	0	6.4	44.1	0	6.8
9.252	0	0.613	44.8	0	7.1	45.5	0	7.2
			40.2	0	7.2	43.4	0	7.8
			4.3		0.8	1.8		0.9
			10.8%		11.6%	4.2%		12.2%
6.483	0	0.465	41.7	0	7.5	41.7	0	7.5
7.283	0	0.530	42.4	0	8.3	43.4	0	8.5
6.483	0	0.465	39.5	0	5.5	45.0	0	6.2
7.223	0	0.526	44.4	0	6.6	44.4	0	6.6
			42.0	0	7.0	43.6	0	7.2
			2.0		1.2	1.4		1.0
			4.9%		17.5%	3.3%		14.0%
6.483	0	0.465	36.9	0	6.7	38.5	0	7.0
7.283	0	0.530	36.9	0	7.2	39.4	0	7.7
6.483	0	0.465	42.9	0	5.9	43.2	0	6.0
7.223	0	0.526	42.7	0	6.3	44.3	0	6.6
			39.9	0	6.5	41.4	0	6.8
			3.4		0.5	2.8		0.7
			8.5%		8.2%	6.9%		10.6%
8.073	0	0.572	34.8	0	7.0	38.6	0	7.8
9.252	0	0.613	35.8	0	7.4	39.5	0	8.2
8.145	0	0.575	37.0	0	5.7	37.0	0	5.7
9.252	0	0.613	39.4	0	6.2	42.3	0	6.7
			36.7	0	6.6	39.3	0	7.1
			2.0		0.8	2.2		1.1
			5.3%		11.6%	5.7%		15.6%
			39.7	0	6.8	41.9	0	7.2
			3.4		0.8	2.6		0.9
			8.5%		12.1%	6.3%		13.0%

Table A-9. Continued.

For θ_{frac} = 0°												
$(\varepsilon_{\theta\theta(I)})_{frac.}$ Msi^{-1}	$(\varepsilon_{\theta\theta(II)})_{frac.}$ Msi^{-1}	$(\varepsilon_{r\theta(I)})_{frac.}$ Msi^{-1}	$(\varepsilon_{r\theta(II)})_{frac.}$ Msi^{-1}	$(\varepsilon_{\theta\theta(T)})_{frac.}$ Msi^{-1}	$(\varepsilon_{r\theta(T)})_{frac.}$ Msi^{-1}	For P_Q				For P_{max}			
						For $\varepsilon_{\theta\theta}$ = 0.0148		For $\varepsilon_{r\theta}$ = 0.0220		For $\varepsilon_{\theta\theta}$ = 0.0148		For $\varepsilon_{r\theta}$ = 0.0220	
						T - factor	$(2\pi d_o)^{1/2}$, $(in.)^{1/2}$	T - factor	$(2\pi d_o)^{1/2}$, $(in.)^{1/2}$	T - factor	$(2\pi d_o)^{1/2}$, $(in.)^{1/2}$	T - factor	$(2\pi d_o)^{1/2}$, $(in.)^{1/2}$
0.142	0	0	0.403	-0.0341	0	0.984	0.325	1	0	0.981	0.389	1	0
0.142	0	0	0.403	-0.0341	0	0.981	0.381	1	0	0.980	0.403	1	0
0.142	0	0	0.403	-0.0341	0	0.986	0.390	1	0	0.985	0.418	1	0
0.142	0	0	0.403	-0.0341	0	0.984	0.424	1	0	0.984	0.430	1	0
						0.984	0.380	1	0	0.982	0.410	1	0
						0.002	0.041			0.002	0.018		
						0.2%	10.8%			0.2%	4.3%		
0.142	0	0	0.403	-0.0341	0	0.912	0.366	1	0	0.983	0.394	1	0
0.142	0	0	0.403	-0.0341	0	0.911	0.371	1	0	0.981	0.409	1	0
0.142	0	0	0.403	-0.0341	0	0.917	0.348	1	0	0.986	0.427	1	0
0.142	0	0	0.403	-0.0341	0	0.907	0.387	1	0	0.985	0.420	1	0
						0.912	0.368	1	0	0.984	0.413	1	0
						0.004	0.016			0.002	0.014		
						0.4%	4.4%			0.2%	3.5%		
0.142	0	0	0.403	-0.0341	0	0.985	0.350	1	0	0.984	0.364	1	0
0.142	0	0	0.403	-0.0341	0	0.984	0.349	1	0	0.983	0.373	1	0
0.142	0	0	0.403	-0.0341	0	0.987	0.407	1	0	0.986	0.409	1	0
0.142	0	0	0.403	-0.0341	0	0.986	0.404	1	0	0.985	0.420	1	0
						0.985	0.378	1	0	0.985	0.391	1	0
						0.001	0.033			0.002	0.027		
						0.1%	8.6%			0.2%	7.0%		
0.142	0	0	0.403	-0.0341	0	0.984	0.330	1	0	0.982	0.364	1	0
0.142	0	0	0.403	-0.0341	0	0.983	0.338	1	0	0.982	0.373	1	0
0.142	0	0	0.403	-0.0341	0	0.987	0.351	1	0	0.987	0.351	1	0
0.142	0	0	0.403	-0.0341	0	0.986	0.373	1	0	0.985	0.401	1	0
						0.985	0.348	1	0	0.984	0.372	1	0
						0.002	0.019			0.002	0.021		
						0.2%	5.4%			0.3%	5.7%		
						0.966	0.368	1	0	0.984	0.397	1	0
						0.033	0.029			0.002	0.025		
						3.4%	7.9%			0.2%	6.3%		

Table A-9. Continued.

For θ_{frac} = 45°													
$(\varepsilon_{\theta\theta(I)})_{frac}$, Msi^{-1}	$(\varepsilon_{\theta\theta(II)})_{frac}$, Msi^{-1}	$(\varepsilon_{r\theta(I)})_{frac}$, Msi^{-1}	$(\varepsilon_{r\theta(II)})_{frac}$, Msi^{-1}	$(\varepsilon_{\theta\theta(T)})_{frac}$, Msi^{-1}	$(\varepsilon_{r\theta(T)})_{frac}$, Msi^{-1}	For P_Q				For P_{max}			
						For $\varepsilon_{\theta\theta}$ = 0.0148		For $\varepsilon_{r\theta}$ = 0.0220		For $\varepsilon_{\theta\theta}$ = 0.0148		For $\varepsilon_{r\theta}$ = 0.0220	
						T - factor	$(2\pi d_o)^{1/2}$, $(in.)^{1/2}$	T - factor	$(2\pi d_o)^{1/2}$, $(in.)^{1/2}$	T - factor	$(2\pi d_o)^{1/2}$, $(in.)^{1/2}$	T - factor	$(2\pi d_o)^{1/2}$, $(in.)^{1/2}$
0.0947	-0.122	0.1883	0.153	0.0254	-0.119	1.012	0.223	0.964	0.284	1.015	0.268	0.957	0.338
0.0947	-0.122	0.1883	0.153	0.0254	-0.119	1.015	0.262	0.957	0.331	1.015	0.278	0.954	0.349
0.0947	-0.122	0.1883	0.153	0.0254	-0.119	1.011	0.266	0.967	0.341	1.012	0.286	0.964	0.364
0.0947	-0.122	0.1883	0.153	0.0254	-0.119	1.012	0.290	0.963	0.369	1.012	0.295	0.963	0.375
						1.013	0.260	0.963	0.331	1.014	0.281	0.960	0.357
						0.001	0.028	0.004	0.036	0.002	0.011	0.005	0.016
						0.1%	10.8%	0.4%	10.8%	0.2%	4.0%	0.5%	4.5%
0.0947	-0.122	0.1883	0.153	0.0254	-0.119	1.013	0.270	0.961	0.343	1.013	0.270	0.961	0.343
0.0947	-0.122	0.1883	0.153	0.0254	-0.119	1.014	0.275	0.957	0.347	1.015	0.282	0.956	0.355
0.0947	-0.122	0.1883	0.153	0.0254	-0.119	1.009	0.255	0.971	0.328	1.011	0.291	0.967	0.373
0.0947	-0.122	0.1883	0.153	0.0254	-0.119	1.011	0.287	0.966	0.367	1.011	0.287	0.966	0.367
						1.012	0.272	0.964	0.346	1.013	0.283	0.963	0.359
						0.002	0.013	0.006	0.016	0.002	0.009	0.005	0.013
						0.2%	4.9%	0.6%	4.6%	0.2%	3.2%	0.5%	3.7%
0.0947	-0.122	0.1883	0.153	0.0254	-0.119	1.012	0.239	0.965	0.305	1.012	0.249	0.964	0.317
0.0947	-0.122	0.1883	0.153	0.0254	-0.119	1.013	0.239	0.963	0.304	1.013	0.256	0.960	0.324
0.0947	-0.122	0.1883	0.153	0.0254	-0.119	1.010	0.277	0.969	0.356	1.010	0.279	0.969	0.358
0.0947	-0.122	0.1883	0.153	0.0254	-0.119	1.011	0.276	0.967	0.353	1.011	0.287	0.966	0.367
						1.011	0.258	0.966	0.330	1.012	0.268	0.965	0.341
						0.001	0.022	0.003	0.029	0.001	0.018	0.004	0.024
						0.1%	8.4%	0.3%	8.8%	0.1%	6.8%	0.4%	7.1%
0.0947	-0.122	0.1883	0.153	0.0254	-0.119	1.012	0.226	0.963	0.287	1.014	0.250	0.960	0.317
0.0947	-0.122	0.1883	0.153	0.0254	-0.119	1.013	0.232	0.962	0.295	1.014	0.256	0.958	0.324
0.0947	-0.122	0.1883	0.153	0.0254	-0.119	1.010	0.239	0.970	0.307	1.010	0.239	0.970	0.307
0.0947	-0.122	0.1883	0.153	0.0254	-0.119	1.011	0.255	0.967	0.326	1.012	0.274	0.965	0.350
						1.011	0.238	0.966	0.304	1.012	0.255	0.963	0.324
						0.001	0.012	0.004	0.017	0.002	0.015	0.006	0.018
						0.1%	5.2%	0.4%	5.6%	0.2%	5.8%	0.6%	5.6%
						1.012	0.257	0.964	0.328	1.013	0.272	0.962	0.345
						0.001	0.022	0.004	0.028	0.002	0.017	0.005	0.022
						0.1%	8.5%	0.4%	8.5%	0.2%	6.3%	0.5%	6.4%

Table 9. Concluded.

For θ_{frac} = 90°													
$(\varepsilon_{\theta\theta(I)})_{frac.}$, Msi^{-1}	$(\varepsilon_{\theta\theta(II)})_{frac.}$, Msi^{-1}	$(\varepsilon_{r\theta(I)})_{frac.}$, Msi^{-1}	$(\varepsilon_{r\theta(II)})_{frac.}$, Msi^{-1}	$(\varepsilon_{\theta\theta(T)})_{frac.}$, Msi^{-1}	$(\varepsilon_{r\theta(T)})_{frac.}$, Msi^{-1}	For P_Q				For P_{max}			
						For $\varepsilon_{\theta\theta}$ = 0.0171		For $\gamma_{r\theta}$ = 0.0220		For $\varepsilon_{\theta\theta}$ = 0.0171		For $\gamma_{r\theta}$ = 0.0220	
						T - factor	$(2\pi d_c)^{1/2}$, $(in.)^{1/2}$	T - factor	$(2\pi d_c)^{1/2}$, $(in.)^{1/2}$	T - factor	$(2\pi d_c)^{1/2}$, $(in.)^{1/2}$	T - factor	$(2\pi d_c)^{1/2}$, $(in.)^{1/2}$
0.0066	-0.094	0.155	-0.126	0.085	0	1.036	0.0137	1	0.243	1.043	0.0166	1	0.291
0.0066	-0.094	0.155	-0.126	0.085	0	1.043	0.0163	1	0.285	1.046	0.0173	1	0.302
0.0066	-0.094	0.155	-0.126	0.085	0	1.033	0.0164	1	0.291	1.035	0.0176	1	0.312
0.0066	-0.094	0.155	-0.126	0.085	0	1.036	0.0179	1	0.316	1.037	0.0182	1	0.321
						1.037	0.016	1	0.284	1.040	0.0174	1	0.306
						0.004	0.002		0.031	0.005	0.001		0.013
						0.4%	10.8%		10.8%	0.5%	3.8%		4.2%
0.0066	-0.094	0.155	-0.126	0.085	0	1.039	0.0167	1	0.294	1.039	0.0167	1	0.294
0.0066	-0.094	0.155	-0.126	0.085	0	1.043	0.0170	1	0.299	1.044	0.0175	1	0.306
0.0066	-0.094	0.155	-0.126	0.085	0	1.028	0.0156	1	0.278	1.032	0.0179	1	0.318
0.0066	-0.094	0.155	-0.126	0.085	0	1.034	0.0177	1	0.313	1.034	0.0177	1	0.313
						1.036	0.017	1	0.296	1.037	0.0174	1	0.308
						0.006	0.001		0.014	0.005	0.001		0.010
						0.6%	5.1%		4.9%	0.5%	3.0%		3.3%
0.0066	-0.094	0.155	-0.126	0.085	0	1.034	0.0147	1	0.261	1.036	0.0154	1	0.271
0.0066	-0.094	0.155	-0.126	0.085	0	1.037	0.0148	1	0.261	1.040	0.0158	1	0.278
0.0066	-0.094	0.155	-0.126	0.085	0	1.030	0.0171	1	0.303	1.031	0.0171	1	0.305
0.0066	-0.094	0.155	-0.126	0.085	0	1.032	0.0170	1	0.301	1.034	0.0177	1	0.313
						1.034	0.016	1	0.281	1.035	0.0165	1	0.292
						0.003	0.001		0.024	0.004	0.001		0.020
						0.3%	8.3%		8.5%	0.4%	6.6%		6.9%
0.0066	-0.094	0.155	-0.126	0.085	0	1.036	0.0139	1	0.246	1.040	0.0155	1	0.272
0.0066	-0.094	0.155	-0.126	0.085	0	1.038	0.0143	1	0.253	1.042	0.0159	1	0.279
0.0066	-0.094	0.155	-0.126	0.085	0	1.029	0.0147	1	0.261	1.029	0.0147	1	0.261
0.0066	-0.094	0.155	-0.126	0.085	0	1.032	0.0157	1	0.278	1.034	0.0169	1	0.299
						1.034	0.0146	1	0.259	1.037	0.0157	1	0.278
						0.004	0.001		0.014	0.006	0.001		0.016
						0.4%	5.1%		5.3%	0.6%	5.8%		5.7%
						1.035	0.0158	1	0.280	1.037	0.0168	1	0.296
						0.004	0.001		0.024	0.005	0.001		0.019
						0.4%	8.5%		8.5%	0.5%	6.2%		6.3%

Table A–10. CT results for bias loading.

Specimen no.	Material Direction θ_{fiber}, degrees	Width, W, inches	Crack length, a, inches	Thick-ness, t', inches	Fiber mass fraction	Adjusted thick-ness[a], t, inches	Thick-ness, ratio, t/a	a/W	P_Q, lbf	P_{max}, lbf	Crack path, $\theta_{fracture}$, degrees	COD_Q, inches	COD_{max}, inches	Slope, COD t/P, psi-1		
														Initial	Final	Change
CT-2LT5-45	45	5.6	2.10	0.218	0.652	0.216	0.1027	0.375	3,956	4,319	45	0.095	0.110	5.09E-06	5.49E-06	7.9%
CT-2LT6-45	-45	5.6	2.35	0.213	0.678	0.218	0.0929	0.420	3,224	3,821	-45	0.091	0.118	6.09E-06	6.74E-06	10.7%
CT-2LT5-135	-45	5.6	2.10	0.219	0.652	0.217	0.1032	0.375	3,865	3,956	-45	0.094	0.110	5.08E-06	6.04E-06	18.9%
CT-2LT6-135	45	5.6	2.35	0.212	0.678	0.218	0.0929	0.420	3,520	3,906	45	0.101	0.122	5.98E-06	6.84E-06	14.5%
Average				0.216	0.665	0.217										
Std. dev.				0.004	0.015	0.001										
COV				1.7%	2.3%	0.6%										
CT-2LT7-45	-45	5.6	2.55	0.455	0.652	0.449	0.1762	0.455	4,809	5,523	-45	0.080	0.111	7.25E-06	9.07E-06	25.1%
CT-2LT8-45	-45	5.6	2.80	0.423	0.678	0.435	0.1553	0.500	4,580	5,199	-45	0.093	0.133	8.61E-06	1.11E-05	28.8%
CT-2LT7-135	45	5.6	2.55	0.453	0.652	0.448	0.1755	0.455	5,574	5,909	45	0.096	0.117	7.37E-06	8.83E-06	19.7%
CT-2LT8-135	45	5.6	2.80	0.425	0.678	0.436	0.1558	0.500	4,901	5,358	45	0.104	0.118	8.79E-06	9.60E-06	9.2%
Average				0.439	0.665	0.442										
Std. dev.				0.017	0.015	0.008										
COV				4.0%	2.3%	1.7%										
Average					0.665											
Std. dev.					0.014											
COV					2.1%											

[a]Values of thickness normalized to 66% fiber mass fraction

[b]Strain is negative.

[c]T-strain changes sign with bias direction

[d]Statistics taken on absolute value of data

Table A-10. Continued.

$K_I t(W)^{1/2}$ / P	K_{II}/K_I	$T(\pi a)^{1/2}$ / K_I	For P_Q			For P_{max}		
			K_I, ksi(in.)$^{1/2}$	K_{II}^d, ksi(in.)$^{1/2}$	T, ksi	K_I, ksi(in.)$^{1/2}$	K_{II}^d, ksi(in.)$^{1/2}$	T, ksi
6.879	0.111	0.293	53.3	5.9	6.1	58.2	6.5	6.6
7.669	-0.110	0.327	47.9	-5.3	5.8	56.7	-6.3	6.8
6.879	-0.111	0.293	51.8	-5.8	5.9	53.0	-5.9	6.0
7.669	0.110	0.327	52.3	5.8	6.3	58.0	6.4	7.0
			51.3	5.7	6.0	56.5	6.3	6.6
			2.386	0.279	0.228	2.398	0.257	0.408
			4.7%	4.9%	3.8%	4.2%	4.1%	6.2%
8.448	-0.110	0.344	38.2	-4.2	4.6	43.9	-4.8	5.3
9.609	-0.109	0.354	42.8	-4.7	5.1	48.5	-5.3	5.8
8.448	0.110	0.344	44.5	4.9	5.4	47.1	5.2	5.7
9.609	0.109	0.354	45.6	5.0	5.5	49.9	5.4	6.0
			42.8	4.7	5.2	47.4	5.2	5.7
			3.259	0.348	0.371	2.579	0.265	0.265
			7.6%	7.4%	7.2%	5.4%	5.1%	4.6%
			47.0	5.2	5.6	51.9	5.7	6.2
			5.280	0.617	0.538	5.400	0.630	0.583
			11.2%	11.9%	9.6%	10.4%	11.0%	9.5%

Table A-10. Continued.

For $\theta_{frac} = 0°$												
$(\varepsilon_{\theta\theta(I)})_{frac.}$ Msi^{-1}	$(\varepsilon_{\theta\theta(II)})_{frac.}$ Msi^{-1}	$(\varepsilon_{r\theta(I)})_{frac.}$ Msi^{-1}	$(\varepsilon_{r\theta(II)})_{frac.}$ Msi^{-1}	$(\varepsilon_{\theta\theta(T)})_{frac.}$ Msi^{-1}	$(\varepsilon_{r\theta(T)})_{frac.}$ Msi^{-1}	For P_Q				For P_{max}			
						For $\varepsilon_{\theta\theta} = 0.0148$		For $\varepsilon_{r\theta} = 0.0220$		For $\varepsilon_{\theta\theta} = 0.0148$		For $\varepsilon_{r\theta} = 0.0220$	
						T - factor	$(2\pi d_o)^{1/2}$, $(in.)^{1/2}$	T - $factor^{cd}$	$(2\pi d_o)^{1/2}$, $(in.)^{1/2}$	T - factor	$(2\pi d_o)^{1/2}$, $(in.)^{1/2}$	T - $factor^{cd}$	$(2\pi d_o)^{1/2}$, $(in.)^{1/2}$
0.109	-0.0715	-0.105	0.328	-0.0482	-0.0544	0.981	0.356	-1.015	0.168	0.979	0.388	-1.017	0.184
0.109	0.0715	0.105	0.328	-0.0482	0.0544	0.982	0.320	1.014	0.152	0.978	0.378	1.017	0.180
0.109	0.0715	0.105	0.328	-0.0482	0.0544	0.981	0.346	1.015	0.164	0.981	0.354	1.015	0.167
0.109	-0.0715	-0.105	0.328	-0.0482	-0.0544	0.980	0.349	-1.016	0.166	0.978	0.386	-1.018	0.184
						0.981	0.343	1.015	0.162	0.979	0.377	1.017	0.179
						0.001	0.016	0.001	0.007	0.001	0.016	0.001	0.008
						0.1%	4.6%	0.1%	4.6%	0.1%	4.1%	0.1%	4.4%
0.109	0.0715	0.105	0.328	-0.0482	0.0544	0.985	0.257	1.012	0.121	0.983	0.294	1.013	0.139
0.109	0.0715	0.105	0.328	-0.0482	0.0544	0.984	0.287	1.013	0.136	0.981	0.325	1.015	0.155
0.109	-0.0715	-0.105	0.328	-0.0482	-0.0544	0.983	0.298	-1.014	0.141	0.982	0.315	-1.014	0.150
0.109	-0.0715	-0.105	0.328	-0.0482	-0.0544	0.983	0.306	-1.014	0.145	0.981	0.334	-1.015	0.159
						0.983	0.287	1.013	0.136	0.982	0.317	1.014	0.151
						0.001	0.022	1.013	0.011	0.001	0.017	1.014	0.009
						0.1%	7.5%	100.0%	7.8%	0.1%	5.4%	100.0%	5.7%
						0.982	0.315	1.014	0.149	0.980	0.347	1.015	0.165
						0.002	0.035	0.001	0.016	0.002	0.035	0.001	0.017
						0.2%	11.0%	0.1%	11.0%	0.2%	10.2%	0.1%	10.2%

Table A-10. Continued.

For $\theta_{frac} = 45°$ when $\theta_{fiber} = 45°$ or $\theta_{frac} = -45°$ when $\theta_{fiber} = -45°$													
$(\varepsilon_{\theta\theta(I)})_{frac.}$ Msi^{-1}	$(\varepsilon_{\theta\theta(II)})_{frac.}$ Msi^{-1}	$(\varepsilon_{r\theta(I)})_{frac.}$ Msi^{-1}	$(\varepsilon_{r\theta(II)})_{frac.}$ Msi^{-1}	$(\varepsilon_{\theta\theta(T)})_{frac.}$ Msi^{-1}	$(\varepsilon_{r\theta(T)})_{frac.}$ Msi^{-1}	For P_Q				For P_{max}			
						For $\varepsilon_{\theta\theta} = 0.0148$		For $\varepsilon_{r\theta} = 0.0220$		For $\varepsilon_{\theta\theta} = 0.0148$		For $\varepsilon_{r\theta} = 0.0220$	
						T - factor	$(2\pi d_o)^{1/2}$, $(in.)^{1/2}$	T - factor^{cd}	$(2\pi d_o)^{1/2}$, $(in.)^{1/2}$	T - factor	$(2\pi d_o)^{1/2}$, $(in.)^{1/2}$	T - factor^{cd}	$(2\pi d_o)^{1/2}$, $(in.)^{1/2}$
0.1109	-0.1850	0.109	0.167	0.0798	0.202	1.034	0.336	1.059	0.328	1.037	0.368	1.065	0.360
0.1109	0.1850	-0.109	0.167	0.0798	0.202	1.032	0.302	-0.950	0.264	1.038	0.360	-0.941	0.310
0.1109	0.1850	-0.109	0.167	0.0798	0.202	1.033	0.327	-0.949	0.285	1.034	0.335	-0.947	0.292
0.1109	-0.1850	0.109	0.167	0.0798	0.202	1.035	0.331	1.061	0.322	1.039	0.369	1.068	0.360
						1.033	0.324	1.005	0.300	1.037	0.358	1.005	0.330
						0.001	0.015	0.064	0.030	0.002	0.016	0.071	0.035
						0.1%	4.7%	6.4%	10.2%	0.2%	4.5%	7.0%	10.5%
0.1109	0.1850	-0.109	0.167	0.0798	0.202	1.026	0.240	-0.959	0.212	1.030	0.277	-0.953	0.242
0.1109	0.1850	-0.109	0.167	0.0798	0.202	1.028	0.270	-0.955	0.237	1.032	0.307	-0.950	0.267
0.1109	-0.1850	0.109	0.167	0.0798	0.202	1.030	0.280	1.052	0.271	1.032	0.298	1.055	0.288
0.1109	-0.1850	0.109	0.167	0.0798	0.202	1.030	0.288	1.053	0.278	1.033	0.316	1.058	0.305
						1.029	0.270	1.005	0.250	1.032	0.299	1.004	0.276
						0.002	0.021	0.055	0.031	0.002	0.017	0.061	0.027
						0.2%	7.9%	5.5%	12.3%	0.1%	5.7%	6.1%	9.9%
						1.031	0.297	1.005	0.275	1.034	0.329	1.005	0.303
						0.003	0.034	0.055	0.039	0.003	0.035	0.061	0.041
						0.3%	11.4%	5.5%	14.2%	0.3%	10.6%	6.1%	13.6%

Table A-10. Continued.

For $\theta_{frac} = 90°$ when $\theta_{fiber} = 45°$ or $\theta_{frac} = -90°$ when $\theta_{fiber} = -45°$													
$(\varepsilon_{\theta\theta(I)})_{frac.}$ Msi^{-1}	$(\varepsilon_{\theta\theta(II)})_{frac.}$ Msi^{-1}	$(\varepsilon_{r\theta(I)})_{frac.}$ Msi^{-1}	$(\varepsilon_{r\theta(II)})_{frac.}$ Msi^{-1}	$(\varepsilon_{\theta\theta(T)})_{frac.}$ Msi^{-1}	$(\varepsilon_{r\theta(T)})_{frac.}$ Msi^{-1}	For P_Q				For P_{max}			
						For $\varepsilon_{\theta\theta} = 0.0148$		For $\varepsilon_{r\theta} = 0.0220$		For $\varepsilon_{\theta\theta} = 0.0148$		For $\varepsilon_{r\theta} = 0.0220$	
						T - factor	$(2\pi d_o)^{1/2}$, $(in.)^{1/2}$	T - factor^{cd}	$(2\pi d_o)^{1/2}$, $(in.)^{1/2}$	T - factor	$(2\pi d_c)^{1/2}$, $(in.)^{1/2}$	T - factor^{cd}	$(2\pi d_o)^{1/2}$, $(in.)^{1/2}$
0.0414	-0.140	0.1870	-0.1870	0.153	0.0544	1.067	0.099	1.015	0.409	1.074	0.100	1.017	0.447
0.0414	0.139	-0.1870	-0.1870	0.153	-0.0544	1.063	0.090	-1.014	0.367	1.076	0.091	-1.017	0.436
0.0414	0.139	-0.1870	-0.1870	0.153	-0.0544	1.065	0.097	-1.015	0.397	1.067	0.097	-1.015	0.407
0.0414	-0.140	0.1870	-0.1870	0.153	0.0544	1.070	0.098	1.016	0.401	1.078	0.099	1.018	0.446
						1.066	0.096	1.015	0.394	1.074	0.097	1.017	0.434
						0.003	0.004	0.001	0.018	0.005	0.004	0.001	0.019
						0.3%	4.5%	0.1%	4.7%	0.5%	4.3%	0.1%	4.4%
0.0414	0.139	-0.1870	-0.1870	0.153	-0.0544	1.051	0.071	-1.012	0.292	1.059	0.072	-1.013	0.336
0.0414	0.139	-0.1870	-0.1870	0.153	-0.0544	1.056	0.080	-1.013	0.328	1.064	0.081	-1.015	0.373
0.0414	-0.140	0.1870	-0.1870	0.153	0.0544	1.059	0.083	1.014	0.341	1.063	0.083	1.014	0.362
0.0414	-0.140	0.1870	-0.1870	0.153	0.0544	1.060	0.086	1.014	0.350	1.066	0.086	1.015	0.383
						1.056	0.080	1.013	0.328	1.063	0.080	1.014	0.364
						0.004	0.006	0.001	0.025	0.003	0.006	0.001	0.020
						0.4%	7.9%	0.1%	7.7%	0.3%	7.8%	0.1%	5.6%
						1.061	0.088	1.014	0.361	1.068	0.089	1.015	0.399
						0.006	0.010	0.001	0.041	0.007	0.010	0.001	0.042
						0.6%	11.3%	0.1%	11.3%	0.6%	11.3%	0.1%	10.5%

Table A-10. Continued.

For θ_{frac} = -45° when θ_{fiber} = 45° or θ_{frac} = -45° when θ_{fiber} = -45°													
$(\varepsilon_{\theta\theta(I)})_{frac.}$ Msi^{-1}	$(\varepsilon_{\theta\theta(II)})_{frac.}$ Msi^{-1}	$(\varepsilon_{r\theta(I)})_{frac.}$ Msi^{-1}	$(\varepsilon_{r\theta(II)})_{frac.}$ Msi^{-1}	$(\varepsilon_{\theta\theta(T)})_{frac.}$ Msi^{-1}	$(\varepsilon_{r\theta(T)})_{frac.}$ Msi^{-1}	For P_Q				For P_{max}			
						For $\varepsilon_{\theta\theta}$ = 0.0171		For $\varepsilon_{r\theta}$ = 0.0220		For $\varepsilon_{\theta\theta}$ = 0.0171		For $\varepsilon_{r\theta}$ = 0.0220	
						T - factor	$(2\pi d_o)^{1/2}$, $(in.)^{1/2}$	T - $factor^{cd}$	$(2\pi d_o)^{1/2}$, $(in.)^{1/2}$	T - factor	$(2\pi d_o)^{1/2}$, $(in.)^{1/2}$	T - $factor^{cd}$	$(2\pi d_o)^{1/2}$, $(in.)^{1/2}$
0.035	-0.095	0.157	0.230	0.0254	-0.202	1.009	0.076	0.947	0.419	1.010	0.083	0.943	0.455
0.035	0.095	-0.157	0.230	0.0254	0.020	1.009	0.069	-0.995	0.394	1.010	0.082	-0.994	0.467
0.035	0.095	-0.157	0.230	0.0254	0.020	1.009	0.074	-0.995	0.427	1.009	0.076	-0.994	0.437
0.035	-0.095	0.157	0.230	0.0254	-0.202	1.009	0.075	0.945	0.409	1.010	0.083	0.940	0.452
						1.009	0.074	0.971	0.412	1.010	0.081	0.968	0.453
						0.000	0.003	0.028	0.014	0.001	0.004	0.031	0.012
						0.0%	4.6%	2.9%	3.4%	0.1%	4.4%	3.2%	2.7%
0.035	0.095	-0.157	0.230	0.0254	0.020	1.007	0.063	-0.996	0.315	1.008	0.063	-0.995	0.361
0.035	0.095	-0.157	0.230	0.0254	0.020	1.008	0.070	-0.995	0.352	1.009	0.070	-0.995	0.399
0.035	-0.095	0.157	0.230	0.0254	-0.202	1.008	0.068	0.953	0.351	1.009	0.068	0.950	0.371
0.035	-0.095	0.157	0.230	0.0254	-0.202	1.008	0.072	0.952	0.359	1.009	0.072	0.948	0.391
						1.008	0.068	0.974	0.344	1.009	0.068	0.972	0.380
						0.001	0.004	0.025	0.020	0.000	0.004	0.026	0.018
						0.1%	5.6%	2.5%	5.8%	0.0%	5.6%	2.7%	4.6%
						1.008	0.071	0.972	0.378	1.009	0.075	0.970	0.417
						0.001	0.004	0.025	0.040	0.001	0.008	0.027	0.041
						0.1%	6.2%	2.5%	10.5%	0.1%	10.2%	2.7%	9.9%

Table A–11. Calculations for t/a=0.10.

Specimen Type	Loading direction	Thickness ratio, t/a	Calculated for P_Q[a]								
			$x_{0(I)}$ ksi(in.)$^{1/2}$	$x_{1(I)}$ ksi(in.)$^{1/2}$	K_I, ksi(in.)$^{1/2}$	$x_{0(II)}$ ksi(in.)$^{1/2}$	$x_{1(II)}$ ksi(in.)$^{1/2}$	K_{II}, ksi(in.)$^{1/2}$	$x_{0(T)}$ ksi	$x_{1(T)}$ ksi	T_s, ksi
CNT	Longitudinal	0.1	25.850	-59.940	85.790	0	0	0	-8.433	15.440	-23.873
ECT	Longitudinal	0.1	83.45	-10.010	93.460	0	0	0	0.975	-2.317	3.292
CT	Longitudinal	0.1	73.4	-14.660	88.060	0	0	0	17.330	-0.191	17.521
CNT	Transverse	0.1	41.390	2.090	39.300	0	0	0	-24.280	-2.759	-21.521
ECT	Transverse	0.1	32.7	-6.211	38.911	0	0	0	0.257	-1.739	1.996
CT	Transverse	0.1	32.91	-6.056	38.966	0	0	0	6.798	0.018	6.780
CT	Bias (+45°)	0.1	14.59	-36.240	50.830	1.424	-4.216	5.640	2.151	-3.837	5.988

[a] $y=x_o + x_1 \log(t/a)$

Table A-11. Continued.

For $\theta_{frac} = 0°$									
$(\varepsilon_{\theta\theta(I)})_{frac}$, Msi^{-1}	$(\varepsilon_{\theta\theta(II)})_{frac}$, Msi^{-1}	$(\varepsilon_{r\theta(I)})_{frac}$, Msi^{-1}	$(\varepsilon_{r\theta(II)})_{frac}$, Msi^{-1}	$(\varepsilon_{\theta\theta(T)})_{frac}$, Msi^{-1}	$(\varepsilon_{r\theta(T)})_{frac}$, Msi^{-1}	For $\varepsilon_{\theta\theta} = \varepsilon_u$		For $\varepsilon_{r\theta} = 0.0220$	
						T factor	$(2\pi d_o)^{1/2}$, $(in.)^{1/2}$	T factor	$(2\pi d_o)^{1/2}$, $(in.)^{1/2}$
0.0624	0	0	0.403	-0.0341	0	1.050	0.329	1	0
0.0624	0	0	0.403	-0.0341	0	0.993	0.339	1	0
0.0624	0	0	0.403	-0.0341	0	0.966	0.310	1	0
0.142	0	0	0.403	-0.0341	0	1.052	0.397	1	0
0.142	0	0	0.403	-0.0341	0	0.995	0.372	1	0
0.142	0	0	0.403	-0.0341	0	0.985	0.369	1	0
0.109	-0.0715	-0.105	0.328	-0.0482	-0.0544	0.981	0.340	-1.015	0.161

Table A-11. Continued.

For θ_{frac} = 45°									
$(\varepsilon_{\theta\theta(I)})_{frac}$, Msi^{-1}	$(\varepsilon_{\theta\theta(II)})_{frac}$, Msi^{-1}	$(\varepsilon_{r\theta(I)})_{frac}$, Msi^{-1}	$(\varepsilon_{r\theta(II)})_{frac}$, Msi^{-1}	$(\varepsilon_{\theta\theta(T)})_{frac}$, Msi^{-1}	$(\varepsilon_{r\theta(T)})_{frac}$, Msi^{-1}	For $\varepsilon_{\theta\theta} = \varepsilon_u$		For $\varepsilon_{r\theta} = 0.0220$	
						T factor	$(2\pi d_o)^{1/2}$, $(in.)^{1/2}$	T factor	$(2\pi d_o)^{1/2}$, $(in.)^{1/2}$
0.0419	-0.193	0.0478	0.197	0.0798	-0.228	0.886	0.215	1.328	0.247
0.0419	-0.193	0.0478	0.197	0.0798	-0.228	1.018	0.270	0.967	0.196
0.0419	-0.193	0.0478	0.197	0.0798	-0.228	1.104	0.276	0.846	0.162
0.0947	-0.122	0.1883	0.153	0.0254	-0.119	0.964	0.242	1.132	0.381
0.0947	-0.122	0.1883	0.153	0.0254	-0.119	1.003	0.250	0.989	0.330
0.0947	-0.122	0.1883	0.153	0.0254	-0.119	1.012	0.252	0.965	0.322
0.1109	-0.185	0.1092	0.167	0.0798	-0.202	1.029	0.319	0.948	0.280

Table A-11. Continued.

For θ_{frac} = 90°									
$(\varepsilon_{\theta\theta(I)})_{frac}$, Msi^{-1}	$(\varepsilon_{\theta\theta(II)})_{frac}$, Msi^{-1}	$(\varepsilon_{r\theta(I)})_{frac}$, Msi^{-1}	$(\varepsilon_{r\theta(II)})_{frac}$, Msi^{-1}	$(\varepsilon_{\theta\theta(T)})_{frac}$, Msi^{-1}	$(\varepsilon_{r\theta(T)})_{frac}$, Msi^{-1}	For $\varepsilon_{\theta\theta} = \varepsilon_u$		For $\varepsilon_{r\theta} = 0.0220$	
						T factor	$(2\pi d_o)^{1/2}$, $(in.)^{1/2}$	T factor	$(2\pi d_o)^{1/2}$, $(in.)^{1/2}$
0.00810	-0.175	0.126	-0.155	0.1937	0	0.762	0.0358	1	0.493
0.00810	-0.175	0.126	-0.155	0.1937	0	1.045	0.0535	1	0.537
0.00810	-0.175	0.126	-0.155	0.1937	0	1.298	0.0626	1	0.506
0.00659	-0.094	0.155	-0.126	0.0849	0	0.903	0.0137	1	0.277
0.00659	-0.094	0.155	-0.126	0.0849	0	1.010	0.0152	1	0.275
0.00659	-0.094	0.155	-0.126	0.0849	0	1.035	0.0155	1	0.275
0.04139	-0.139	0.187	-0.187	0.1535	0.0544	1.066	0.0953	1.015	0.390

Table A-11. Continued.

For θ_{frac} = -45°									
$(\varepsilon_{\theta\theta(I)})_{frac}$, Msi^{-1}	$(\varepsilon_{\theta\theta(II)})_{frac}$, Msi^{-1}	$(\varepsilon_{r\theta(I)})_{frac}$, Msi^{-1}	$(\varepsilon_{r\theta(II)})_{frac}$, Msi^{-1}	$(\varepsilon_{\theta\theta(T)})_{frac}$, Msi^{-1}	$(\varepsilon_{r\theta(T)})_{frac}$, Msi^{-1}	For $\varepsilon_{\theta\theta} = \varepsilon_u$		For $\varepsilon_{r\theta} = 0.0220$	
						T factor	$(2\pi d_o)^{1/2}$, $(in.)^{1/2}$	T factor	$(2\pi d_o)^{1/2}$, $(in.)^{1/2}$
0.0419	0.193	0.0478	0.197	0.0798	0.228	0.886	0.215	1.328	0.247
0.0419	0.193	0.0478	0.197	0.0798	0.228	1.018	0.270	0.967	0.196
0.0419	0.193	0.0478	0.197	0.0798	0.228	1.104	0.276	0.846	0.162
0.0947	0.122	0.1883	0.153	0.0254	0.119	0.964	0.242	1.132	0.381
0.0947	0.122	0.1883	0.153	0.0254	0.119	1.003	0.250	0.989	0.330
0.0947	0.122	0.1883	0.153	0.0254	0.119	1.012	0.252	0.965	0.322
0.0348	0.0951	-0.1568	0.230	0.0254	0.202	1.010	0.136	-0.948	0.287

Table A-11. Concluded.

For θ_{frac} = -90°									
$(\varepsilon_{\theta\theta(I)})_{frac}$, Msi^{-1}	$(\varepsilon_{\theta\theta(II)})_{frac}$, Msi^{-1}	$(\varepsilon_{r\theta(I)})_{frac}$, Msi^{-1}	$(\varepsilon_{r\theta(II)})_{frac}$, Msi^{-1}	$(\varepsilon_{\theta\theta(T)})_{frac}$, Msi^{-1}	$(\varepsilon_{r\theta(T)})_{frac}$, Msi^{-1}	For $\varepsilon_{\theta\theta} = \varepsilon_u$		For $\varepsilon_{r\theta} = 0.0220$	
						T factor	$(2\pi d_o)^{1/2}$, $(in.)^{1/2}$	T factor	$(2\pi d_o)^{1/2}$, $(in.)^{1/2}$
0.00810	0.175	0.1263	-0.1553	0.1937	0	0.762	0.0358	1	0.493
0.00810	0.175	0.1263	-0.1553	0.1937	0	1.045	0.0535	1	0.537
0.00810	0.175	0.1263	-0.1553	0.1937	0	1.298	0.0626	1	0.506
0.00659	0.094	0.1553	-0.1263	0.0849	0	0.903	0.0137	1	0.277
0.00659	0.094	0.1553	-0.1263	0.0849	0	1.010	0.0152	1	0.275
0.00659	0.094	0.1553	-0.1263	0.0849	0	1.035	0.0155	1	0.275
-0.03820	0.140	-0.0616	-0.0616	0.1535	0.0544	-0.942	0.0735	-0.985	0.156

Appendix B. Detail Drawings of Tests specimen and apparatus

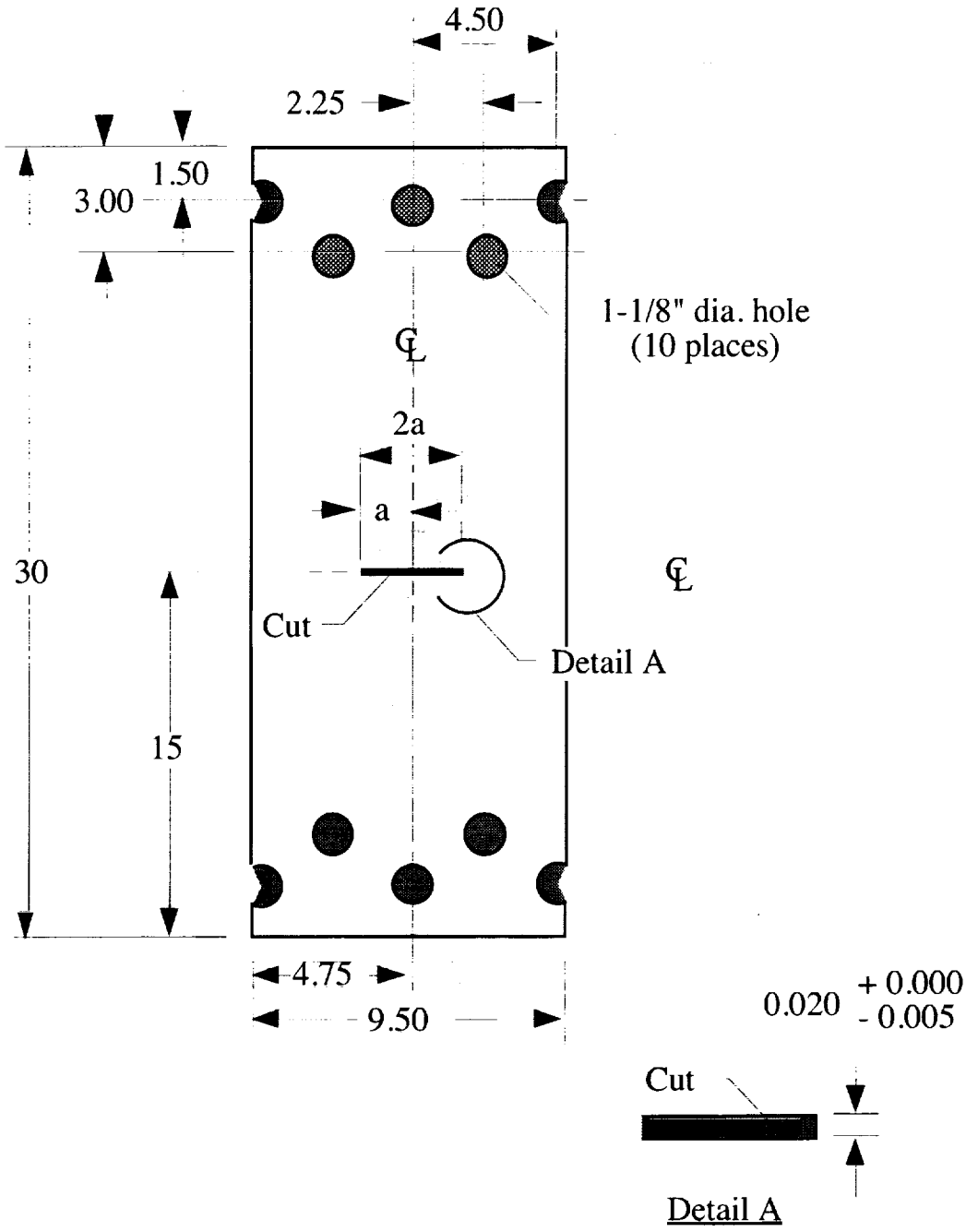

All dimensions are shown in inches.

Figure B–1. Drawing of 9.50-inch-wide center notch tension (CNT) specimens.

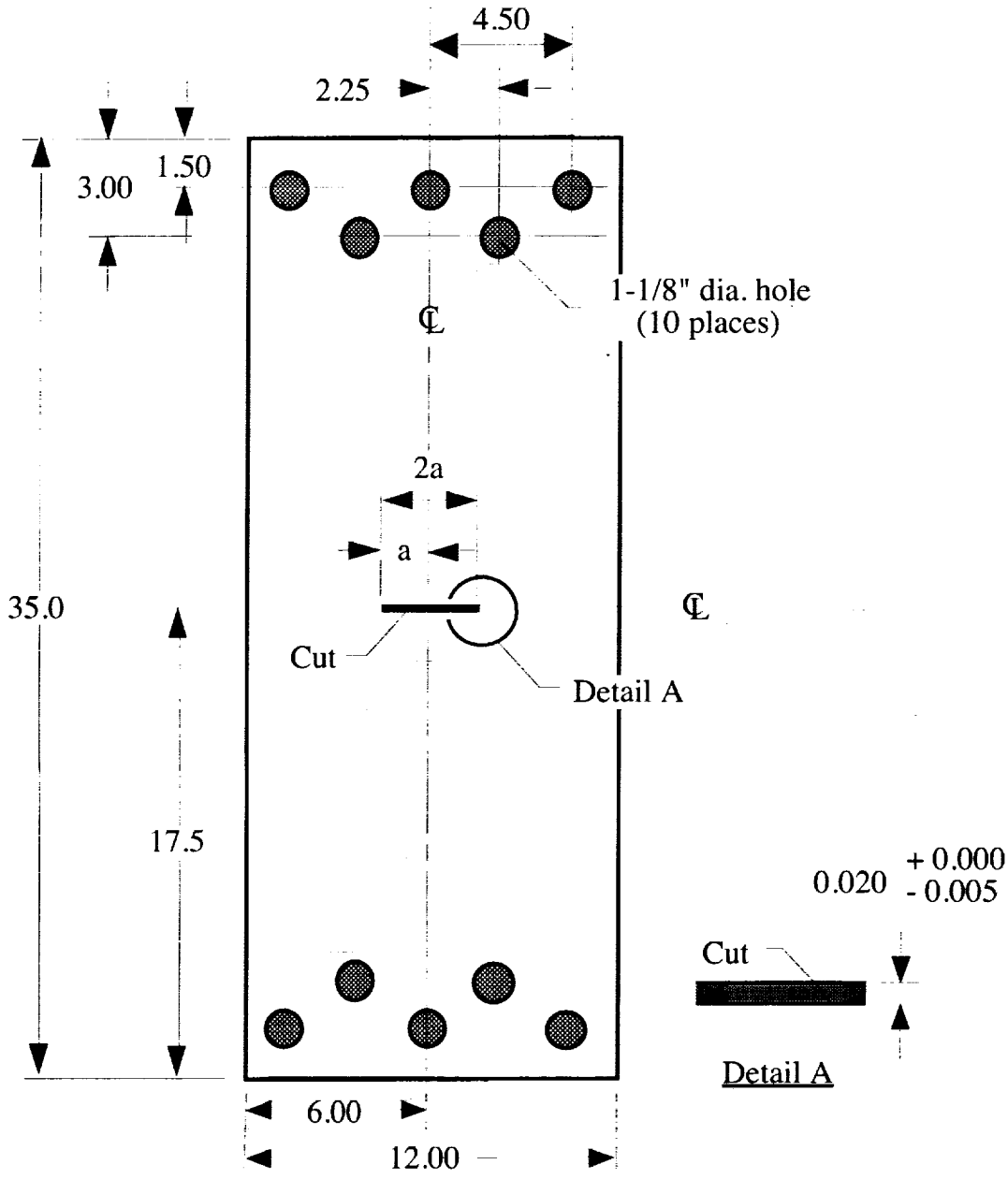

All dimensions are shown in inches.

Figure B–2. Drawing of 12.0-inch-wide center notch tension (CNT) specimens.

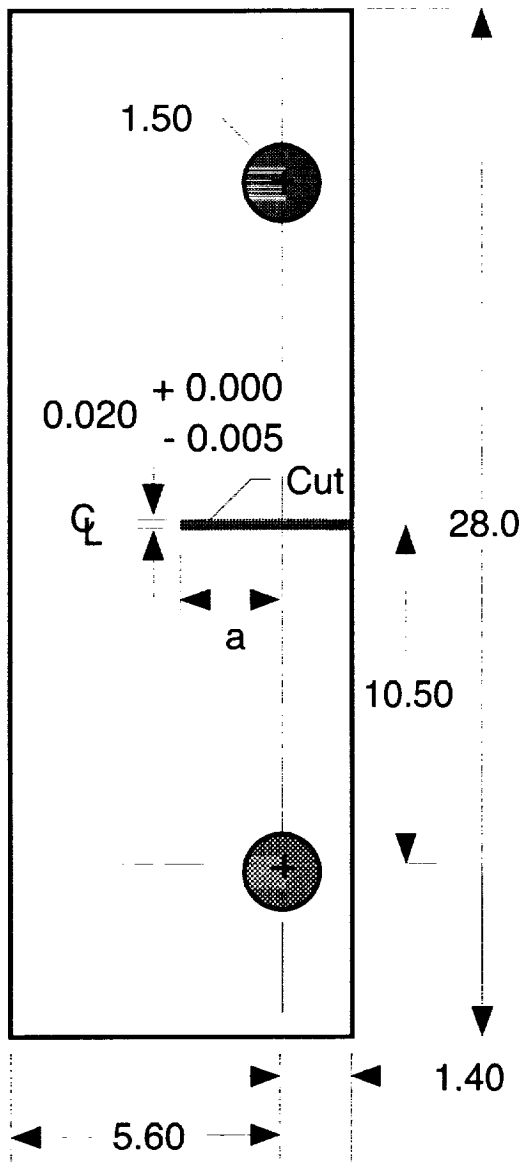

All dimensions are shown in inches.

Figure B–3. Drawing of 7.0-inch-wide extended compact tension (ECT) specimens.

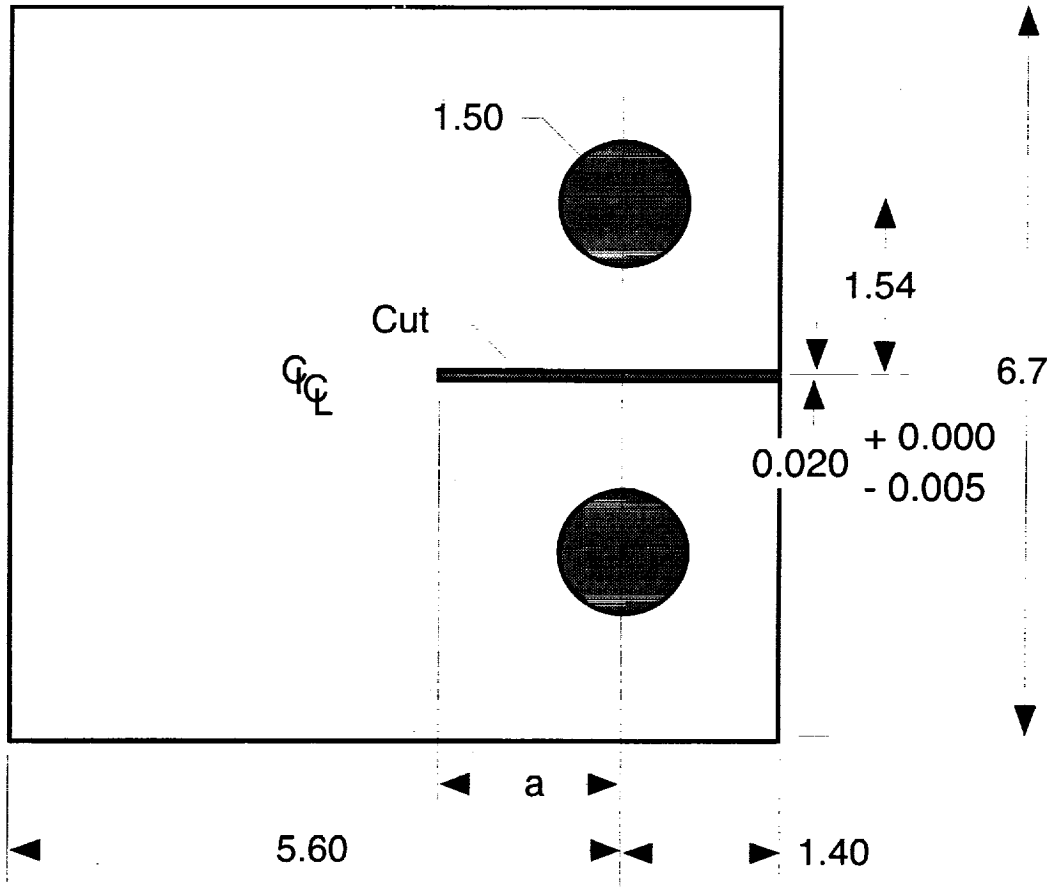

All dimensions are shown in inches.

Figure B–4. Drawing of 7.0-inch-wide compact tension (CT) specimens.

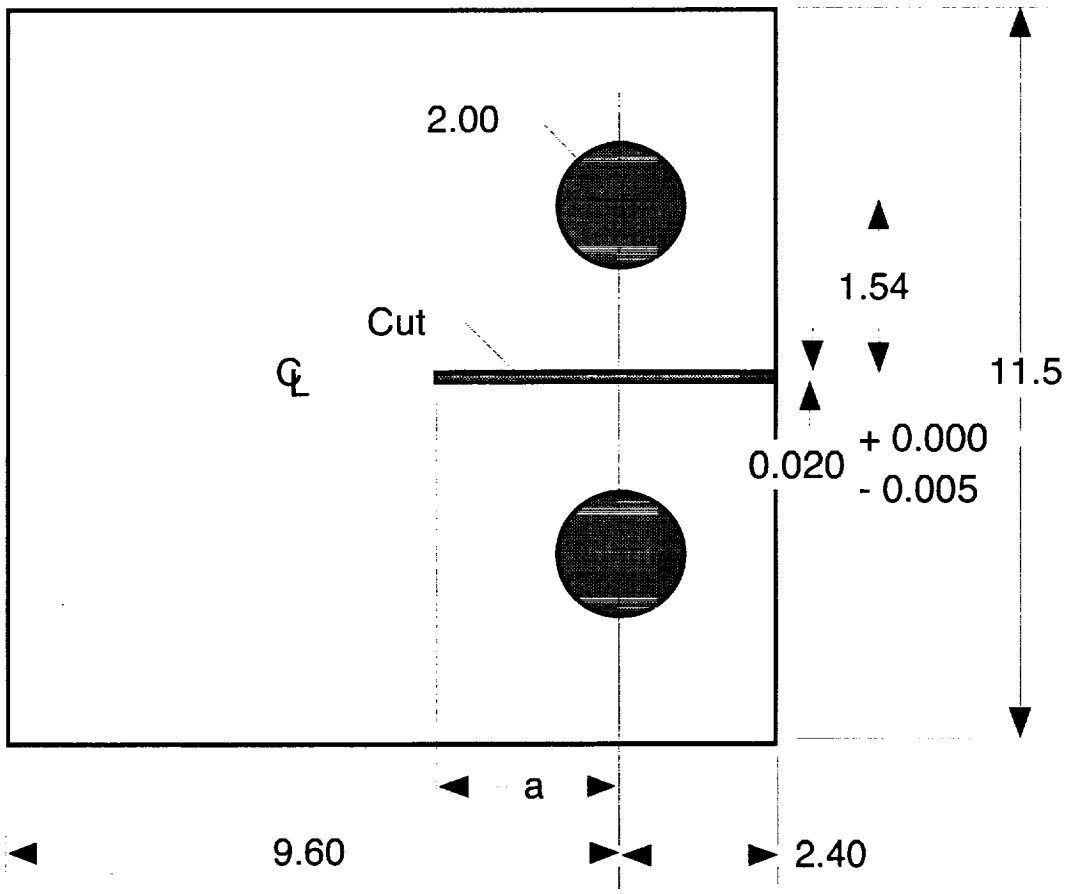

All dimensions are shown in inches.

Figure B–5. Drawing of 12.0-inch-wide compact tension (CT) specimens.

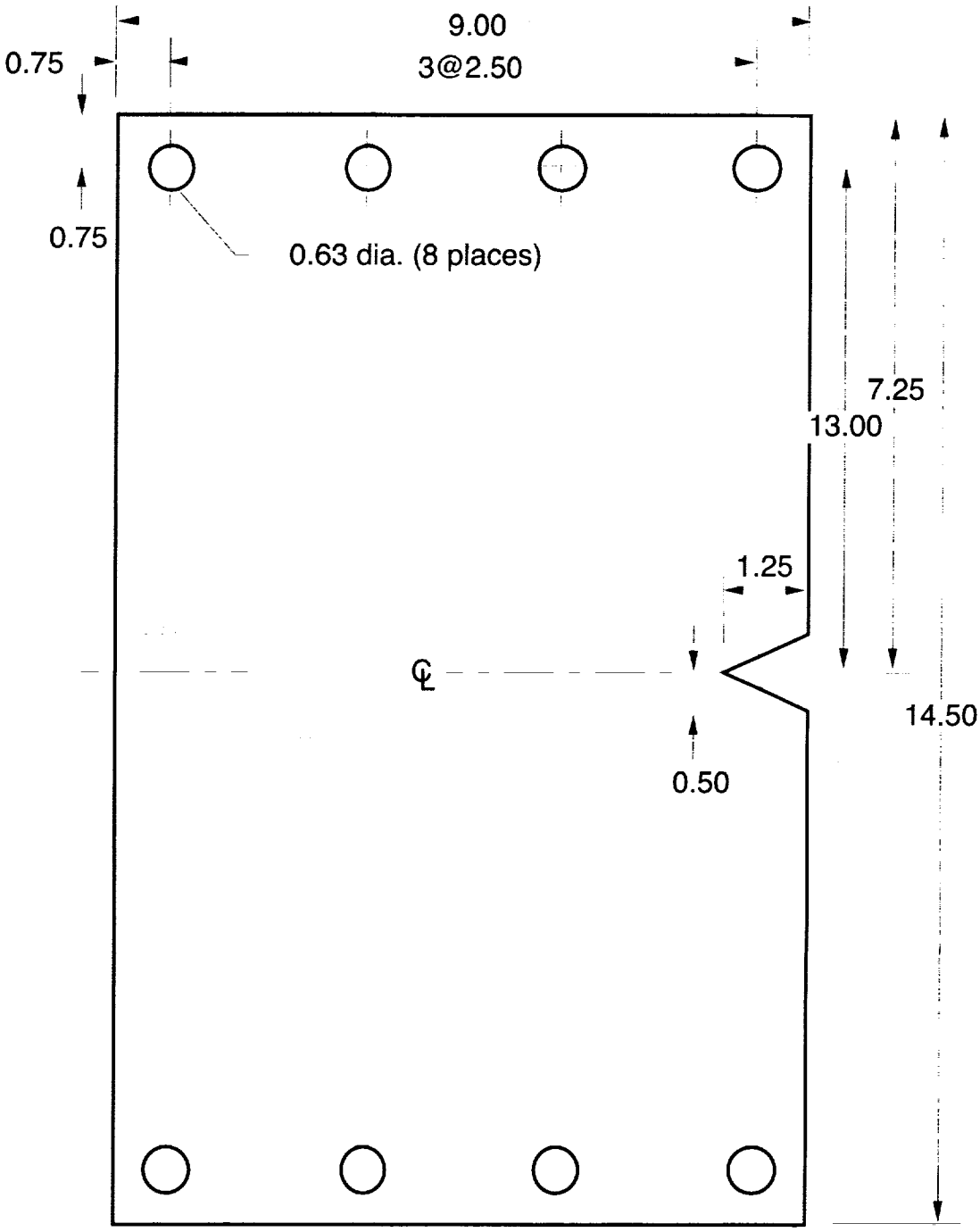

Note - Four pieces required, lined on one side with 1/16-inch Teflon sheet

All dimensions shown in inches.

Figure B–6. Drawing of guide plates for CNT specimens.

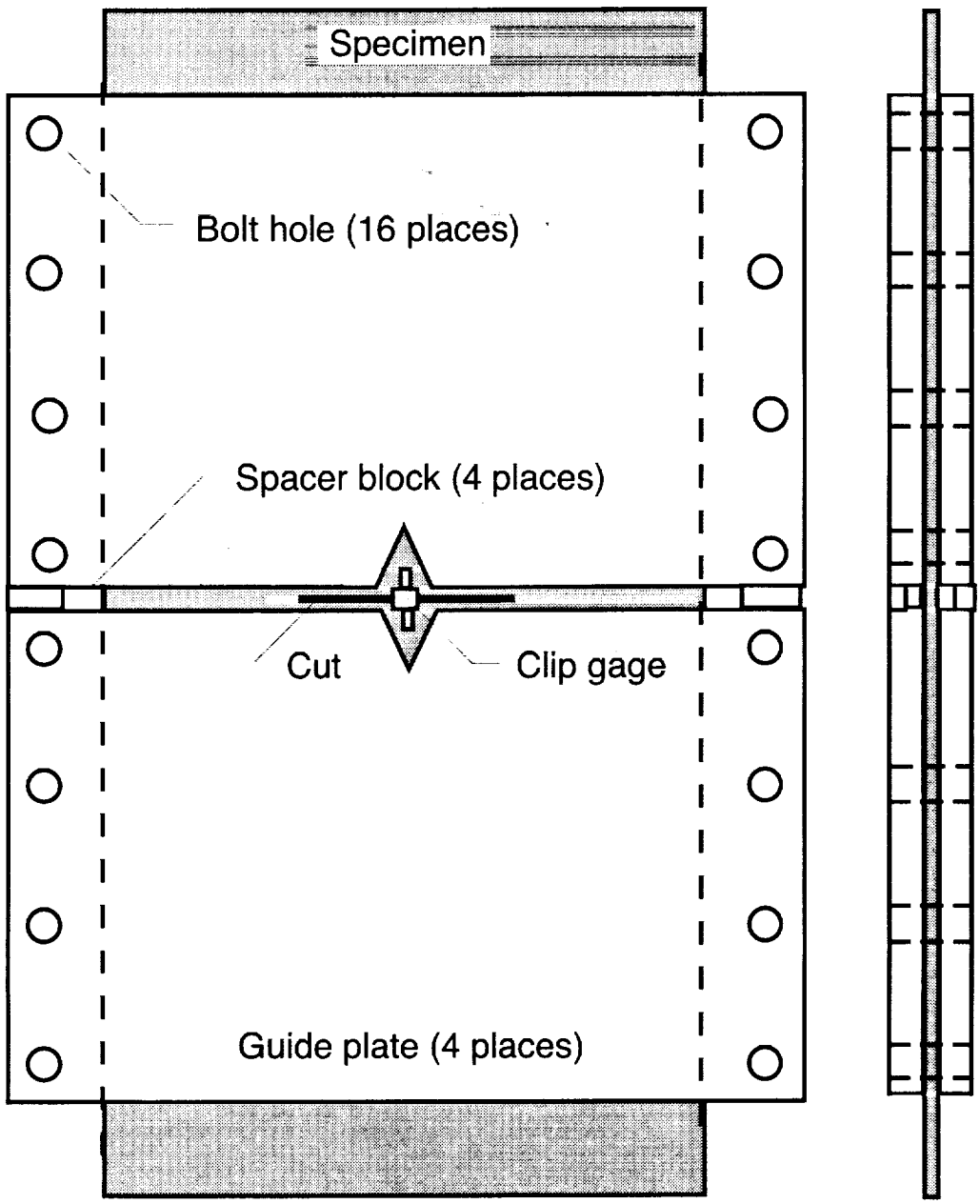

Figure B–7. Arrangement of guide plates and clip gage for CNT specimens.

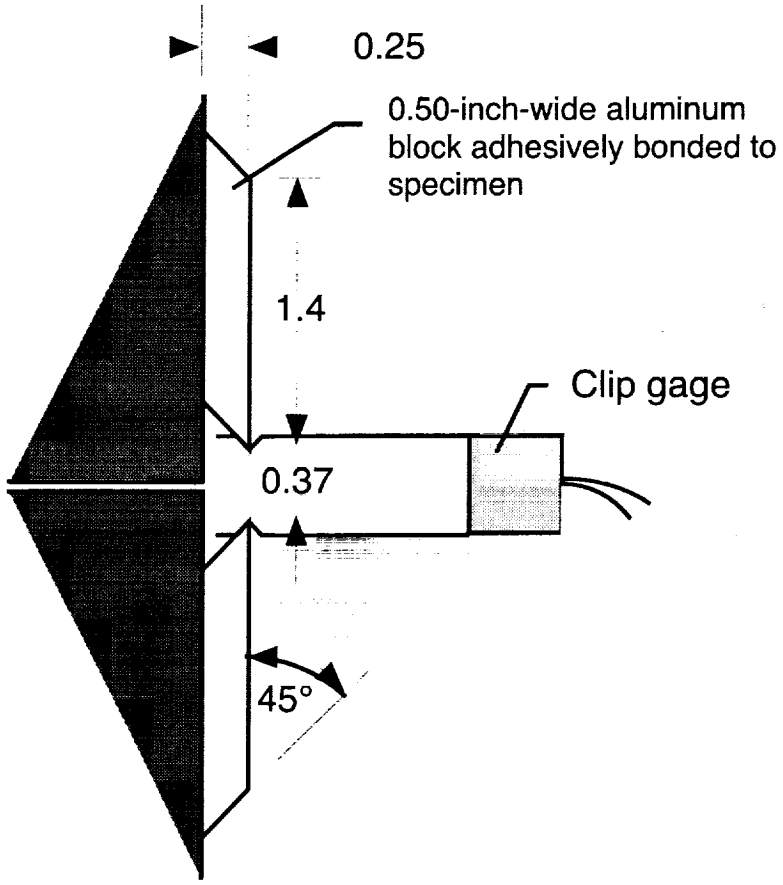

All dimensions are shown in inches.

Figure B–8. Installation of clip gage for CNT specimens.

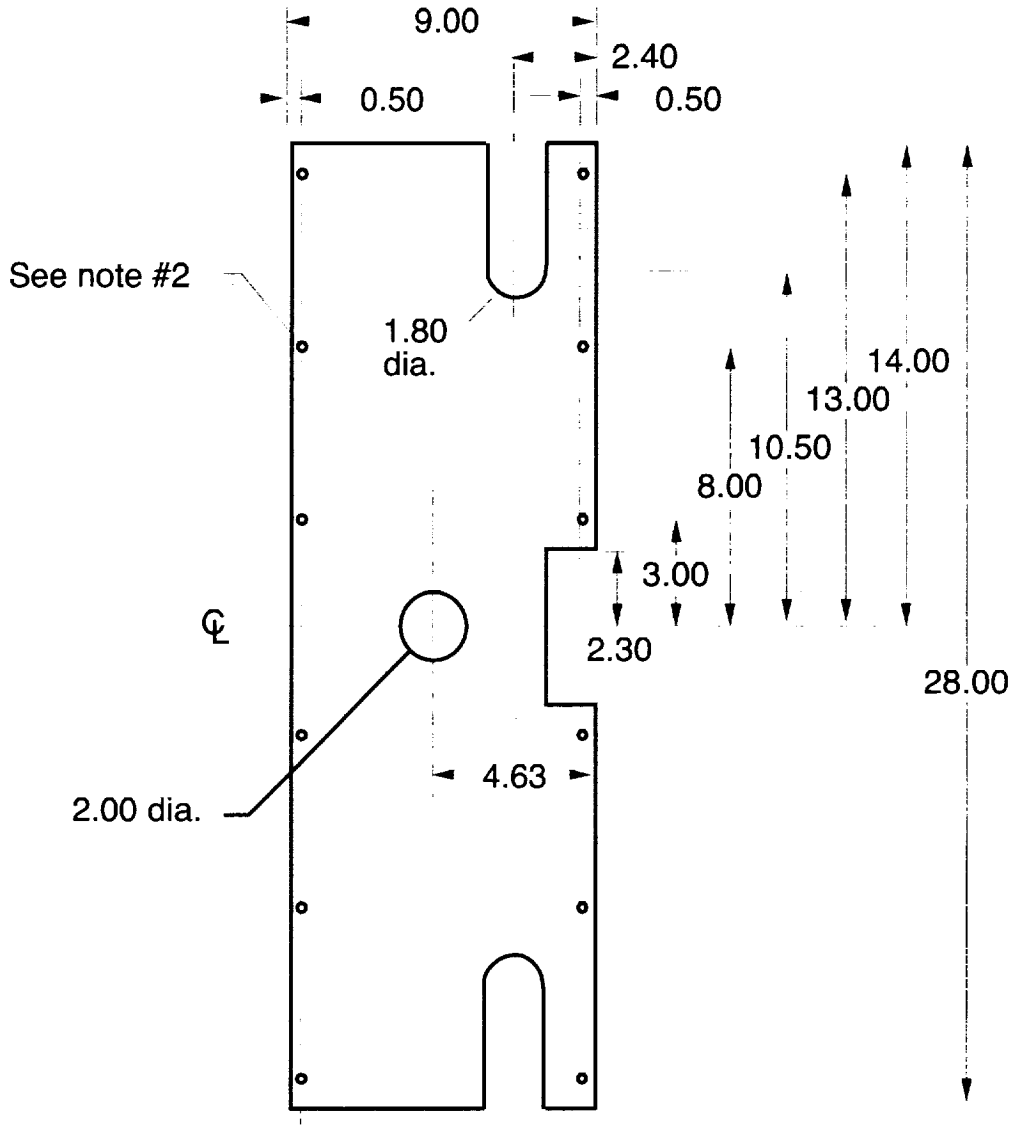

Notes -
1. Two pieces required, lined on one side with 1/16-inch Teflon sheet
2. Piece #1 - countersink for 1/4-20x1 flathead screws, 5 places
   Piece #2 - drill and tap for 1/4-20x1 thread, 5 places

All dimensions shown in inches.

Figure B–9. Drawing of guide plates for ECT specimens.

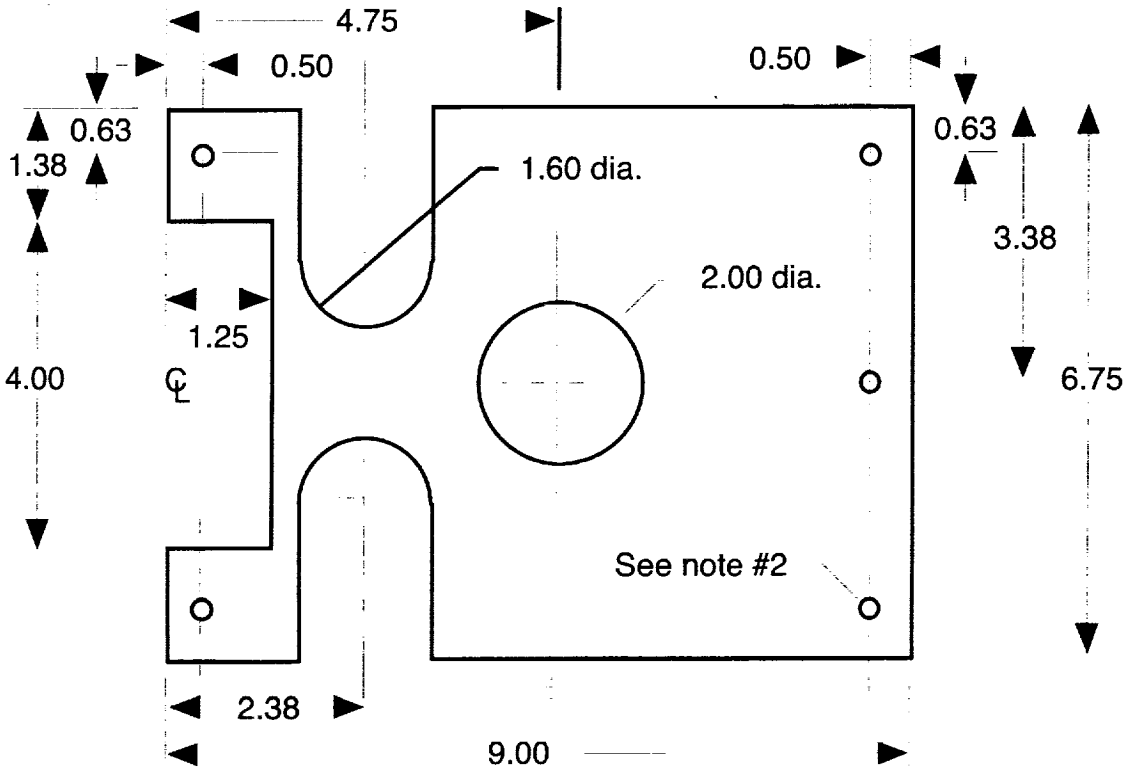

Notes -
1. Two pieces required, lined on one side with 1/16-inch Teflon sheet
2. Piece #1 - countersink for 1/4-20x1 flathead screws, 5 places
   Piece #2 - drill and tap for 1/4-20x1 thread, 5 places

All dimensions shown in inches.

Figure B–10. Drawing of guide plates for 7.0-inch-wide CT specimens.

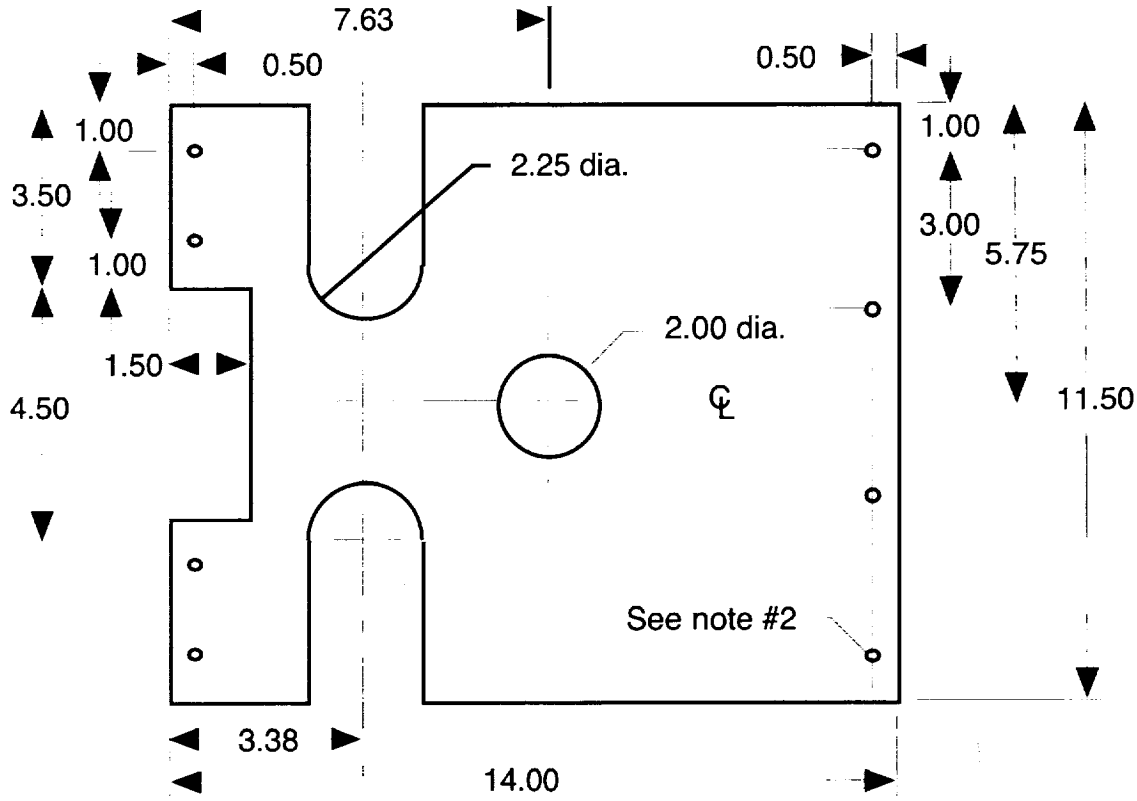

Notes -lined on one side with 1/16-inch Teflon sheet
2. Piece #1 - countersink for 1/4-20x1 flathead screws, 5 places
Piece #2 - drill and tap for 1/4-20x1 thread, 5 places

All dimensions shown in inches.

Figure B–11. Drawing of guide plates for 12.0-inch-wide CT specimens.

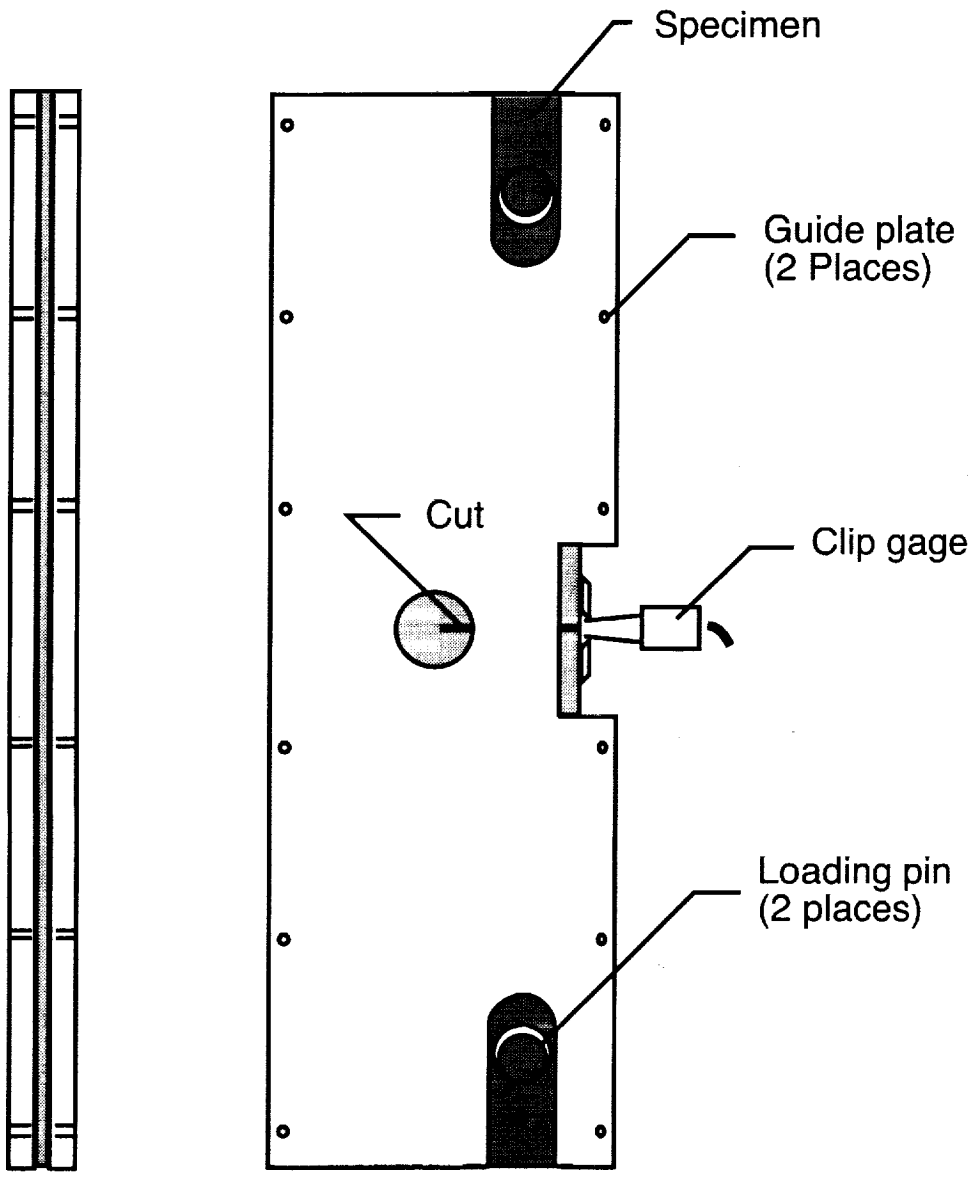

Figure B–12. Arrangement of guide plates and clip gage for ECT specimens.

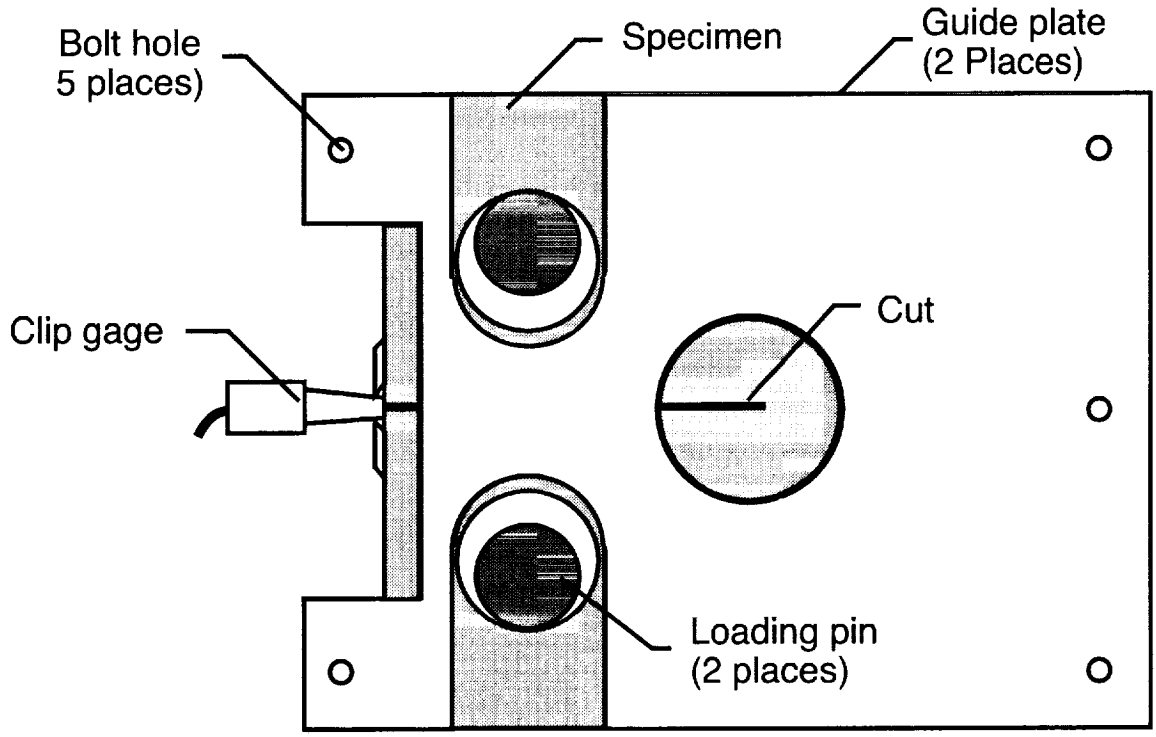

Figure B–13. Arrangement of guide plates and clip gage for CT specimens.

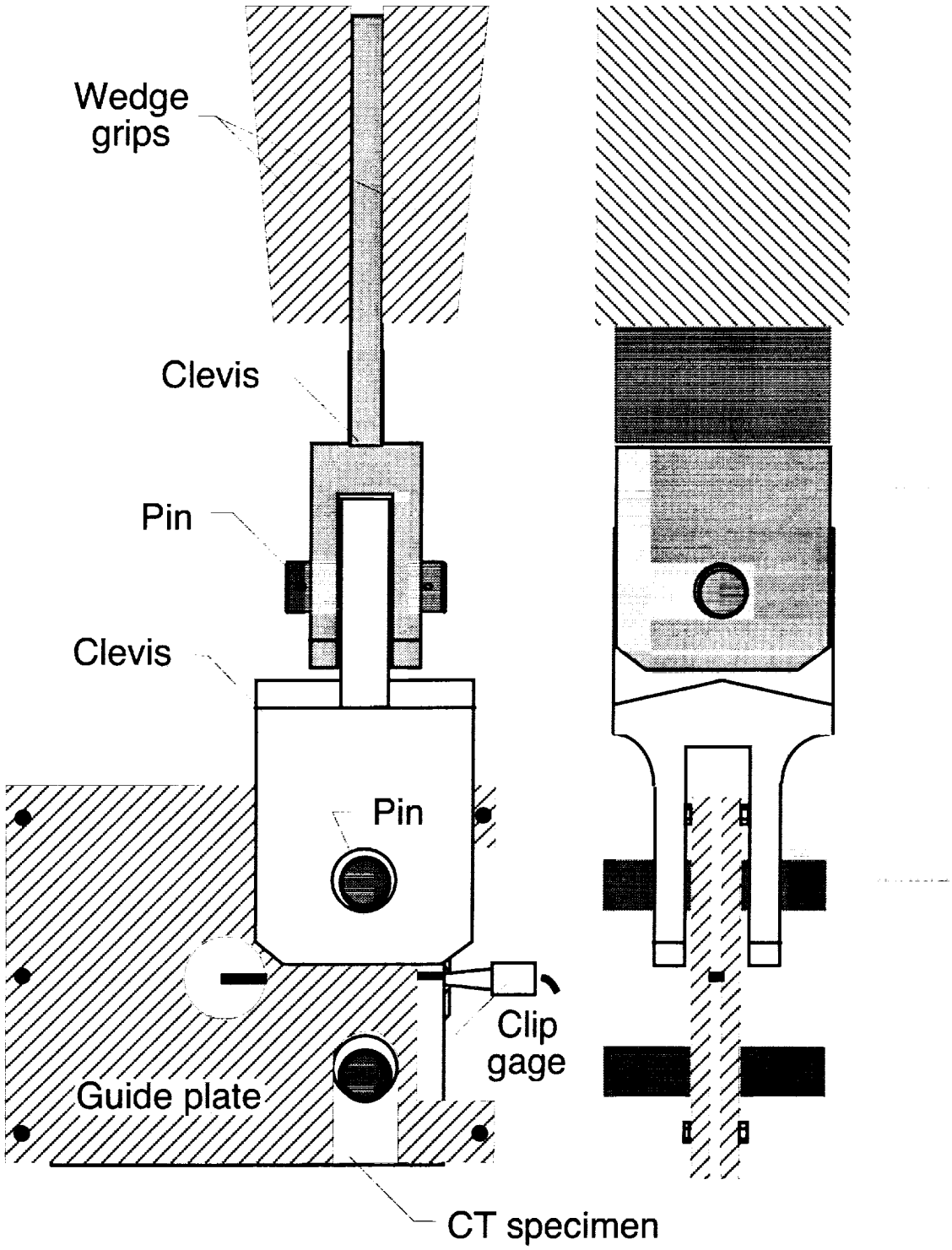

Figure B–14. Clevis arrangement for ECT and CT specimens.

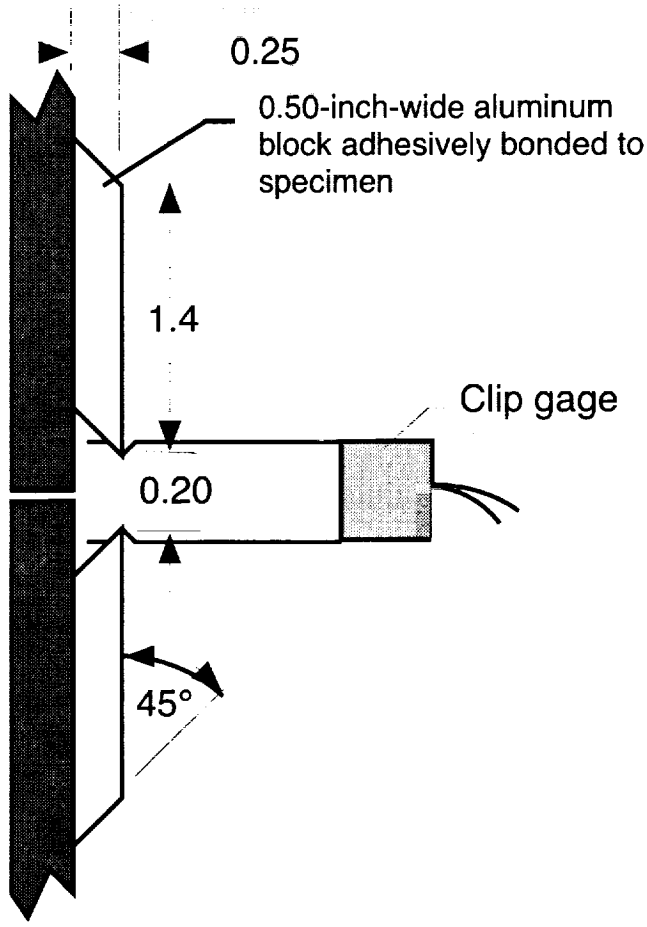

All dimensions are shown in inches.

Figure B–15. Installation of clip gage for ECT and CT specimens.

REPORT DOCUMENTATION PAGE

Form Approved
OMB No. 0704-0188

1. AGENCY USE ONLY (Leave blank)	2. REPORT DATE	3. REPORT TYPE AND DATES COVERED
	May 2001	Technical Memorandum

4. TITLE AND SUBTITLE
Fracture Berhavior of a Stitched Warp-Knit Carbon Fabric Composite

5. FUNDING NUMBERS
242-82-76-10

6. AUTHOR(S)
Clarence C. Poe, Jr., James R. Reeder, and F. G. Yuan

7. PERFORMING ORGANIZATION NAME(S) AND ADDRESS(ES)
NASA Langley Research Center
Hampton, VA 23681-2199

8. PERFORMING ORGANIZATION REPORT NUMBER
L-18080

9. SPONSORING/MONITORING AGENCY NAME(S) AND ADDRESS(ES)
National Aeronautics and Space Administration
Washington, DC 20546-0001

10. SPONSORING/MONITORING AGENCY REPORT NUMBER
NASA/TM-2001-210868

11. SUPPLEMENTARY NOTES
Poe and Reeder: Langley Research Center, Hampton, VA
Yuan: North Carolina State University, Raleigh, NC

12a. DISTRIBUTION/AVAILABILITY STATEMENT
Unclassified-Unlimited
Subject Category 24 Distribution: Standard
Availability: NASA CASI (301) 621-0390

12b. DISTRIBUTION CODE

13. ABSTRACT (Maximum 200 words)

Tests were conducted on several types of fracture specimens made from a carbon/epoxy composite. The composite material was stitched prior to introducing epoxy resin. Boeing used this material to develop a composite wing box for a transport aircraft in the NASA Advanced Composites Transport Program. The specimens included compact, extended compact, and center notched tension specimens. The specimens were cut from panels with three orientations in order to explore the effects of anisotropy. The panels were made with various thicknesses to represent a wing skin from tip to root. All fractures were not self-similar depending on specimen type and orientation. Unnotched tension specimens were also tested to measure elastic constants and strengths. The normal and shear strains were calculated on fracture planes using a series representation of strain fields for plane anisotropic crack problems. The fracture parameters were determined using a finite element method. Characteristic distances for critical tension and shear strains were calculated for each specimen and a failure criterion based on the interaction of tension and shear strains was proposed.

14. SUBJECT TERMS	15. NUMBER OF PAGES
Composites; Fracture Mechanics; Crack Turning; Textile	112
	16. PRICE CODE: A06

17. SECURITY CLASSIFICATION OF REPORT	18. SECURITY CLASSIFICATION OF THIS PAGE	19. SECURITY CLASSIFICATION OF ABSTRACT	20. LIMITATION OF ABSTRACT
Unclassified	Unclassified	Unclassified	UL

NSN 7540-01-280-5500

Standard Form 298 (Rev. 2-89)
Prescribed by ANSI Std. Z-39-18
298-102